Development of high performance tribological coatings for application onto hip joint prostheses

Paul Knox MEng (Hons)

A thesis submitted in partial fulfilment of the requirements of the University of Wolverhampton for the degree of Doctor of Philosophy

December 4, 2009

This work or any part thereof has not previously been presented in any form to the University or to any other body whether for the purposes of assessment, publication or for any other purpose (unless otherwise indicated). Save for any express acknowledgements, references and/or bibliographies cited in the work, I confirm that the intellectual content of the work is the result of my own efforts and of no other person.

Signature .....

Date .....

Abstract

In this thesis Graphit-iC^{TM}, an amorphous carbon coating developed by Teer Coatings Ltd. was modified and deposited onto CoCr and UHMWPE substrates in order to improve the wear properties. It was identified that depositing a hard coating onto a soft substrate would cause high stresses and lead to coating delamination. Consequently the polyethylene substrates were ion implanted with nitrogen to reduce the hardness differential at the substrate-coating boundary. The coating was characterised using a pin on disc method in order to determine wear and friction. Hardness and fatigue was characterised using nano-indentation and the coating adhesion was measured using scratch testing.

Application of the coatings resulted in a significant reduction in wear. Wear factors as low as 3.65×10^{-18}m^3/Nm were achieved for coated CoCr substrates compared to 3.53×10^{-15}m^3/Nm reported in the literature for uncoated CoCr. The coating resulted in friction coefficients between 0.12 and 0.19 with hardness ranging from 6.65 and 15.63GPa. Similarly coating UHMWPE resulted in a reduction in the wear factor to less than 9.6×10^{-17}m^3/Nm.

It was concluded that the deposition of amorphous carbon coatings can improve wear of hip joint prostheses, although consideration must be made for the adhesion of the coating to the substrate so that it does not contribute to an early failure of the device. Improved adhesion can be achieved by reducing the hardness differential between the coating and adhesion, either through softening the coating or by using interlayers.

Contents

List of Figures

List of Tables

Abbreviations

AFM	Atomic Force Microscopy
CFUMSIP	Closed Field Unbalanced Magnetron Sputter Ion Plating
CMM	Coordination Measuring Machine
CoCr	Cobalt Chromium
CVD	Chemical Vapour Deposition
DLC	Diamond-like Carbon
HDPE	High Density Polyethylene
LDPE	Low Density Polyethylene
MOM	Metal on Metal
PMMA	Polymethylmethacrylate
POD	Pin on Disc
POM	Polymer on Metal
PTFE	Polytetrafluoroethylene
PVD	Physical Vapour Deposition
RBS	Rutherford Backscattering
SEM	Scanning Electron Microscopy
TiN	Titanium Nitride
UHMWPE	Ultra High Molecular Weight Polyethylene
XPS	X-ray Photoelectron Spectroscopy

Acknowledgements

The author would firstly like to thank Ramona and his family for supporting him during his studies.

A significant mention should be made to Dr C Wang his Director of Studies and Dr G. Pearce, his supervisor. Also Colin Durnall and Jim Stamps who helped with sample preparation and examination and Matthew Burley for the integration code.

He is also grateful to Sue Field and everyone at Teer Coatings Ltd. who provided financial support and advice as well as coating and testing equipment. They all dedicated large amounts of their time to helping him understand coatings, their deposition and testing.

Companies that have supported him at various stages throughout the project, either by supplying of raw materials or testing equipment include Firth Rixon Ltd, Perplas Ltd, Stryker Howmedica, Zeeko Ltd and Micro Materials Ltd.

Time on equipment and advice was also received from Phil Charlton and Prof L. Blunt, University of Huddersfield; Prof J. Sullivan, Dr S. Saied, Dr B. Shi and Dr T. Zaharia, Aston University; Dr C. Jeynes, Dr M. Webb, and Dr N. Peng, University of Surrey and Prof Fisher, Dr I. Udofia and Dr S. Williams, University of Leeds.

Support from a medical perspective was welcomed from Mr J Patrick and Gunther Selzer at the Robert Jones and Agnes Hunt Orthopaedic Hospital; Mr Cleake at

the Worcester Royal Infirmary and Mr T Sadique of Manor Hospital, Walsall.

Financial support was received from EPSRC.

Finally the author would like to thank Gareth at Osteotec Ltd. for time off work to write up his thesis as well as Jayne and Daniel who suggested it would probably be best to submit before retirement.

1. Introduction

The hip joint is a ball and socket joint composed of the acetabular cup in the pelvic bone and the femoral head, it is supported by strong muscles and ligaments which provide stability and a large range of movement. This anatomy does not always last a person's entire life, failure can result in pain and disability and occur through numerous mechanisms, biological and mechanical in nature.

Artificial replacements can be implanted to repair the failed joint. From an engineering perspective these must be designed with the necessary mechanical strength and be able to endure the biological environment in which they are placed, otherwise they will also fail. In the past, design factors which have led to failure of a joint include joint geometry and poor material choice or manufacture, leading to excessive and unexpected wear and corrosion. In order to reduce the incidence of implant failure, it is important that the entire system is fully characterised; from the anatomy of the joint and the biological response, through to the microstructure of the material and the design geometry.

In 2005 there were 61,881 reported hip replacement operations (up from 48,987 in 2004) in England and Wales, according to a comprehensive report of joint operations carried out in the UK (National Joint Registry for England and Wales, 2006). Of these, 55,812 were primary replacements and 5,769 were revision surgeries. This compares to the more complete, but less detailed National Health Service hospital episode statistics compiled by the Department of Health, which recorded 63,418 "Total prosthetic replacements of hip joint" (OPCS-4 codes W37,

W38 and W39) from April 2005 until March 2006 (Department of Health, 2006).

The UK national joint registry's inception was in 2002 (National Joint Registry for England and Wales, 2007). For longer term data it is necessary to look at the registries of other countries, in particular the Swedish Hip Arthroplasty Registry, which is the longest standing. The Swedish registry reports that over the past 10 years the survival rate of total hip replacements was 92.5%, the remainder failed and required revision (Swedish Hip Arthroplasty Register, 2006). At a cost of approximately £3000-4000 for a primary total hip replacement and more for revision (Faulkner *et al.*, 1998), the failure of hip joint prostheses is a significant burden to Great Britain's National Health Service and other healthcare providers around the world. By reducing the rate of hip joint failure, cost savings can be made, in addition to reducing the pain and general risks associated with any surgery to the patient.

The reduction of wear and subsequent extension of life of a hip joint replacement would bring both economic benefits and a better quality of life to the patients who have to undergo replacement surgery. Reduction of wear can be achieved by modifying the materials used for the replacement. In particular by applying a surface coating at the femoral-acetabular interface which is able to withstand the forces that the joint is exposed to.

This thesis will examine the deposition of a high performance carbon coating known as Graphit-iC^{TM} (Teer *et al.*, 2004) onto orthopaedic materials, Graphit-iC^{TM} is a graduated amorphous carbon coating with chromium as an interlayer

deposited directly onto the substrate and then used to dope the carbon layer; sp^3 ratio is less than 0.5%. This coating has not yet been applied to orthopaedic components, but has been shown to have low wear and friction characteristics in other industries compared to some other diamond-like carbon (DLC) coatings.

1.1 Hypothesis

The production of wear particles from metal on metal (MOM) and polymer on metal (POM) hip joint replacements and the adverse effect that they have on the body has been a continual problem since they were first implanted. Surface coatings are believed to have the potential to reduce the wear of hip joints, but to date have had limited success; this is in part due to poor adhesion of the coating.

Amorphous carbon coatings have extremely low wear and good adhesion; they have been successfully used in other industries such as machine tooling, and it is hypothesised that they will be able to reduce the wear of hip joint replacements. This thesis will examine the deposition of amorphous carbon coatings onto orthopaedic materials.

1.2 Aims

- To characterise Graphit-iC^{TM} and associated coatings in terms of wear, friction, hardness, toughness and adhesion when deposited onto cobalt chromium (CoCr)

- To optimise the Graphit-iC^{TM} coating produced by Teer Coatings Ltd. for improved performance on hip joint replacements.

- To deposit an amorphous carbon coating on ultra high molecular weight polyethylene (UHMWPE) with a wear factor superior to uncoated UHMWPE and with adhesion and toughness that is suitable for hip joint replacements.

1.3 Thesis Structure

Chapter 1 introduces the work carried out in this thesis.

Chapter 2 presents work that has been published on the topic of this thesis. It outlines the basic joint anatomy and its methods of failure. Followed by the replacements that are available to overcome this. The shortcomings of current replacements are discussed and the use of coatings as a method to reduce these.

Chapter 3 describes the deposition process and parameters used for the coatings that are developed in the course of these studies.

Chapter 4 characterises the hardness of the coatings deposited in Chapter 3 using nano-indentation. Other characteristics such as the reduced modulus are also reported on.

Chapter 5 describes a scratch test method used to characterise the adhesion of the coatings to the CoCr and UHMWPE substrates.

Chapter 6 investigates the toughness and fatigue properties of the coatings using

a low cycle, accelerated fatigue, micro impact test.

Chapter 7 discusses methods of wear testing, this leads on to characterisation of wear and friction for the deposited coatings using a pin on disc method.

Chapter 8 concludes the thesis; the findings of the literature review are discussed and the subsequent characterisations from Chapters 4 through to 7 summarised.

2. Development of Total Hip Joint Replacement

2.1 Introduction

The gross anatomy of the hip joint is first discussed leading to how it can fail and what can be done to resolve the issue, including hip joint replacement. The history and development of hip joint prostheses is discussed, identifying the deficiencies and how design has been improved to resolve some of these issues. Coatings, particularly DLC, are identified as a way of reducing problems; these are explained with methods of testing their performance prior to implantation into a patient.

2.2 The Natural Hip Joint

2.2.1 Anatomy and Physiology

The hip joint comprises the femoral head and acetabulum of the pelvis which consists of the ilium, ischium, and pubis. In the younger person these bones are separate, but in early adulthood they fuse into one. The ilium is located superiorly, while the pubis is located anteriorly and the ischium posteriorly (Gray, 1858).

The hip joint is a ball and socket joint with 3 degrees of freedom; allowing the leg to flex, extend, adduct, abduct and internally and externally rotate. The largest muscles in the body span the joint to enable this range of motion and

provide it with the strength, movement and support needed. Some of the muscles which allow these movements are gluteus maximus (extension); iliopsoas and pectineus (flexion); gluteus medius and minimus (abduction) and the adductors bevis, longus and magnus (adduction) (Thompson and Floyd, 1997).

In addition to the muscles which span the joint, support is provided by three ligaments. The ligaments link the pelvis and femoral bones, they are known as the iliofemoral, pubofemoral and ischiofemoral ligaments (Gray, 1858).

The articulating surfaces of the acetabular cup and femoral head are covered by hyaline cartilage. Hyaline cartilage is a connective tissue of chondrocytes embedded in a matrix of proteoglycans and collagen fibres. The cartilage is avascular, obtaining nutrients from synovial fluid by diffusion. During movement synovial fluid can be forced into pores in the hyaline cartilage which improves the nutritional supply. The diffusion process by which nutrients reach the cartilage means that repair of cartilage is slow (Gray, 1858; Maroudas, 1970, 1976).

The joint is enclosed by a synovial capsule; synovium lines the internal surfaces of the cavity space and contains the synovial fluid. Synovial fluid is derived from blood plasma (Dumbleton, 1981) but has additional constituents produced by fibroblasts in the synovium which improve the lubrication such that friction levels of 0.001 are achieved (Batchelor and Chandrasekaran, 2004). The lubricating properties of synovial fluid are mainly derived from the presence of lubricin, a glycoprotein and hyaluronic acid, a long chained polymer which gives the fluid non-Newtonian characteristics such that when the fluid is sheared, the viscosity

Table 2.1: Range of movement at the hip joint (Thompson and Floyd, 1997)

Motion	Angle (°)
Extension / Flexion	-30 - 130
Adduction / Abduction	-30 - 35
Internal / External Rotation	-45 - 50

decreases (shear thinning) (Ogston and Stanier, 1953; Dumbleton, 1981). This property improves lubrication of the joint for different activities - when a subject is standing still, the viscosity is high, whereas when a subject walks, the liquid becomes less viscous.

When walking, the gait forces are bimodal and reach between 2 and 5 times body weight (Bergmann *et al.*, 2001; Paul, 1967; Rydell, 1966); during a year the number of joint cycles is over 1 million (Morlock *et al.*, 2001). Genda *et al.* (2001) reports the peak stresses to be 1.67MPa for females and 1.38MPa for males. The difference in stress is due to the difference in femoral head size observed in the genders - 23.8mm and 26.0mm for females and males respectively. The peak stress observed in the joint is dependent on the condition of the articulating cartilage however, measuring this effect is difficult (Genda *et al.*, 2001). These forces and stresses will also vary between activities, such as walking, stair climbing and running.

During the gait cycle the joint will flex and extend through a range normal for that person, although the total range of movement that the joint is capable of is greater (Table 2.1).

Table 2.2: Indications for primary hip replacement in the UK, 2005 (National Joint Registry for England and Wales, 2006)

Indication (may be more than one)	Incidence (%)
Osteoarthritis	94
Avascular necrosis	3
Dysplasia of the hip	1
Fractured neck of femur	1
Seropositive rheumatoid arthritis	1
Other	4

2.2.2 Hip Joint Failure

The national joint registry for England and Wales (National Joint Registry for England and Wales, 2006) reports on the reasons for approximately 80% of primary hip joint replacement operations in England and Wales. The most common reason necessitating replacement is osteoarthritis, occurring in 94% of all reported cases. Other reasons include rheumatoid arthritis, fracture and avascular necrosis (Table 2.2).

Osteoarthritis is a degenerative disease the prevalence of which increases with age. It results from damage to the hyaline cartilage which can become split and softened, known as fibrillation. The damage to the cartilage leads to its wearing away; in severe cases bone on bone contact will occur when the cartilage has been completely removed. This leads to changes to the structure of the bone; new bone forms around the edges of the joint, these bone formations are known as osteophytes (Duckworth, 1995). Osteoarthritis leads to joint pain and stiffness for the person. Initially lifestyle changes can be suggested as treatment, such as weight loss. The use of analgesia can reduce the pain and discomfort (Kumar and Clark, 1999). In the longer term surgical intervention is necessary. Options

for surgical intervention include (Duckworth, 1995):

Arthroscopic lavage which will clear the joint space of any debris but is a palliative approach which does not address the underlying problem.

Osteotomy whereby the inter-trochanteric region is cut, it will relieve symptoms for a few years, but the mechanism by which it works is not fully understood.

Arthrodesis whereby the joint is fused is extremely successful for removing pain but is debilitating.

Arthroplasty whereby the joint is remodelled; typically in the hip joint a total or part replacement is inserted to prevent fusion of the joint after the procedure.

Patients are increasingly undergoing arthroplasty. Sweden, which has the longest running joint arthroplasty register reports an increasing trend for the past 40 years (Figure 2.1) (Swedish Hip Arthroplasty Register, 2006). Less data is available in the UK however, the UK hospital episode statistics report that in 1999-2000 48,520 hip joint replacements (including revision) were carried out. This increased to 63,418 in 2005-2006 (Office of Population, Censuses and Surveys: Classification of interventions and procedures, 4th Revision (OPCS4) codes W37-W39).

The increasing number of hip joint replacements can be attributed to surgeons implanting into younger (<60) patients (Swedish Hip Arthroplasty Register, 2006), an ageing population and increasing demands from patients for longer, more active lives (Wells *et al.*, 2002), which would preclude arthrodesis.

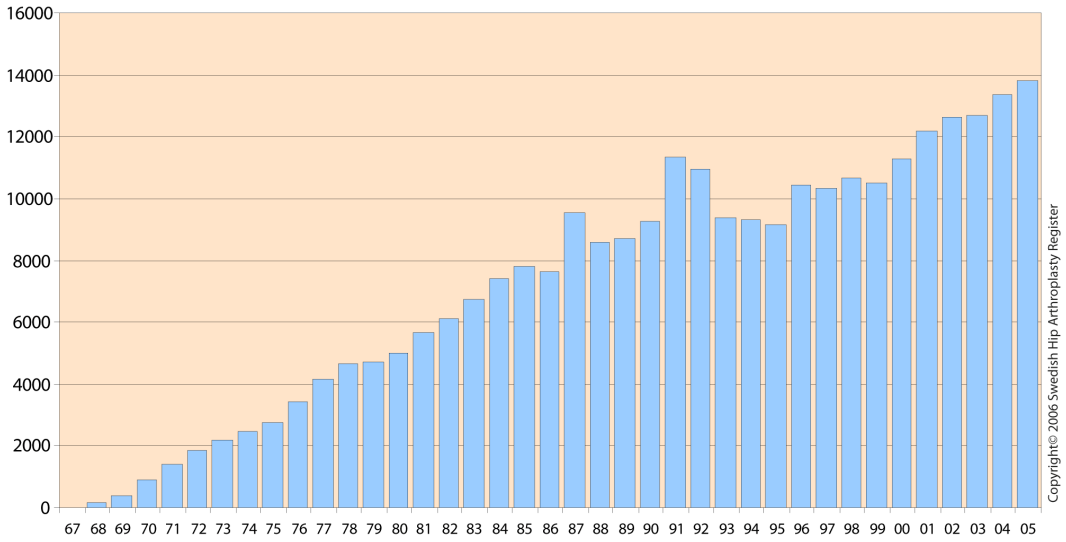

Figure 2.1: Primary THRs performed in Sweden between 1967 (6 operations) and 2005 (13,822 operations) (Swedish Hip Arthroplasty Register, 2006)

2.3 Significant Hip Joint Prostheses through the 1990s

2.3.1 Pre 1940 - Early Hip Joint Prostheses

The first hip joint arthroplasties were not total replacements, but instead partial replacements, they were carried out towards the end of the 19th century. Glück (1891) was one of the first surgeons, utilising an ivory ball prosthesis, to replace the femoral head of a patient.

In 1923 Smith-Petersen removed the articulating surface and replaced it with a mould (Figure 2.2) made of glass however, they broke while they were in the patient. As an alternative to glass Smith-Petersen tried viscaloid however, this produced an excessive foreign body response and so in 1933 a tougher form of

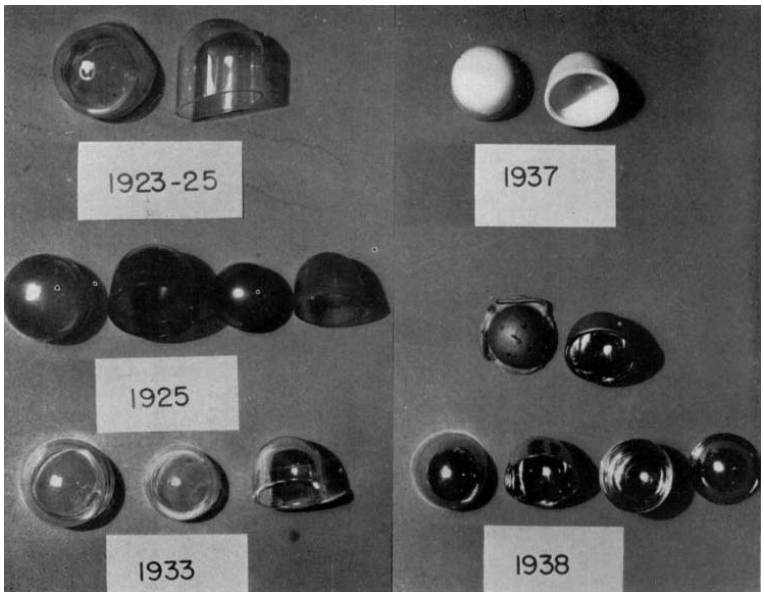

Figure 2.2: Smith-Petersen moulds of glass, viscaloid, pyrex, bakelite and CoCr
(Reproduced with permission and copyright © of the British Editorial Society of Bone and Joint Surgery (Smith-Petersen, 1948))

glass, pyrex, was used; however, these were still not strong enough and some broke in the patient. Later, in 1938, a mould from CoCr alloy known as vitallium was used. These did not break like glass and did not produce the same tissue response that was observed with viscaloid (Smith-Petersen, 1948).

The mould was intended to be temporary while the bone repaired and shaped itself to the cap geometry. This was not always the case, some remaining in place and continuing to function after considerable time; in one case an 86 year old patient received the implant 60 years prior (Anon, 2007). More typically however, within two years of replacement only 45% of cases had an excellent or good outcome (Law, 1962).

In 1939 Wiles implanted the first total joint replacement, it was made from stainless steel; the acetabular cup was screwed into the bone while the femoral compo-

Figure 2.3: X-ray of a hip arthroplasty carried out by Wiles Adapted from (Amstutz and Grigoris, 1996)

nent was attached to the outside of the femur (Figure 2.3). Unfortunately records of this first implant and the further five patients he implanted subsequent devices into were lost in the Second World War. In 1951 only one of the six patients remained alive; the implant had disintegrated (Amstutz and Grigoris, 1996).

2.3.2 1950s - McKee-Farrar Prostheses

In 1951 McKee implanted three prostheses into patients at a hospital in Norwich, UK. Two were of stainless steel and one of CoCr. The steel implants loosened after one year however, the CoCr implant survived three years; consequently further implants that were to be designed by McKee used CoCr (McKee and Watson-Farrar, 1966).

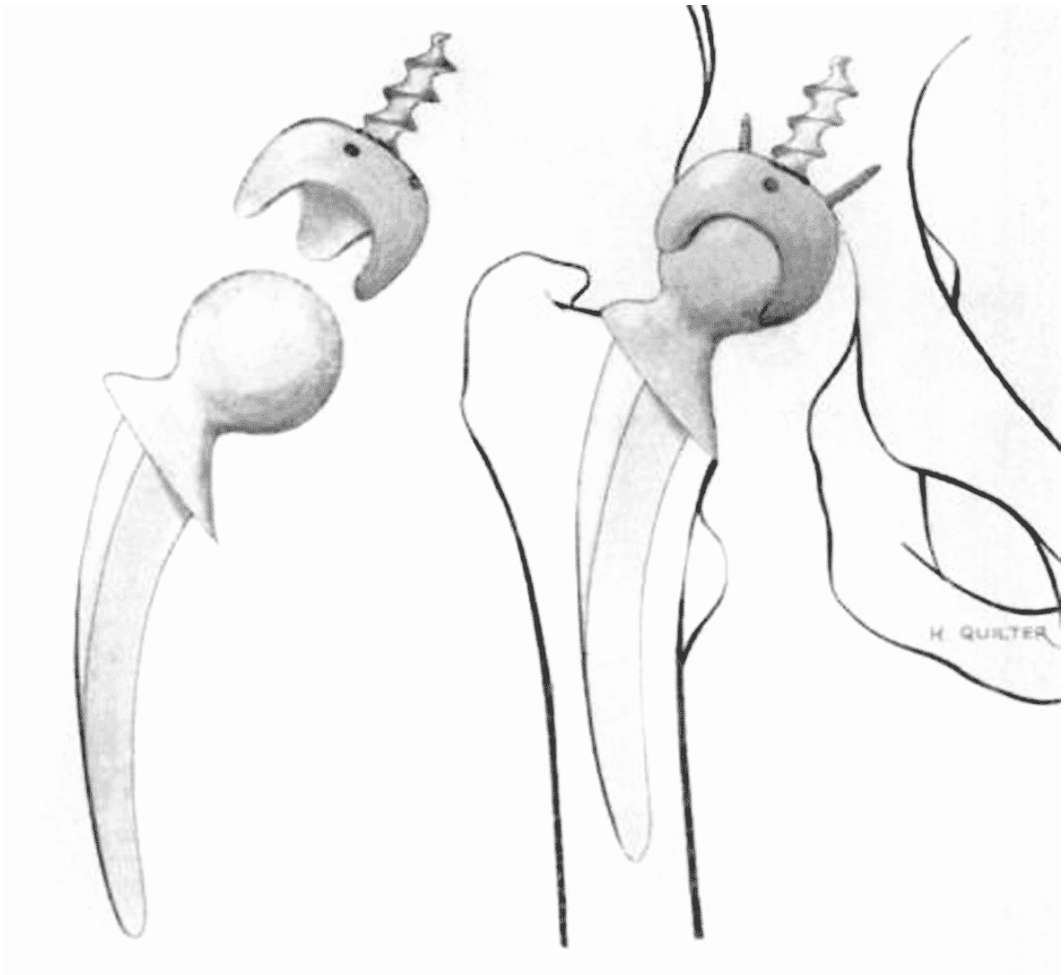

Figure 2.4: McKee prosthesis with a screw fit acetabular and modified Thompson femoral component (McKee and Watson-Farrar, 1966)

As well as material choice, McKee also identified the importance of fixation when he implanted 40 prostheses into patients from 1956 until 1960. These prostheses utilised a Thompson femoral component which he observed being used for partial replacements while he was visiting the USA. McKee modified the Thompson prosthesis to have a smaller head so that it could articulate against the acetabular component which was screwed into the acetabulum (Figure 2.4). This implant gave 51% good to fair results. McKee observed that when one of the components became loose, pain would occur. (McKee and Watson-Farrar, 1966)

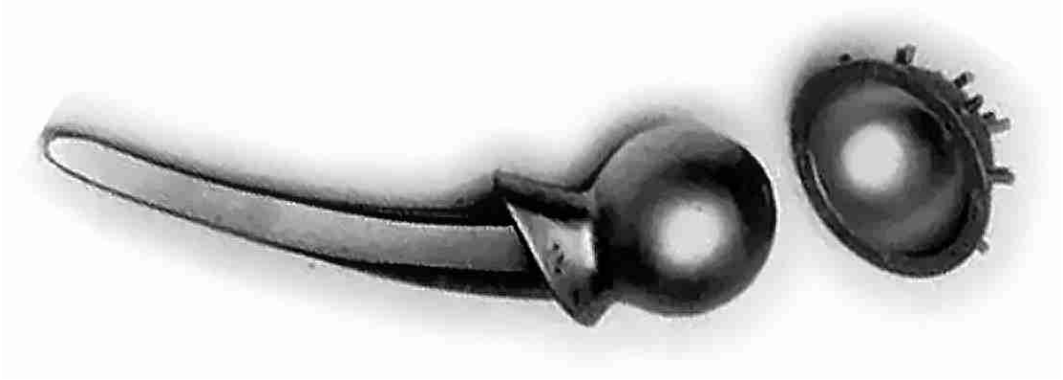

Figure 2.5: Cemented McKee prosthesis Reproduced with permission and copyright © of the British Editorial Society of Bone and Joint Surgery (McKee and Watson-Farrar, 1966)

In 1960 Charnley used polymethylmethacrylate (PMMA) as a bone cement to secure a Thompson femoral component; it occurred to McKee that cement could be used similarly for securing the acetabular component. By 1961 McKee was implanting a redesigned acetabular component which was studded to aid fixation by cement. The studded design of the cup negated the need for a thread so that the acetabular cup could be firmly embedded into the pelvis instead of being screwed into the pelvis, sitting proud and concentrating the load into a small area. A more natural anatomical position was achieved. Embedding the cup also allowed for more room and the cup size to be larger so that a standard Thompson component could be adopted (Figure 2.5) (McKee and Watson-Farrar, 1966).

2.3.3 1960s - Charnley and Ring Prostheses

Charnley implanted his first design in the late 1950s; the prosthesis utilised a polytetrafluoroethylene (PTFE) acetabular cup articulating against a PTFE cap which replaced the surface of the femoral head. The selection of PTFE as the material was to reduce the friction. Charnley was however concerned that the

design would restrict nutrients to the bone remaining in the femoral head. Consequently Charnley started using the stainless steel Moore femoral component which he fixed into the femur using PMMA cement. At the time the Moore component had a femoral head diameter of 42mm, Charnley thought that a smaller head would be better as it would reduce the frictional torque; Charnley reduced the head size to 22.25mm (Waugh, 1990)

Short term results of these implants were promising, although in 1962 Charnley became aware that the particles generated from the joint were causing an adverse tissue reaction. This required revision of the implant and stopped the use of PTFE as an articulating material (Waugh, 1990).

Instead Charnley swapped to high molecular weight polyethylene (HMWP), which is now known as UHMWPE. UHMWPE appeared from simulator testing to produce less wear than PTFE and less of an adverse tissue response. Besides briefly using a press-fit acetabular cup after concerns were raised about fixation of the cup using PMMA; this was to be the implant that Charnley made available for general use in 1970. A few minor design changes have also been incorporated.

The Ring prosthesis, originally used in 1964 was of cementless design (Ring, 1968). Peter Ring did not believe that PMMA was beneficial for long term fixation due to poor adhesion to bone. Instead, a threaded stem similar to that used in McKee's early designs was used to secure the acetabular component into the pelvis. Ring chose to use CoCr for the implants. Concerns were raised in these early designs about the strength of the acetabular stems which could snap (Figure 2.6). In

Figure 2.6: X-ray of a failed Ring prosthesis

1965 the design was modified so that the prosthesis tapered at the joint between cup and thread to increase strength and allow countersinking (Ring, 1968).

A review was carried out by Ring (1974) on his prostheses. This included the original designs and the newer versions. Results between the two show improvement, the older version requiring revision in 14% of 169 cases after five to eight years while the newer version had a revision rate of 2% after five years.

2.3.4 1970s - Ceramic and Exeter Hip Joints

The Exeter hip joint comprises a stainless steel femoral component and a UHMWPE acetabular cup developed in 1969. The development came about as a result of

loosening of the Mckee-Farrar prostheses being implanted at the Princess Elizabeth Orthopaedic Centre in Exeter, UK. Surgeons were concerned that the loosening was caused by friction between the metal components; this concern stopped them from using the Ring prosthesis. The POM alternative developed by Charnley with low friction was a suitable alternative however, surgeons at Exeter were unwilling to use the lateral surgical approach used in the Charnley implant. Instead they wanted to continue using a posterior approach.

The Exeter joint design contained two changes to joints of the time: the removal of a collar on the neck of the implant and a double taper to the stem to aid with cement fixation. The lack of collar on the stem was because designers came to believe that the collar did not offer protection from atrophy of the bone underneath the collar. This was because they had observed resorption of the bone under the collar in Mckee-Farrar prostheses.

At the same time as the Exeter hip was being developed, the ceramic joints were being implanted for the first time. In 1970 Boutin implanted an alumina cup and head into a patient, the alumina head was attached to a titanium alloy stem. This was initially by means of gluing but when this and a screw fix were unsuccessful a taper lock method was developed (Boutin *et al.*, 1988).

Both cemented and uncemented alumina cups were tried and had a survivability of 87.94% and 88.36% respectively at eight years. Of the 560 cemented cups that were implanted three fractured. It was postulated that this was due to either the ceramic microstructure, residual stresses from manufacture or a poor fitting to the

Figure 2.7: Birmingham hip resurfacing joint (Used with permission of Smith and Nephew)

stem. It was found that the careful control of microstructure and residual stresses by manufacturing quality is important to the success of the implant (Boutin *et al.*, 1988), this will be discussed later in section 2.4.1.

2.3.5 1990s - Birmingham Hip Resurfacing Joint

Resurfacing prostheses (Figure 2.7) conserve the bone stock of the patient; instead of using the femoral shaft for support, the femoral neck is used. Bone stock preservation is beneficial, particularly for the younger (<60) patient who may be expected to undergo a number of revision surgeries in their lifetime (Bell *et al.*, 1985).

The implantation of resurfacing joints is not indicated for as wide a group of patients as traditional total joint replacements. Significant stresses are focused on the femoral neck so good bone stock is required for support (McMinn, 2003).

A number of different hip resurfacing joints have been developed including Charnley's first PTFE prosthesis discussed in Section 2.3.3 (Charnley, 1963). Another significant resurfacing joint was the Wagner (Bell *et al.*, 1985). Both of these designs were unsuccessful; the Charnley because of concerns about preservation of bone stock through lack of nutrients (Waugh, 1990) and the Wagner due to loosening of the acetabular component associated with a tissue response to wear particles (Bell *et al.*, 1985).

More recently, in 1991, early trials on the CoCr Birmingham hip resurfacing joint developed and designed by McMinn have been implanted. Initially a pilot study was carried out to examine the effect of fixation methods, three different types were attempted. Press-fit, cement and hydroxyapatite. The press-fit acetabular cup suffered from aseptic loosening in 10% of cases so was stopped. The cemented acetabular cup was also rejected over fears of loosening. McMinn advocated the use of a hydroxyapatite coated cup and a cemented femoral stem (McMinn, 2003). The hydroxyapatite was initially deposited onto a smooth metal cup, the prosthesis being named the McMinn resurfacing joint however, it was further developed to have a porous coating after concerns that adhesion would be a problem after the hydroxyapatite had been absorbed into the bone, this was to become known as the Birmingham hip resurfacing prosthesis (McMinn, 2003).

Early results (between 2-12 year follow up) from this fixation method are good; of 1,503 (1,209 of which were Birmingham hip resurfacings) only one failure occurred as a result of aseptic loosening (McMinn, 2003).

2.4 Current Hip Joint Prostheses

The most commonly implanted cemented and cement-less acetabular cups in the UK in 2006 were the Stryker Howmedica's Contemporary cup (5,734 cases) and Depuy's Pinnacle cup (5,698 cases) respectively, both are UHMWPE components. The most commonly implanted cemented stem was the stainless steel Exeter stem manufactured by Stryker Howmedica (17,743 cases) while the Titanium alloy Corail stem manufactured by Depuy (6,038 cases) was the most commonly implanted cement-less hip (National Joint Registry for England and Wales, 2007).

The Stryker Howmedica's Exeter stem used in combination with its contemporary cup is the most common combination used in the UK, although the stem is also matched with other cups; Stryker Howmedica's Trident cup, Depuy's Elite Plus Ogee cup and Stryker Howmedica's Duration cup, in order of decreasing incidence.

Second to the Exeter combinations is the Depuy Corail stem and pinnacle cup, which is then followed by the Charnley implant.

Hip resurfacing operations are recorded separately however, the CoCr Birmingham hip resurfacing head manufactured by Smith and Nephew accounted for 3,288 operations, 52.1% of the resurfacing heads to be used in the UK.

Individual studies report of the efficacy of these current designs however, an overview of all hip joint replacements indicates that the reason for revision surgery is, in 60% of cases, due to aseptic loosening. This is followed by lysis (21%), pain

(20%) and wear (13%) (National Joint Registry for England and Wales, 2007).

2.4.1 Materials

Currently polyethylene is the only polymer to be used for replacement of the hip joint and only as the acetabular component although polyetheretherketone (PEEK) is currently being investigated for its suitability as a bearing material (Wang *et al.*, 1999a).

Polyethylene can be classified into several subcategories defined by their molecular weight and the degree of cross linking in the polymer chains. UHMWPE has a molecular weight of 2-6$\times 10^6$g/mol and elastic modulus of 0.8-1.6GPa; the yield strength and ultimate strength are 21-28MPa and 39-48MPa respectively. Crystallinity ranges between 39-75% and is dependent on processing conditions as well as environmental conditions and molecular weight (Kurtz, 2004).

Polyethylene is derived from an ethene monomer (CH_2=CH_2) which is polymerised into its high molecular weight form using the Zeigler process (Kurtz, 2004). This process occurs at sub 100°C and in one atmosphere to produce a polymer with low levels of cross linking. The polymerisation process results in a powder form which is moulded or extruded into shape. (Kurtz, 2004).

Cross-linking of the polymer chains of polyethylene has been examined (Grobbelaar *et al.*, 1978; Oonishi *et al.*, 1992). Cross-linking is achieved by free radical formation as a result of irradiation. Early investigations were carried out by Grobbelaar *et al.* (1978); it was established that cross-linking would increase ten-

sile strength and abrasive resistance although doses over 400kGy were noted to cause increased brittleness and increase wear. By introducing cross-linking agents such as acetylene and chlorotrifluoroethylene Grobbelaar *et al.* (1978) were able to reduce the irradiation levels required to cause cross-linking.

Three metals are used in hip joint prostheses; these are stainless steel, cobalt chromium alloys (CoCr) and titanium alloys. The steel used in hip joint replacement is typically a low carbon (0.03%wt), austenitic steel. It contains 17-19%wt chromium, 14-16%wt nickel and 2.3-4.2%wt molybdenum as major constituents, among others when complying with ISO 5832-1 (Technical Committee ISO/TC 150 Subcommittee 1, 1997a); the iron content consists of the balance of material - at least 57.035%wt. It has a modulus of approximately 200GPa (Davis, 2003); this causes concerns of stress shielding. According to Wolff's law, the bone, which will be shielded from the stress will remodel to become weaker. This can lead to loosening of the joint.

The problem is similar with CoCr alloys which have an modulus of approximately 210GPa (Davis, 2003). If specified to ISO 5832-4 (Technical Committee ISO/TC 150 Subcommittee 1, 1997b) CoCr is largely composed of 26.5-30%wt chromium, 4.5-7.0%wt molybdenum and up to 1%wt nickel with at least 58.65%wt cobalt (Technical Committee ISO/TC 150 Subcommittee 1, 1997b). CoCr alloys are either cast or wrought; the microstructure of cast CoCr is coarse dendritic structure with carbides at interdendritic points within the grains having precipitated out during cooling, carbides are also found at the grain boundaries (Chiba *et al.*, 2007). Wrought CoCr has a finer structure with carbides forming mainly at the

grain boundaries with sizes between 1-5μm (Wimmer *et al.*, 2001).

During the cooling of castings, areas of microporosity can form within the structure. A fully dense alloy has superior mechanical properties and so heat treatment processes such as hot isostatic pressing (HIP) can be used to reduce the porosity. The hot forging process of wrought CoCr reduces the microporosity so can also lead to improved mechanical properties (Cawley *et al.*, 2003). However, the heat treatment affects the alloy microstructure and presence of carbides within CoCr. The carbide grains which are 5 times harder than the surrounding metal matrix improve wear resistance of the alloy (Schmidt *et al.*, 1996). Heat treatment reduces the carbide content of the alloy and consequently reduces the wear performance (Cawley *et al.*, 2003).

Titanium alloy has a lower modulus of elasticity, 110GPa (Davis, 2003). When specified to ISO 5832-3 the major constituents are aluminium 5.5-6.75%wt and vanadium 3.5-4.5%wt. Titanium makes up at least 88.105%wt of the alloy (Technical Committee ISO/TC 150 Subcommittee 1, 1996).

Alumina and Zirconia are ceramics used in hip joint replacement. Both are crystalline oxides of Aluminium and Zirconium respectively. Alumina is currently used as the femoral head material in 24.7% of cases in the UK (National Joint Registry for England and Wales, 2007) whereas zirconia only accounts for 0.3%.

These ceramics are hard and have a high Young's modulus however, they are brittle, with a low fracture toughness and low bending strength, their properties can be seen in Table 2.3 (Hamadouche and Sedel, 2000).

Table 2.3: Properties of alumina and zirconia

Property	Alumina	Zirconia
Young's Modulus (GPa)	380	210
Hardness (Vickers)	2,000	1,200
Fracture Toughness K_{IC}	5	7

It is the fracture toughness and bending strength which have caused concerns about ceramics used in joint replacement. Studies have reported fractures (Boutin *et al.*, 1988; Piconi and Maccauro, 1999; Weisse *et al.*, 2003; Habermann *et al.*, 2006) however, control of the microstructure and manufacturing methods can reduce the incidence.

Ceramic components are manufactured from powder usually by hot isostatic pressing. The process heats and places the powder under pressure so that the particles fuse together; reducing porosity, increasing density and making the material more homogeneous. This process is important because the fracture toughness of a ceramic is dependent on the size of defects within the material, the flaws can be reduced in size and quantity by decreasing porosity of the ceramic and having a smaller grain size. Improved homogeneity of the microstructure will increase the toughness of the material (Ostrowski and Rödel, 1999).

International standards attempt to address this; ISO 13356 (Technical Committee ISO/TC 150, Subcommittee 1, 1997) specifies that zirconia should not have a grain size greater than 0.6μm while ISO 6474 (Technical Committee ISO/TC 150, Subcommittee 1, 1994) specifies that alumina should not have a grain size greater than 7.0μm with a standard deviation of less than 3.5μm. Advice from the USA's medical device regulatory authority, the Food and Drug Administration

(FDA), suggests that burst tests on ceramic materials should exceed an average of 46kN with no measurement lower than 20kN (Orthopedic Devices Branch, 1995). Sedel (2000) reports that in the 1970s the burst strength was only 38kN however, it increased to 90kN in 1998.

2.4.2 Biocompatibility

Implanting a foreign material into the body will elicit a response from the body. This will either have a negative impact on the body itself, or on the material which has been implanted. Besides the basic physical properties that a material has, it's selection for implantation into the body is because it elicits a minimal response from the body.

Metals implanted into the body are susceptible to attack from the environment they are placed in. The body fluids around the joint are corrosive to metals, corrosion can occur through a number of mechanisms, such as galvanic and crevice corrosion.

Galvanic corrosion occurs when two different metals are used with differing electro-potentials. The body fluids act as an electrolyte and enable a galvanic current to flow; the metals oxidise, gaining a positive charge and can dissolve into the surrounding electrolyte. This form of corrosion is observed in modular prostheses utilising stainless steel and cobalt alloys (Kummer and Rose, 1983).

Electrochemical corrosion can also occur when only a single metal is present; in this case it is the liquid that provides the electrochemical gradient by way

of differing ion concentrations at one area of the implant compared to another area. This condition normally occurs in crevices where the fluids can stagnate; significant differences in ion concentration can develop. This environment can be found between the femoral stem and head in modular implants. Kummer and Rose (1983) studied the potential for galvanic corrosion of CoCr and titanium alloy and established that there would be no significant problem with the use of these two alloys; however, the study failed to take into consideration the effect of crevice corrosion. It was later found that the galvanic potential between the two materials accelerated crevice corrosion at the interface between femoral stem and head (Collier *et al.*, 1992).

Ultimately corrosion of the materials placed in the body, will result in failure of the joint, although this only accounts for a small proportion of all revision surgeries, if any; the National Joint Registry for England and Wales (2007) reports "other" causes for revision to be 5% of cases. Of more importance is the effect of materials on the body, this can lead to osteolysis and aseptic loosening, which account for 21% and 60% of all revision operations respectively. Concern has not been raised about the effect of a bulk implant material on the body, concern has arisen over the production of wear products from the bulk implant.

Of the materials currently in use in hip joint prostheses, UHMWPE is noted for having the highest wear rate; $56.4mm^3/10^6$ cycles reported by Saikko *et al.* (2001b) when articulating against CoCr in a hip joint simulator. The debris produced can cause a soft tissue response and osteolysis. Osteolysis is a result of macrophages responding to the presence of wear particles. Macrophages attempt

to phagocytose the wear particles by releasing cytokines and triggering other cells to respond which lead to inflammation and bone resorption (Green *et al.*, 1998). The quantity and size of particles determine the macrophage response and subsequent level of osteolysis. Particles in the range of 0.3-10μm have been found to be the most active (Green *et al.*, 1998).

There is also concern about the effect of metallic wear particles in the body; unlike polyethylene particles which are within the micrometre size range, metal particles can be nano-sized (Doorn *et al.*, 1998). Particles of this size have the potential to disperse throughout the body and not just remain in the joint space. Wear debris has led to increased metal levels in urine and blood (Coleman *et al.*, 1973) as well as the liver, spleen and lymph nodes (Langkamer *et al.*, 1992). It has been reported that the metal wear particles are a cause of chromosomal damage (Daley *et al.*, 2004), which could potentially cause cancer. Studies generally show an increased risk of cancer in hip joint replacement patients (Gillespie *et al.*, 1988; Nyren *et al.*, 1995; Visuri *et al.*, 1996) however, the evidence is not sufficient to demonstrate the cause.

2.4.3 Tribology

The wear of hip joint prostheses is dependent on the interface between the femoral head and acetabular cup. This section reviews the factors which affect the wear and methods by which the wear can be reduced.

The materials used for the femoral head and acetabular cup have a significant

effect on the wear rate; other factors will have an effect, but not so profound. Studies have been carried out extensively on the effect of wear with various different material combinations. This can be either be in-vitro simulated testing, which is discussed later, or from in-vivo data obtained from x-rays or explanted implants.

Typically POM replacements such as the Charnley and Exeter hips wear the most; followed by MOM and then ceramic on ceramic (COC). Hall *et al.* (1996) retrieved and analysed the UHMWPE acetabular cups of 129 Charnley implants; an average wear factor of 2.1×10^{-15}m^3/Nm was recorded with linear penetration equating to 0.2mm/year and wear volumes of 55mm^3/year over a median implant life of 10.7 years (range 0.75-22). These results are comparable with data from others, including Kabo *et al.* (1993); Livermore *et al.* (1990); Hall *et al.* (1998). The study by Kabo *et al.* (1993) examined 60 polyethylene acetabular components, 40 from conventional replacement and 20 from surface replacement. Differing head sizes were examined; sizes of 22mm, 26mm, 28mm and 32mm from conventional hip replacement recorded linear wear rates of 0.127, 0.229, 0.234 and 0.214mm/year respectively. There is an increasing trend of linear wear with increasing head size and corresponding wear volume, although sample sizes are low. The larger study by Hall *et al.* (1998) did not confirm this correlation, showing no significant difference in linear wear with increasing femoral head size. Hall *et al.* (1998) did observe increasing volumetric wear with increasing head size. They reported that femoral head sizes of 11, 14.3, 16 and 19mm exhibited wear rates of 52, 62, 89, 137mm^3/year respectively.

Smaller head sizes were proposed by Charnley (1970) as a method of reducing frictional torque which is directly proportional to the femoral head size as can be seen in Equation 2.1 (μ=friction coefficient, r=radius, L=load and τ=torque)

$$\tau = rL\mu \tag{2.1}$$

It was thought that high torque would lead to loosening of the prosthesis however, Hall *et al.* (1997) have since presented evidence that indicates torque is unlikely to have a significant effect on loosening. Smaller head sizes also have the benefit of enabling a thicker acetabular cup which can accommodate more linear wear without wearing through. In light of the soft tissue response to UHMWPE debris, the case for smaller head sizes to reduce wear is persuasive.

Metal on metal implants wear less than UHMWPE; Sieber *et al.* (1998) recorded linear wear rates in 115 28mm CoCr implants and 3 32mm diameter CoCr implants implanted for an mean time of 22 months (range 2-98), by measuring the retrieved implants dimensions and comparing them to an ideal sphere. Linear wear rates were observed to be between 20 and 80μm/year for five "moderately" worn components however the majority had linear wear rates of less than 20μm/year. The wear rates were high for the first year - 25μm/year, dropping to 5μm/year after three years. These wear rates are similar to those observed by Schmidt *et al.* (1996) who recorded linear wear rates of 13 Mckee-Farrar acetabular cups to be 4.9μm/year after an average implantation time of 16.3 years; linear wear of 17 Mckee-Farrar femoral heads was also recorded as 6.6μm/year after an average

14.5 years of implantation.

Conversely to POM implants, larger femoral head sizes in MOM implants lead to reduced wear (Smith *et al.*, 2001). This is because of the lubricating regime; it is possible for MOM joints to achieve full fluid film lubrication whereby the lubricating fluid fully separates the asperities of the two components.

To achieve fluid film lubrication, there must be sufficient separation between the two components. The separation required is dependent on the surface roughness of the material. Johnson *et al.* (1972) expanded on the Greenwood and Williamson theory of contact between random rough surfaces (Greenwood and Williamson, 1966) to establish that fluid film lubrication occurs when the ratio of film thickness to the standard deviation of asperities about their mean line is greater than 3. The rough surfaces of UHMWPE (Technical Committee ISO/TC 150, Subcommittee 4 (1996) requires an R_a of less than 2μm and so would require a thick film before fluid film lubrication could occur. Metal implants however have a smoother surface, the ISO standard requiring a R_a values of less than 0.05μm, therefore a fluid film can develop with a thinner lubricating film.

The film thickness achieved in a joint is dependent on the fluid viscosity, entraining velocity and load. Design of the implant cannot control the viscosity or load, but the entraining velocity will increase with larger head diameters. Unsworth (2006) reports that the MOM Birmingham Hip Resurfacing joints are able to achieve the necessary film thickness for fluid film lubrication.

Measuring in-vivo wear in retrieved ceramic on ceramic joints can be difficult

because the low levels of wear introduce large errors when measuring the deviation from an assumed perfect sphere for the calculations (Boutin *et al.*, 1988). Mahoney and Dimon (1990) have reported linear wear rates of 10μm/year from the femoral component, which when combined with the wear of the acetabular total 19μm/year. These values however are greater than those reported by Mittelmeier and Heisel (1992) who obtained linear wear measurements of 2.6μm/year for the femoral head and totalling 8.0μm/year when combined with wear from the acetabular component over 16 years. These values are considerably lower than metal on metal implants.

2.5 Hip Joint Coatings

The development of hip joint prostheses, the materials that are currently used and the problems associated with them have been reviewed. It has been identified that the main causes of failure are aseptic loosening and osteolysis; these causes have been linked with the generation of wear particles. It has also been shown that metals and polyethylene joints continue to be the most popular, despite polyethylene being the largest wear producing material and the potential risks of metal ion production. A reduction in wear particle generation should be expected to reduce the incidence of failure of hip joint prostheses.

Surface modification of these materials has been tried in hip joint prostheses to reduce wear (Taeger *et al.*, 2003; Joyce, 2007; Harman *et al.*, 1997; Raimondi and Pietrabissa, 2000) after having been used successfully in other industries

requiring good wear performance, such as aerospace (Voevodin *et al.*, 1999), electronics (Robertson, 2001) and in non-wearing medical applications such as stents (Hauert, 2004).

Two surface coatings have been applied to the femoral acetabular interface and implanted into patients, these are titanium nitride (TiN) and diamond-like carbon (DLC) coatings. TiN has seen the more extensive in-vivo use, and is manufactured and marketed by Endotec, USA. Results on TiN in-vivo performance have been published by Raimondi and Pietrabissa (2000) reporting delamination of the coating from a titanium substrate articulating against UHMWPE. Harman *et al.* (1997) also observed delamination caused by the presence of voids in the coating when large coating droplets were removed during a post-coating polishing process.

In-vivo results of DLC coatings have not been reported on so extensively and the author could not find any company marketing their use. Taeger *et al.* (2003) reports on the delamination of DLC coated hip prostheses while Hauert (2003) refers to 190 implanted knee implants showing increased wear and delamination however, little detail is given. Joyce (2007) has also recently reported on a retrieved DLC coated great toe implant, this exhibiting signs of delamination.

2.5.1 Diamond-like and Amorphous Carbons

The deposition of the first diamond-like carbon coatings can be credited to Aisenberg and Chabot (1971). They coined the term diamond-like carbon because of

the similarities with diamond that they observed: transparency, similar index of refraction, insulating, high hardness, resistant to acid, partially crystalline with a lattice similar to diamond and a similar dielectric constant. Since their study additional deposition methods have been developed and the coatings that are deposited vary widely in both properties and structure.

As a result the term DLC has become ambiguous. The DLC described by Aisenberg and Chabot (1971) has a high sp^3 content which formed microcrystalline structures within the amorphous structure. Coatings developed following Aisenberg and Chabot (1971) can be more amorphous with less sp^3 content, others retaining high sp^3 content but with little to no crystalline structure (tetrahedral amorphous carbons, ta-C). Confusion arises in the literature because the point at which a coating is no longer diamond-like is not defined. The term is also complicated by the inclusion of varying amounts of hydrogen in some coatings - hydrogenated amorphous coatings, these can be even less diamond-like.

Structurally DLC's contain sp^3 and sp^2 bonding; these are two of the three hybridisations of carbon. With sp^3 bonding, all four of the valance electrons are located in a hybrid orbital. They all form covalent σ bonds in a tetrahedral arrangement, the bonding which is seen in diamond. The sp^2 hybridisation of carbon has only 3 of the four valance electrons located in a hybrid orbital and able to form 3 σ bonds. The forth electron lies in a p orbital and is only able to form a weaker covalent π bond. This is typically seen in graphite.

The sp^2/sp^3 ratio of amorphous carbon coatings is the strongest single influence

on the physical properties, a higher sp^3 fraction increasing hardness and elastic modulus. The exact mechanism by which sp^3 bonds form is not currently known, although the basic principle of subplantation, initially proposed by Lifshitz *et al.* (1990) has generally been accepted through mathematical modelling (Kaukonen and Nieminen, 2000; Kohary and Kugler, 2001). As carbon ions bombard the coating surface during deposition, they penetrate into the coating where they cause densification and can form sp^3 bonds (Lifshitz *et al.*, 1990). The energy of the ions determines the fraction of sp^3 formation. Ion energies of around 140eV have been shown to be the most efficient for producing a high sp^3 fraction (Fallon *et al.*, 1993).

Modification of the sp^3 content may address the physical properties of a coating and therefore the tribological properties that are required for hip joint prostheses but it does not address the problem that has been observed with implanted coatings: delamination.

Delamination of a coating occurs when the forces applied to the coating exceeds the strength of adhesion between the coating and substrate (Wang *et al.*, 1991). In addition to any external forces which may be applied, amorphous carbon coatings have intrinsic stresses which can limit their adhesive strength resulting from their deposition by stressing the interface between the coating and substrate. The reduction of these stresses can improve the adhesive strength of a coating (Wang *et al.*, 1991). Intrinsic stresses are linked to the energy with which ions bombard the coating surface during deposition; greater energy will lead to larger intrinsic stresses (Knotek *et al.*, 1991; Donnet and Erdemir, 2008; Davis, 1993;

Windischmann, 1992)

Introduction of metal interlayers, between the coating and substrate reduce the residual stresses and improves the adhesion of coatings (Holmberg *et al.*, 2000; Chen and Hong, 2005). Multilayers reduce the stresses further (Zhang *et al.*, 2005b; Sheeja *et al.*, 2003), or gradient transitions across the coatings so as to prevent distinct boundaries which provide a route for crack propagation (Lyubimov *et al.*, 1992).

2.5.2 Titanium Nitride

TiN is a transition metal nitride ceramic that can be deposited onto materials to give a hard, corrosion resistant layer with good wear properties. The properties of the coating are dependent on the microstructure, stoichiometry and thickness.

TiN typically has a microstructure of columnar grains. When deposited using chemical vapour deposition (CVD) techniques these columns grow in a common, preferred direction (Echigoya *et al.*, 1991); physical vapour deposition (PVD) techniques result in columnar orientation in the direction of coating growth (Burnett and Rickerby, 1988). Orientation of the grains affect the coating properties (Yeh *et al.*, 2008; Azushima *et al.*, 2008; Abadias, 2008).

Throughout the deposition processes it is possible to control the ratio of Ti:N to form a TiN_{χ} coating. Variation in this stoichiometry alters the hardness of the coating (Stanislav *et al.*, 1990), numerous studies have been carried out investigating this with varying results, most probably due to the variation in coat-

ing parameters and conditions (O'Hern *et al.*, 1989; Arnell *et al.*, 1996; Chevallier and Chabert, 1981). Arnell *et al.* (1996) report that the hardest coating is achieved when χ has a value of 0.9, these achieved microhardness values up to 4,000kgf/mm^2 (39GPa) while Chevallier and Chabert (1981) reported that when χ has a value of 0.7, microhardness ranged from 3,500-4,000kgf/mm^2 (34-39GPa).

The thickness of TiN coatings is not constrained by the residual stresses in the same way as DLC coatings. TiN also has residual stress in the GPa's however, they can achieve much thicker coatings as the stresses decrease in thicker coatings (Chou *et al.*, 2002; Machunze and Janssen, 2008). As with DLC coatings their structure can also be modified with multilayers and interlayers to reduce the internal stresses (Huang *et al.*, 2006).

TiN is currently applied to hip joint prostheses and is used in other applications such as machine tooling that requires a very hard coating. Initial TiN coatings that were applied to hip prostheses were susceptible to delamination and failure, raising fears for all coatings and slowing progress in the area (Harman *et al.*, 1997; Raimondi and Pietrabissa, 2000).

The paper by Raimondi and Pietrabissa (2000) is one of the few retrieval studies on TiN coated hip joints. It shows that there are a number of wear mechanisms that the coatings undergo which lead to failure. Fretting was observed in two of the four explanted joints and scratching and surface roughening indicated that the coating was susceptible to third body wear. The hard wear particles that are produced from TiN will also exacerbate wear of UHMWPE counter-faces (Onate

et al., 2001; Batista *et al.*, 2002; Zu *et al.*, 2001; Dobrzanski *et al.*, 2001). Onate *et al.* (2001) showed that after five million cycles of in vitro testing in a knee simulator, the UHMWPE debris produced with a TiN coating was 3.531mg, in comparison to 0.690mg for a similar uncoated joint and 0.150mg for a DLC coated joint.

Harman *et al.* (1997) reports that in the case of joints manufactured by Endotec, the coating contained a nonuniform droplet size. The larger droplets formed asperities which increased the roughness, could scratch the counter-face and were exposed to high contact pressures causing them to become dislodged. The dislodged particles were free to move around in the bearing and exacerbated wear. A more controlled deposition would improve the coating in this case.

Although the poor adhesion, lack of resilience to third body wear and effect of coating debris on the counter-face wear has caused research to look towards alternative coatings, TiN continues to be the main hip joint coating solution available on the market.

2.5.3 Sputter Deposition of Coatings

Coatings can be deposited by two main methods: CVD and PVD, within these methods there are a variety of different techniques This study will focus on a specific PVD method known as sputtering.

As implied by the names, PVD is a process whereby the coating is deposited using physical methods; particles are physically removed from a source and transported

to the substrate to be coated. CVD methods use chemical methods to transport the coating particles.

The CVD process was first documented in 1897 by de Lodyguine who patented a method of depositing tungsten on carbon filaments (Lodyguine, 1897). CVD deposition can be generalised as a process by which a precursor gas undergoes chemical deposition on the substrate to deposit the atoms which comprise the intended coating. The chemicals involved in the CVD processes can be toxic and temperatures involved can cause problems for the substrate. In the case of TiN deposition, $TiCl_4$ is used and temperatures reaching 1,000°C can be obtained (Eskildsen *et al.*, 1999). If the coating is being applied to steel, the benefits of any thermal treatment applied to the substrate prior to coating could be negated (Eskildsen *et al.*, 1999).

A PVD process was first described by Edison (1884), this has become known as cathodic arc deposition. Cathodic arc deposition focuses a high current, low voltage beam on a tightly confined spot on the target - the source material for the coating. The energy density within this spot leads to rapid evaporation and ejection of material from the target. The ejected material can spread throughout an evacuated chamber and deposit on any exposed surfaces.

Sputtering is a technique, whereby atoms are ejected from a source material as they are bombarded by an inert gas plasma (Sigmund, 1969). At its most basic, this can involve a single target cathode contained within an anode chamber. The introduction of a gas and a potential difference between the anode and cathode

will cause the formation of a plasma. The ions within the plasma will be accelerated towards the cathode and bombard its surface. Provided this bombardment imparts sufficient energy into the surface atoms, they will break free from the surface and spread throughout the deposition chamber and deposit onto any exposed surfaces (Kelly and Arnell, 2000). The collisions of the gas on the target also lead to the production of secondary electrons; the electrons can ionise further gas particles and therefore feed and sustain the process (Stallard, 2005; Kelly and Arnell, 2000).

This basic method is limited and not particularly efficient. It will only function when the target material is conductive, the deposition rates are slow and plasma ionisation efficiency is poor (Kelly and Arnell, 2000). Magnetron sputtering allows the sputtering of any material, even if non-conductive; it can also improve deposition rates and ionisation efficiency. The magnetrons are placed behind the target and a radio frequency field used to enable the plasma to form. The magnetic fields from the magnetrons can be configured to constrain the secondary electrons so that they remain close to the target and therefore improve ionisation efficiency which will lead to increased bombardment of the target and greater sputter rates (Kelly and Arnell, 2000). Further improvements can be made by closing the magnetic field to prevent ions escaping the field which will increase plasma density (Teer, 1991).

The use of unbalanced magnetrons has been investigated by Window and Savvides (1986). Window and Savvides (1986) established that by modifying the magnetic field with unbalanced magnetrons the substrate being coated could be bombarded

with ions from the plasma. This bombardment modifies the surface and alters the coating as it is being deposited. The coating nucleation, morphology, composition and crystallinity are all altered which can lead to harder, more wear resistant coatings (Window and Savvides, 1986).

Introduction of a reactive gas to the plasma can further increase the range of coatings that can be deposited to compounds including oxides, nitrides and carbides (Safi, 2000). By this method, a titanium target with nitrogen reactive gas can deposit a TiN coating.

2.6 Summary

Artificial replacement of all or part of the hip joint has been carried out since the late 19th Century. Since the first implant, problems have been identified which lead to the failure of the replacement, necessitating a further revision operation in most cases.

Today the largest cause of prosthesis failure is aseptic loosening which is commonly attributed to excessive wear of the implants materials, particularly UHMWPE. Surface coatings can be applied to the prostheses to reduce the wear. TiN and DLC coatings have been used previously, although not extensively. In the few reports that are available on their clinical performance coating adhesion is a problem.

DLC coatings can be extensively modified with dopants or with transition layers

to improve their wear and adhesion, this capability has resulted in their extensive use in other industries such as the tooling and semiconductors; their use has not been fully exploited in the orthopaedic industry.

3. Coating Deposition

3.1 Introduction

The deposition of coatings onto CoCr and UHMWPE substrates is described within this chapter. A total of six different coatings were deposited using a PVD technique. Five were deposited onto CoCr substrates, while one was deposited onto UHMWPE substrates. In addition some of the UHMWPE substrates were ion implanted with nitrogen ions prior to coating deposition.

The interface between a DLC coating and UHMWPE will have a large hardness difference. Under the loads experienced in a hip joint, up to five times body weight (Bergmann *et al.*, 2001; Rydell, 1966; Paul, 1967), the UHMWPE will compress and deform which will cause high stresses to be exerted on the coating. It is likely that the coating will fail because it will be unable to deform with the substrate. By altering the hardness of the UHMWPE and coating so that a smooth transition from the soft UHMWPE to hard coating is achieved the stress concentration can be reduced and improve the coating's adhesive properties. Although the hardness of DLC coatings can be modified and range between 7-65GPa (Donnet and Erdemir, 2008), this are significantly harder than UHMWPE which has a hardness of 0.26GPa (shown later in Table 4.3), in order to obtain a similar hardness between coating and UHMWPE it is necessary to increase the hardness of the UHMWPE. This can be achieved by ion implantation, which is a surface modification technique that can be used to modify surface properties, including hardness, of a material such as UHMWPE.

Ions are accelerated towards UHMWPE, they penetrate the surface and impart energy to the material by momentum transfer until they come to rest. The energy imparted to the atoms can break bonds, ionise and scatter other atoms. As the scattered atoms move through the substrate in a similar fashion to the original ions they further modify the structure as they disrupt surrounding atoms. With more energy, the bombarding ions are able to penetrate deeper into the substrate causing additional disruption. The depth that they penetrate and the effect they have on the UHMWPE is dependent on the ion mass and the energy.

Ion implantation of medical implants has been investigated. The implantation can harden the surface and potentially reduce the wear. Nitrogen implantation has been studied on metallic substrates including titanium alloys (Torregrosa *et al.*, 1995); CoCr (Onate *et al.*, 2001; Bowsher *et al.*, 2004) and polymeric substrates used in hip joints (Shi *et al.*, 2001).

Ion implantation for MOM joints should not be viewed as particularly beneficial. Run in wear of these joints is high and can remove 25μm in the first year (Sieber *et al.*, 1998). Using stopping and range of ions in matter (SRIM) (Ziegler *et al.*, 2008), a software package which uses the projected range algorithm developed by J. P. Biersack (Ziegler *et al.*, 1985) it can be found that an ion energy of approximately 400MeV would be required to achieve a depth of 25μm in CoCr with nitrogen. Bowsher *et al.* (2004) demonstrate this problem with a hip simulator study of ion implanted CoCr MOM joints with the 0.2μm implantation depth being removed early on in the simulation.

Ion implantation into UHMWPE is likely to have a more noticeable improvement on wear of implants, their high levels of wear could be reduced. The low density of polyethylene also means that the ion implantation energy does not have to be as high to achieve micron depths in the substrate, 325KeV will achieve a depth of 1.06μm (Appendix A). Studies into ion implantation of UHMWPE have shown that the ion bombardment leads to increased cross-linking and forms a diamond-like surface layer (Marcondes *et al.*, 2004).

3.2 Ion Implantation of UHMWPE Components

For this study UHMWPE was ion implanted with nitrogen using the Danfysik machine at the University of Surrey (2007). Ions were accelerated away from the cold penning ion source to an analysing magnet which filtered unwanted elements and isotopes. A further accelerator increased the beam energy to it's final energy before passing through focusing quadrupole magnets and a scanning magnet which enabled the beam to be scanned across the surface of the UHMWPE target (Figure 3.1).

Two groups of UHMWPE samples were ion implanted, the first group was unmodified and implanted with a beam energy of 15KeV. The second group had been pre-coated with a 40nm layer of chromium using the closed field unbalanced magnetron sputter ion plating (CFUMSIP) method developed by Teer Coatings Ltd. (2007) and described later in Section 3.3; with these precoated samples a beam energy of 45KeV was used to account for the layer of chromium. The

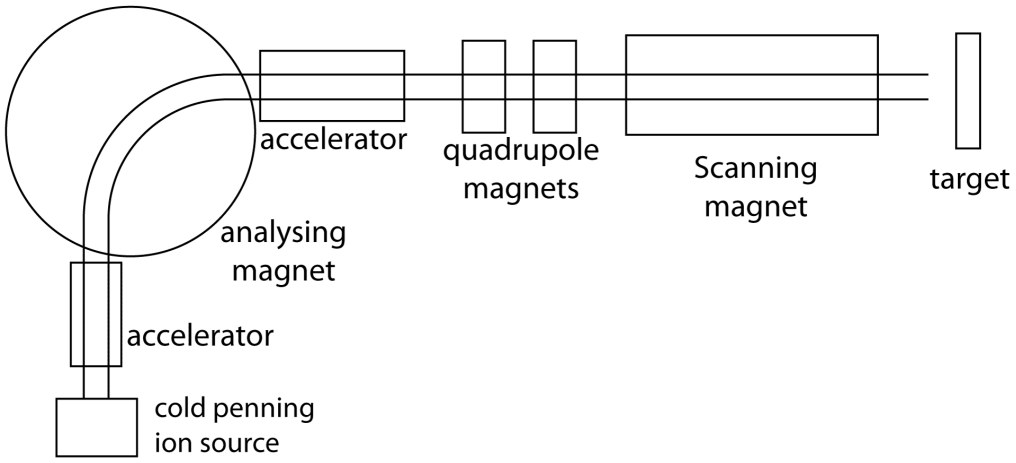

Figure 3.1: Schematic of Danfysik ion implanter

40nm layer was confirmed using scanning electron microscopy (SEM) (Figure 3.2). Two different doses were used for the two groups of UHMWPE, these were 1×10^{15}particles/cm^2 and 5×10^{15}particles/cm^2.

Consequently the following five conditions of UHMWPE were produced for testing

1. Unmodified UHMWPE
2. Nitrogen implanted UHMWPE at 15KeV with a dose of 1×10^{15}particles/cm^2
3. Nitrogen implanted UHMWPE at 15KeV with a dose of 5×10^{15}particles/cm^2
4. Precoated (with chromium) UHMWPE, nitrogen ion implanted at 45KeV with a dose of 1×10^{15}particles/cm^2
5. Precoated (with chromium) UHMWPE nitrogen ion implanted at 45KeV with a dose of 5×10^{15}particles/cm^2

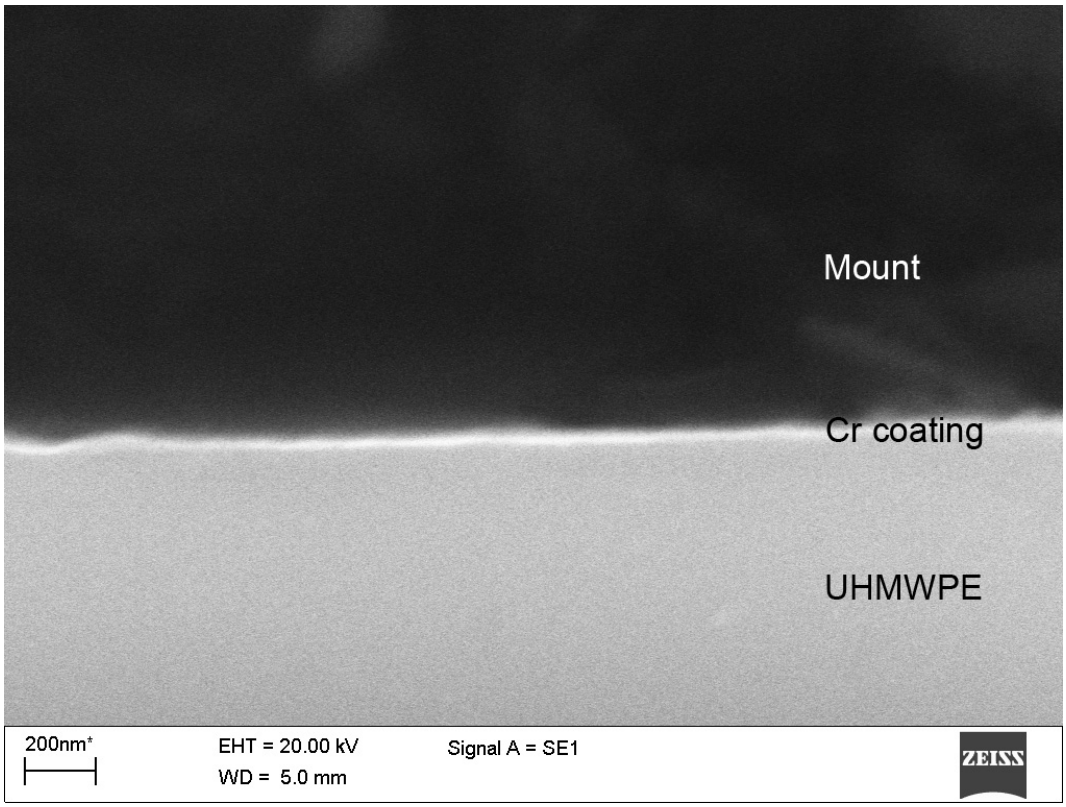

Figure 3.2: SEM of Cr layer deposited onto UHMWPE prior to ion implantation

3.3 Coating Deposition

Coatings used in this study were deposited using the UDP-650-FOD at Teer Coatings Ltd. (2007), this is a CFUMSIP process (Figure 3.3). The device consists of a front opening door with four magnetron targets equally spaced around the outside, the targets are made from materials that will be deposited into the coating, but for this study, the rear target was chromium, with the two side targets being carbon and the front target made from CoCr. The centre of the chamber contains the sample holder which rotates at five revolutions per minute throughout the coating cycle and is held at a negative bias relative to the chamber so that ions accelerate towards the sample holder. A cross section of the machine can be seen in Figure 3.3.

The coatings that were deposited are derived from the Graphit-iC^{TM} coating developed by Teer Coatings Ltd. (Teer *et al.*, 2004). The Graphit-iC^{TM} coating has been studied extensively (Yang *et al.*, 2000; Teer *et al.*, 2004; Teer, 2001; Coldwell *et al.*, 2004; Stallard *et al.*, 2004; Stallard, 2005; Camino *et al.*, 1999); Stallard *et al.* (2004) reports low wear factors of 4.5×10^{-18}m^3/Nm and critical scratch loads of 98N. It is thought that the coating has the potential to perform similarly in the orthopaedic field.

The Graphit-iC^{TM} coating comprises a chromium layer, between 50 and 200nm thick, deposited directly onto the substrate, with a bias of 120V. When the chromium layer is approximately 50nm and the process has been running for 2,160 seconds the bias is immediately dropped to 60V, for the following 1,800

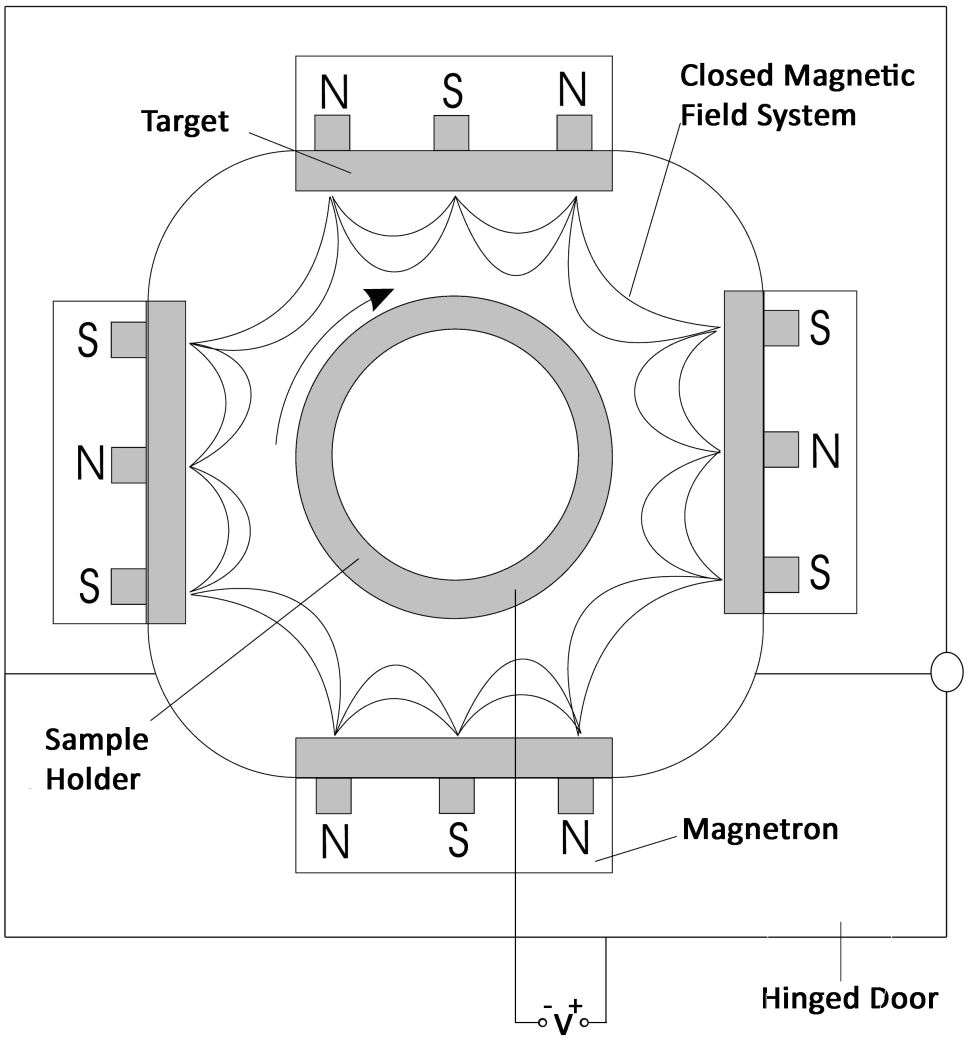

Figure 3.3: Cross section of Teer Coating's closed field unbalanced magnetron sputtering chamber

Figure 3.4: Idealised representation of a graduated Graphit-iC^{TM} coating

seconds the current to the chromium magnetron is decreased and current to the carbon magnetron is increased. This creates a graduated coating so that by the time the process is finished the surface of the coating comprises mostly of carbon, illustrated in Figure 3.4. Parameters of this coating along with all the others deposited can be seen in Tables 3.1 - 3.6.

Table 3.1: Deposition parameters of Coating 1: 40V bias

		Magnetron Current (A)				
Time (s)	Cycle description	Chromium	Carbon	Chromium	Carbon	Substrate Bias Voltage (V)
1800	ion clean	0.4	0.3	0.4	0.3	400
360	Cr layer	4	0	0	0	120
1800	Ramp	4→0.25	0→3.5	0	0→3.5	40
18000	GiC	0.25	3.5	0	3.5	40

Table 3.2: Deposition parameters of Coating 2: Graphit-iC™

		Magnetron Current (A)				
Time (s)	Cycle description	Chromium	Carbon	Chromium	Carbon	Substrate Bias Voltage (V)
1800	ion clean	0.4	0.3	0.4	0.3	400
360	Cr layer	4	0	0	0	120
1800	Ramp	4→0.25	0→3.5	0	0→3.5	60
18000	GiC	0.25	3.5	0	3.5	60

Table 3.3: Deposition parameters of Coating 3: 80V bias

		Magnetron Current (A)				
Time (s)	Cycle description	Chromium	Carbon	Chromium	Carbon	Substrate Bias Voltage (V)
1800	ion clean	0.4	0.3	0.4	0.3	400
360	Cr layer	4	0	0	0	120
1800	Ramp	4→0.25	0→3.5	0	0→3.5	80
18000	GiC	0.25	3.5	0	3.5	80

Table 3.4: Deposition parameters of Coating 4: 60 to 40V transition bias

		Magnetron Current (A)				
Time (s)	Cycle description	Chromium	Carbon	Chromium	Carbon	Substrate Bias Voltage (V)
1800	ion clean	0.4	0.3	0.4	0.3	400
360	Cr layer	4	0	0	0	120
1800	Ramp	4→0.25	0→3.5	0	0→3.5	60
300	GiC	0.25	3.5	0	3.5	60
17700	GiC	0.25	3.5	0	3.5	60→40

Table 3.5: Deposition parameters of Coating 5: CoCr interlayer

		Magnetron Current (A)				
Time (s)	Cycle description	Chromium	Carbon	Cobalt Chromium	Carbon	Substrate Bias Voltage (V)
1800	ion clean	0.4	0.3	0.4	0.3	400
420	CoCr layer	0	0	4	0	120
60	CoCr layer	0	0	4	0	120→60
60	CoCr layer	0	0	4	0	60
60	CoCr→Cr	0→4	0	4→0	0	60
120	Cr	4	0	0	0	60
1800	Ramp	4→0.25	0→3.5	0	0→0.35	60
18000	GiC	0.25	3.5	0	3.5	60

Table 3.6: Deposition parameters of Coating 6: Graphit-iC^{TM} deposited onto UHMWPE Samples A-E

		Magnetron Current (A)				
Time (s)	Cycle description	Chromium	Carbon	Chromium	Carbon	Substrate Bias Voltage (V)
400	ion clean	0.2	0.1	0.2	0.1	300
900	Cr layer	2	0	0	0	80→45
3600	Ramp	2→0.15	0→2.1	0	0→2.1	45
23400	GiC	0.15	2.1	0	2.1	45

Varying the substrate bias alters coating nucleation, morphology and crystallinity; increasing the bias will create a harder coating with greater sp^3 content. Zhang *et al.* (2000) reports coatings of this nature to have an sp^3 content of less than 0.5%. Provided that the samples are position in the chamber so that as they are rotated around they each face all the magnetrons for the same period of time and from the same distance, they can be considered similar. Subsequent coating depositions are also highly reproducible, provided the samples are loaded into the chamber similarly and the deposition parameters are maintained (Field, 2009).

Coatings 1-5 were each deposited onto a CoCr pin and 5 CoCr discs. The sixth coating (Table 3.6) was deposited onto the UHMWPE substrates, which had been ion implanted with nitrogen (Section 3.2). Deposition onto the UHMWPE was run for 6.5 hours instead of the 5 used for depositing onto CoCr, this was because the magnetrons were run at a lower power so that the temperature generated in the coating chamber, which is normally approximately 200°C, would not damage the UHMWPE.

Prior to loading samples into the deposition chamber they were cleaned with acetone and then placed in an ultrasonic bath for 10 minutes. Once clean the samples are placed onto the sample holder and the chamber evacuated to a pressure of 2.5×10^{-5} torr. Argon was introduced into the chamber at a rate of $1\times10^{-5}m^3$/min and an argon plasma created using an RF power source. In addition to the samples CoCr and UHMWPE samples, one M42 tool steel (American Society for Testing and Materials, 2004) sample was placed in the chamber for each coating run. This is a routine quality control sample that Teer Coatings

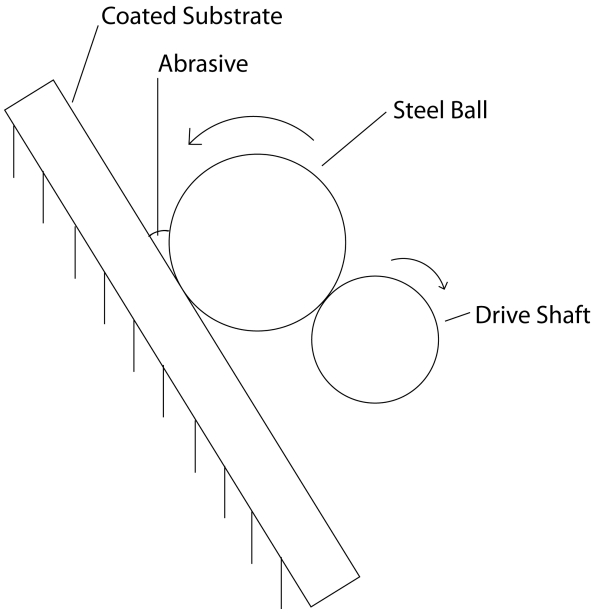

Figure 3.5: Side profile of the device used in the ball crater method

Ltd. use for comparison with any other coating run they have carried out.

Prior to coating deposition the substrates undergo an "ion clean" for 30 minutes which causes the argon plasma ions to bombard and etch the substrate surface. During the ion clean the substrate bias is set high, approximately 450V in comparison to a more 40-80V range used during deposition. After the ion clean the coating process begins.

Following deposition the M42 tool steel sample from each deposition process was used to determine the coating thickness using the ball crater technique. Shown schematically in Figure 3.5 with a photo illustrating how the ball is rests on the drive shaft in Figure 3.6. The coated substrate is inclined at an angle and a steel ball rotated against it. The process causes a circular wear scar to appear through the coating; this can be accelerated by using an abrasive such as diamond paste.

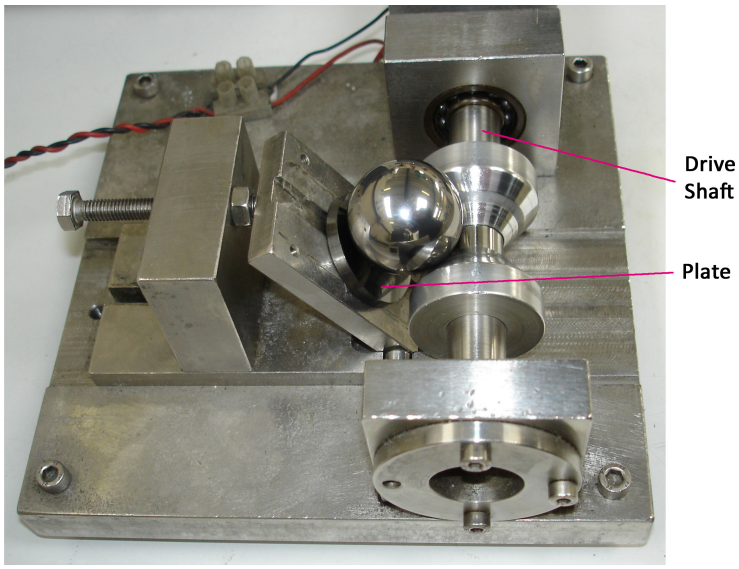

Figure 3.6: Photo of ball crater device illustrating how the ball is held in place

When the coating has been worn through it is possible to observe and measure, under an optical microscope two concentric circles seen in Figure 3.7. It is possible to calculate the coating thickness using Equation 3.1

$$Thickness = \frac{xy}{diameter\ of\ steel\ ball} \tag{3.1}$$

By using this method it was possible to determine the thickness of each of coating, these are shown in Table 3.7.

Table 3.7: Coating thicknesses

Sample	Description	Thickness (μm)
1	40V Bias	2.3
2	Graphit-iC^{TM}	2.0
3	80V Bias	2.0
4	60 to 40V Transition Bias	2.0
5	CoCr Interlayer	2.2
A-E	Graphit-iC^{TM} deposited onto ion implanted UHMWPE	2.0

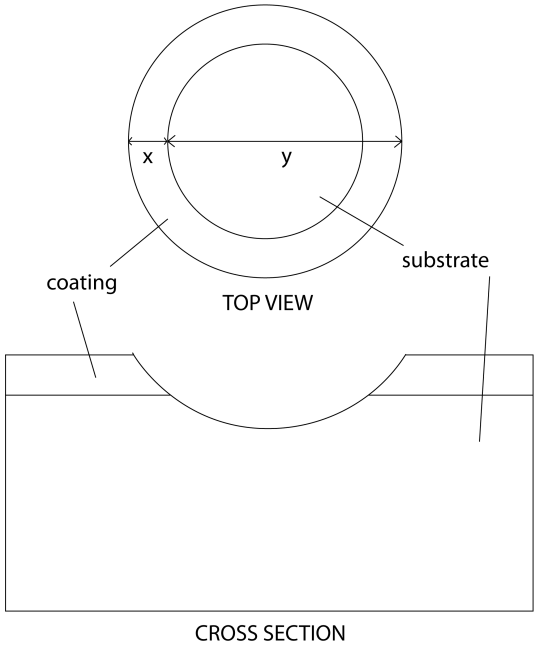

Figure 3.7: Schematic of the crater produced during the ball crater method

3.4 Summary

This chapter has described the method by which coated samples were prepared for study in this thesis. Consequently the following CoCr pins and discs are to be tested, they will be described as seen in Table 3.8 and designated in graphs by their associated number.

Table 3.8: CoCr pin and plate samples for study

Sample Number	Description
1	40V bias coated CoCr
2	Graphit-iC^{TM} coated CoCr
3	80V bias coated CoCr
4	60 to 40V transition bias coated CoCr
5	CoCr interlayer coated CoCr
6	Uncoated CoCr

Similarly, all UHMWPE plates have been coated with Graphit-iC^{TM} and modified by ion implantation, they will be described as seen in Table 3.9 and designated

in graphs and tables by their associated letter:

Table 3.9: UHMWPE plate samples for study, all coated with Coating 6

Sample Letter	Description
A	Nitrogen implanted UHMWPE at 15KeV with a dose of 1×10^{15}particles/cm^2
B	Nitrogen implanted UHMWPE at 15KeV with a dose of 5×10^{15}particles/cm^2
C	Precoated (with chromium) UHMWPE, nitrogen ion implanted at 45KeV with a dose of 1×10^{15}particles/cm^2
D	Precoated (with chromium) UHMWPE nitrogen ion implanted at 45KeV with a dose of 5×10^{15}particles/cm^2
E	Unmodified UHMWPE

4. Coating Hardness

4.1 Introduction

Standard indentation techniques are not capable of resolving any information from the coatings deposited onto CoCr and UHMWPE in this study. The indentation deforms both the coating and the substrate resulting in a composite hardness measurement. To examine the properties of coatings it is necessary to use reduce the loads from the newtons and kilo-newtons that are typically used in standard hardness tests such as the Rockwell C to milli-newtons which minimise the substrate deformation. Using milli-newton loads for hardness measurement reduces the substrate deformation and is a technique known as nano-indentation.

Because of the small loads used in nano-indentation the technique tends not to examine the resulting indent but instead records a load-depth profile through both the loading and unloading procedure. This means that elastic and plastic properties can also be examined. An extensive review has been carried out by Oliver and Pharr (2004) in which the calculation of material properties from nano-indentation is discussed.

The nano-indentation technique is extremely sensitive to environmental changes; temperature and pressure will have a large effect on results when attempting to control sub-nanometre movements and μN loads. Complex control equipment is required to support the method. The Micro Materials Ltd nanotest machine utilises a lever on a pivot. An electromagnet controls the load while capacitor

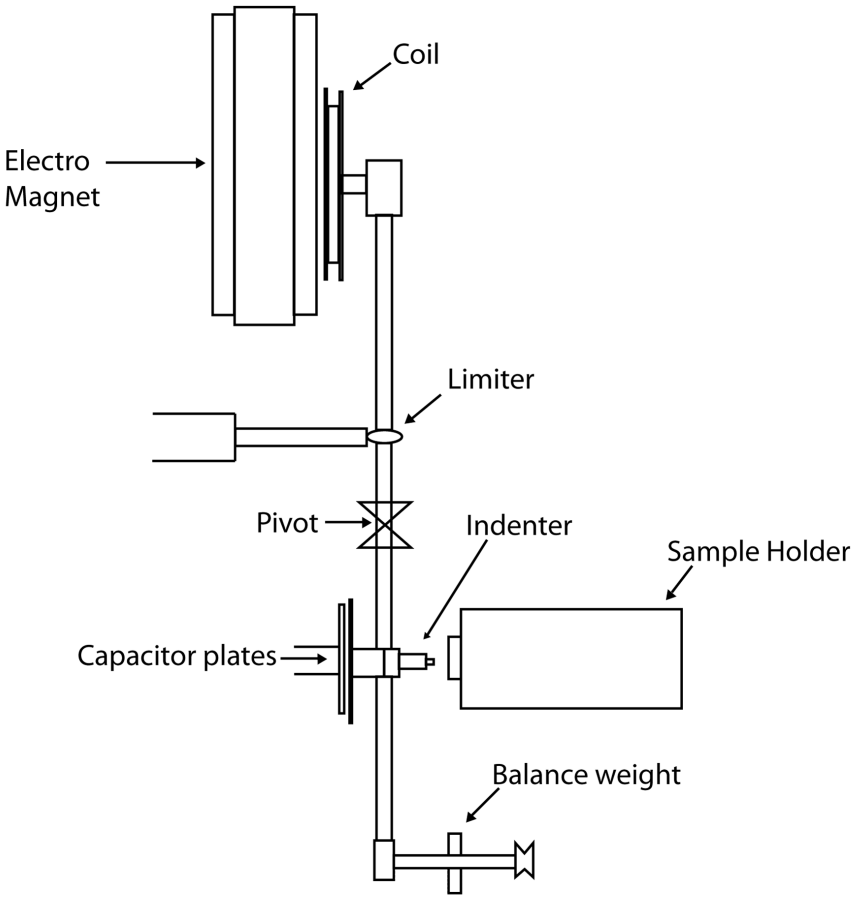

Figure 4.1: Micromaterials NanoTest schematic

plates accurately determine the position (Figure 4.1).

As with standard hardness tests, the hardness is calculated from the maximum load to residual area ratio (Equation 4.1).

$$Hardness(H) = \frac{Load_{max}}{Area(h_{max})} \tag{4.1}$$

The load is known and the indentation can be measured under a microscope. The Nanotest machine from Micro Materials Ltd instead uses an indentor with

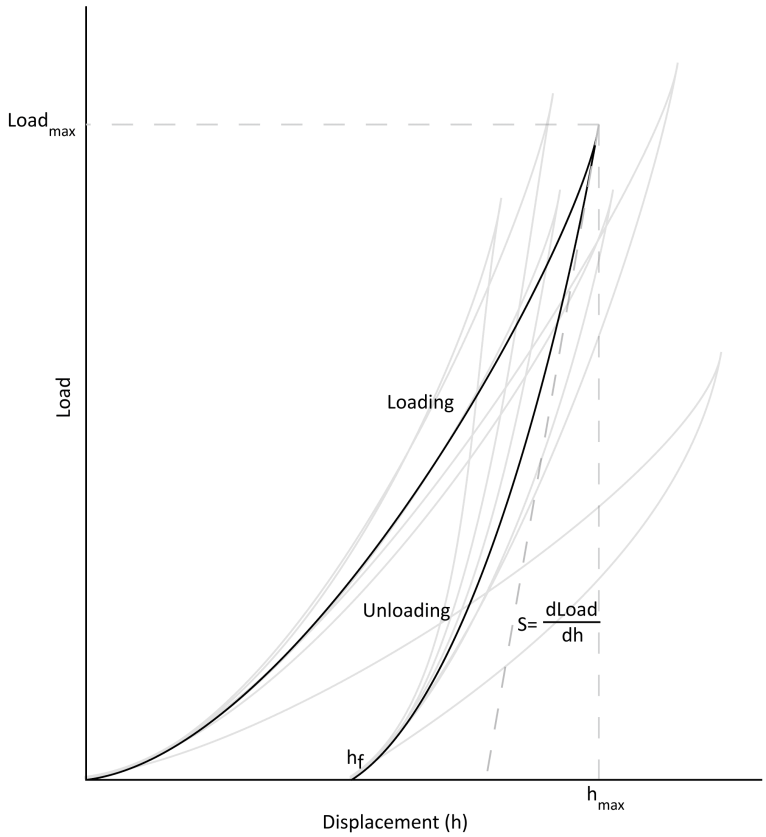

Figure 4.2: Typical graph produced from nano-indentation

known geometry, normally a Berkovich tip. The equipment records both the load and depth penetration; knowing the depth and the geometry of the indentor it is possible to calculate the area and therefore hardness without observing the indentation under a microscope (Figure 4.2). Multiple indents are used to reduce statistical error and are indicated for illustrative purposes in Figure 4.2. From the graph it is also possible to calculate the stiffness, this is from the gradient of the unloading curve (Figure 4.2 and Equation 4.2).

$$Stiffness(S) = \frac{dLoad}{dh} \tag{4.2}$$

The indentation technique is also capable of determining the reduced modulus which is related to the material's elastic modulus by equation 4.3 (Oliver and Pharr, 2004), where E_r=reduced modulus, E_i=indentor elastic modulus, E_s=Sample elastic modulus, ν_i=Poisson's ratio for indentor, ν_s=Poisson's ratio for sample.

$$\frac{1}{E_r} = \frac{1-\nu_s^2}{E_s} + \frac{1-\nu_i^2}{E_i} \tag{4.3}$$

The reduced modulus is calculated from the stiffness parameter and the contact area Equation 4.4 (Oliver and Pharr, 2004): where E_r=Reduced modulus, S=Stiffness, A=Indent area

$$\frac{1}{S} = \frac{\pi^{0.5}}{2E_r A^{0.5}} \tag{4.4}$$

4.2 Method

4.2.1 CoCr Samples

Indents on CoCr plates (Samples 1-5) were carried out over a depth range of 30nm to 300nm in 30nm increments so that the hardness at varying depths could be calculated (Table 4.2, Appendix B), each indent was repeated three times and separated by 50μm. Sample 6 was not examined because it was uncoated and could therefore be accurately measured for hardness using traditional techniques. At 30nm indentation depth the hardest coating was found to be the 80V bias coating (Sample 3, Table 3.8) (12.03$\pm$2.03GPa) while the softest coating was found

to be 40V bias coating (Sample 1, Table 3.8) (7.92±2.51GPa). These hardness measurements remained unchanged throughout the coating as the indentations increased to 300nm. At 300nm their hardness was recorded at 11.01±0.97GPa and 7.84±1.05GPa respectively. Similarly the Graphit-iC^{TM} coating (Sample 2, Table 3.8) which was coated with a substrate bias of 60V had a constant hardness throughout the coating; at 30nm and 300nm the hardness was measured to be 11.24±1.73GPa and 10.16±0.36GPa respectively; at 210nm the hardness increased to 14.82±7.67GPa for Graphit-iC^{TM} although this was due to a single outlier which can be seen in Figure B.7, probably caused by debris on the sample.

The 60V to 40V transitional bias coating (Sample 4, Table 3.8) and CoCr interlayer coating (Sample 5, Table 3.8) both exhibit trends of increased hardness as depth increases (Figure 4.3). The transition bias coating (Sample 4, Table 3.8) has a hardness of 8.78±2.03GPa at 30nm and 10.91±0.27GPa at 300nm, while the CoCr interlayer coating (Sample 5, Table 3.8) hardness increases from 10.32±0.88 to 15.63±0.94GPa at 30nm and 300nm respectively. At 300nm the CoCr interlayer coating has the highest recorded hardness of this study.

There was found to be a statistical difference (ANOVA $p<0.05$) between the 40V, 60V (Graphit-iC^{TM}) and 80V bias coatings. It follows that the 60 to 40V transition bias coating would have a similar hardness to the 40V bias coating when indenting to 30nm and this was the case ($p>0.05$).

The reduced modulus of the coatings were recorded for the coating when indentation was at 300nm (Table 4.1). It was found that the coating with the

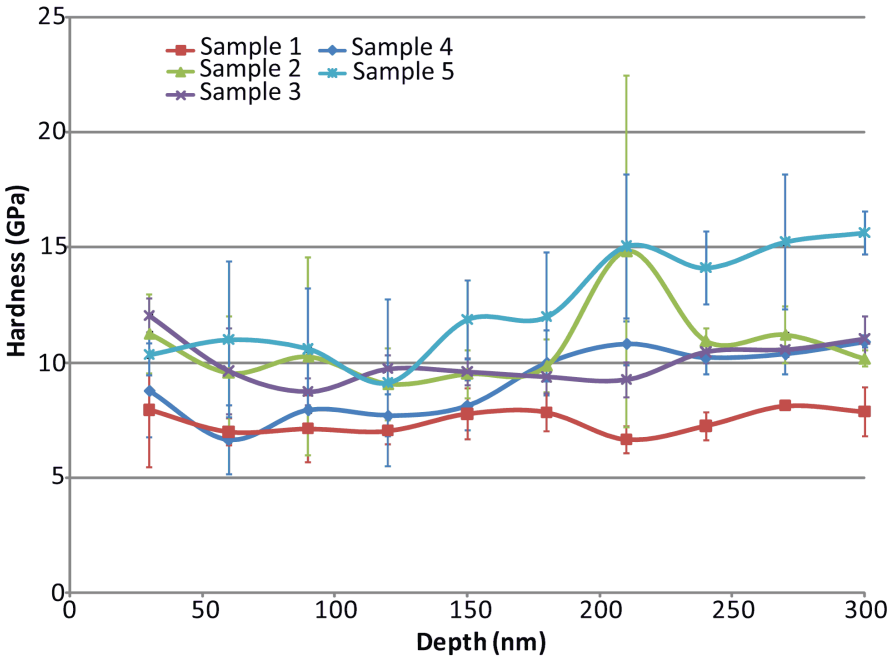

Figure 4.3: Hardness of amorphous carbon coatings deposited onto CoCr substrate as a function of depth

Table 4.1: Reduced modulus of amorphous carbon coatings deposited onto CoCr, as measured by nanoindentation

	Reduced Modulus (GPa)
Sample 1	96.12±9.9
Sample 2	146.51±2.55
Sample 3	143.20±7.7
Sample 4	144.27±4.07
Sample 5	173.48±10.25

greatest reduced modulus was the CoCr interlayer (sample 5, Table 3.8) which measured 173.48GPa, this compared to the 40V (sample 1) which obtained the lowest reduced modulus of 96.12GPa (Figure 4.4).

Table 4.2: Hardness (GPa) of amorphous carbon coatings deposited onto CoCr over various depths, as measured by nanoindentation, within two standard deviations

Depth (nm)	30	60	90	120	150	180	210
Sample 1	7.92±2.51	6.96±0.58	7.11±1.45	7.01±0.59	7.75±1.12	7.82±0.82	6.65±0.59
Sample 2	11.24±1.73	9.55±2.44	10.25±4.29	9.05±1.57	9.49±1.04	9.84±1.15	14.82±7.67
Sample 3	12.03±0.74	9.62±1.86	8.72±0.59	9.71±0.57	9.58±0.59	9.35±0.69	9.24±0.75
Sample 4	8.78±2.03	6.62±1.49	7.91±0.81	7.69±0.92	8.12±1.10	9.97±1.41	10.82±0.94
Sample 5	10.32±0.88	10.99±3.38	10.57±2.62	9.11±3.64	11.86±1.72	11.98±2.81	15.05±3.14

Depth (nm)	240	270	300
Sample 1	7.22±0.62	8.11±0.07	7.84±1.05
Sample 2	10.92±0.54	11.20±1.22	10.16±0.36
Sample 3	10.44±0.49	10.55±0.16	11.01±0.97
Sample 4	10.21±0.75	10.36±0.90	10.91±0.27
Sample 5	14.11±1.58	15.23±2.92	15.63±0.94

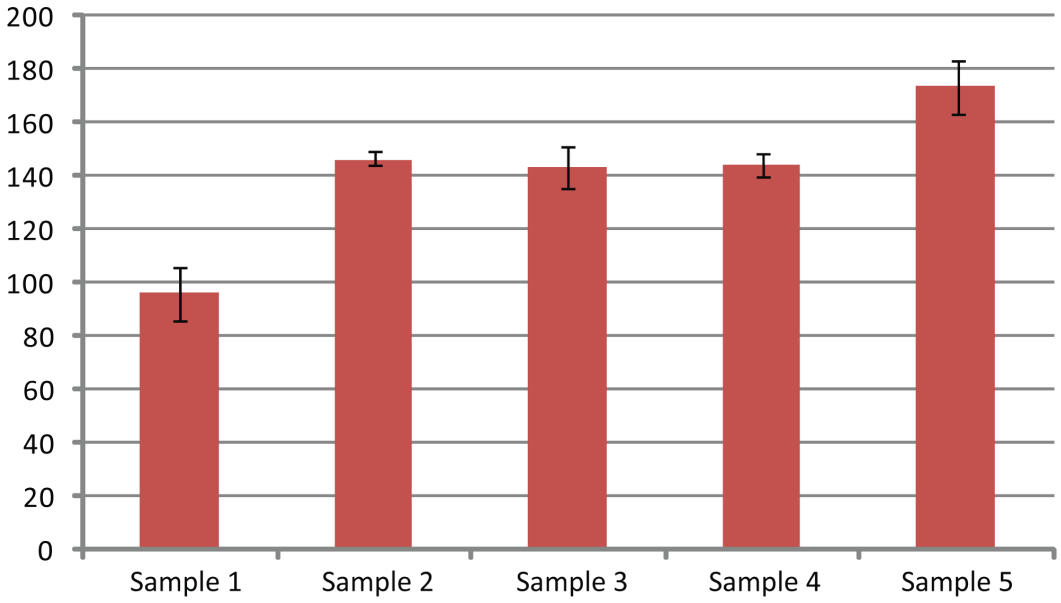

Figure 4.4: Reduced modulus (GPa) of amorphous carbon coatings deposited onto CoCr

4.2.2 Ion Implanted UHMWPE Samples

Nano-indentation was carried out on one of the UHMWPE discs for each modified sample described in Section 3.4 by indenting to a depth of 250nm. Because of the sensitivity of the technique and the variability of the UHMWPE, 10 repeats were used to reduce statistical error. Depth profiling was not carried out because the UHMWPE substrate is soft and will rapidly dominate the hardness measurements.

Table 4.3 contains the hardness measurements for the ion implanted UHMWPE, the depth profile graphs can be found in Appendix B, Figure B.11. Samples nitrogen implanted at 15KeV were found to have a significantly lower hardness (Sample A: 0.1287±0.041GPa, Sample B: 0.12474±0.02GPa) than Sample E (0.26287±0.065GPa) which had not been ion implanted ($p<0.05$); although when an initial layer of chromium was deposited there was no difference in hardness (Sample C: 0.26957±0.053GPa, Sample D 0.2586±0.051) to Sample E ($P>0.05$) UHMWPE. The sample with the highest modulus was the unmodified UHMWPE (Sample E, Table 3.9) with the lowest being Sample A (Table 3.9) - UHMWPE ion implanted with an energy of 15KeV and dose of 1×10^{15}particles/cm^2 (Figure 4.6).

A statistical difference in hardness was found between the samples ion implanted with 15KeV nitrogen (A and B) and the unmodified UHMWPE ($p<0.05$), but no difference between the precoated samples (C and D) to the UHMWPE ($p>0.05$).

Table 4.3: Hardness and reduced modulus of modified UHMWPE discs, within 2 standard deviations

Sample	Hardness (GPa)	Reduced Modulus (GPa)
Sample A	0.12 ± 0.04	1.10 ± 0.34
Sample B	0.12 ± 0.02	1.24 ± 0.23
Sample C	0.27 ± 0.05	1.94 ± 0.27
Sample D	0.26 ± 0.05	2.06 ± 0.33
Sample E	0.26 ± 0.07	2.48 ± 0.76

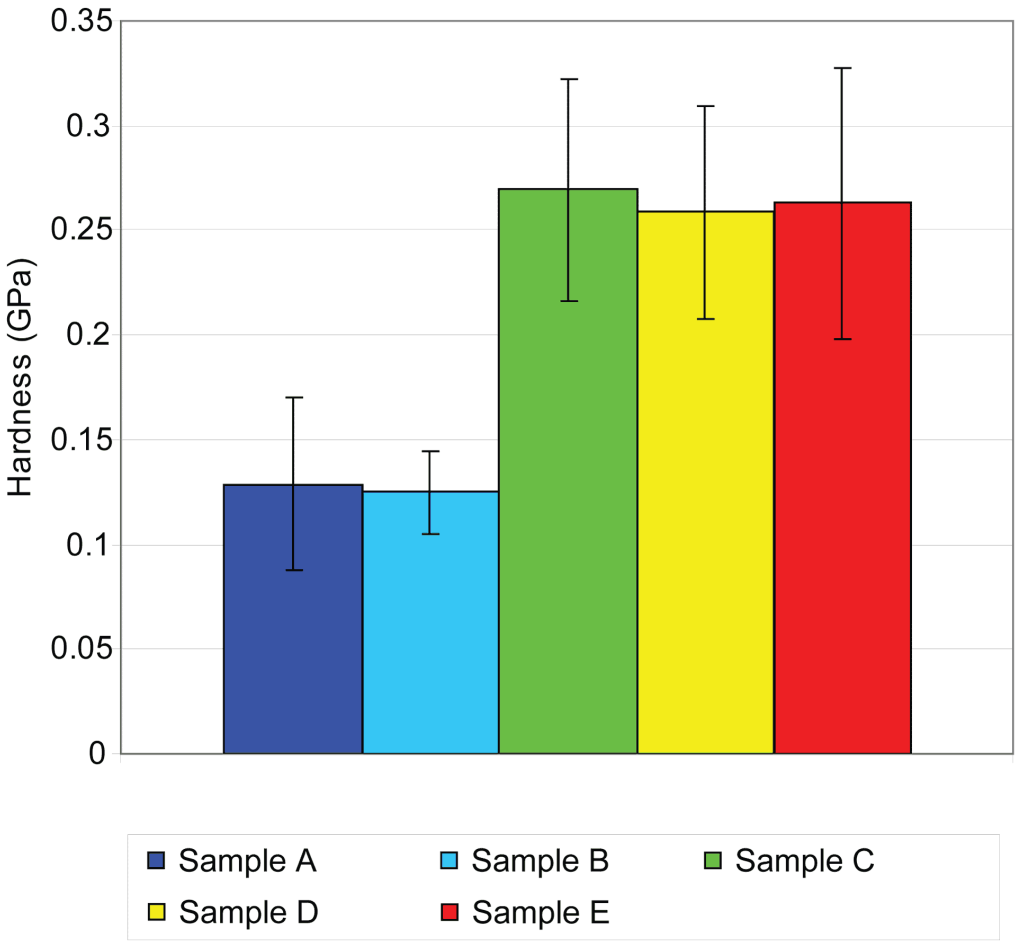

Figure 4.5: Hardness of ion implanted and coated substrates at a depth of 250nm

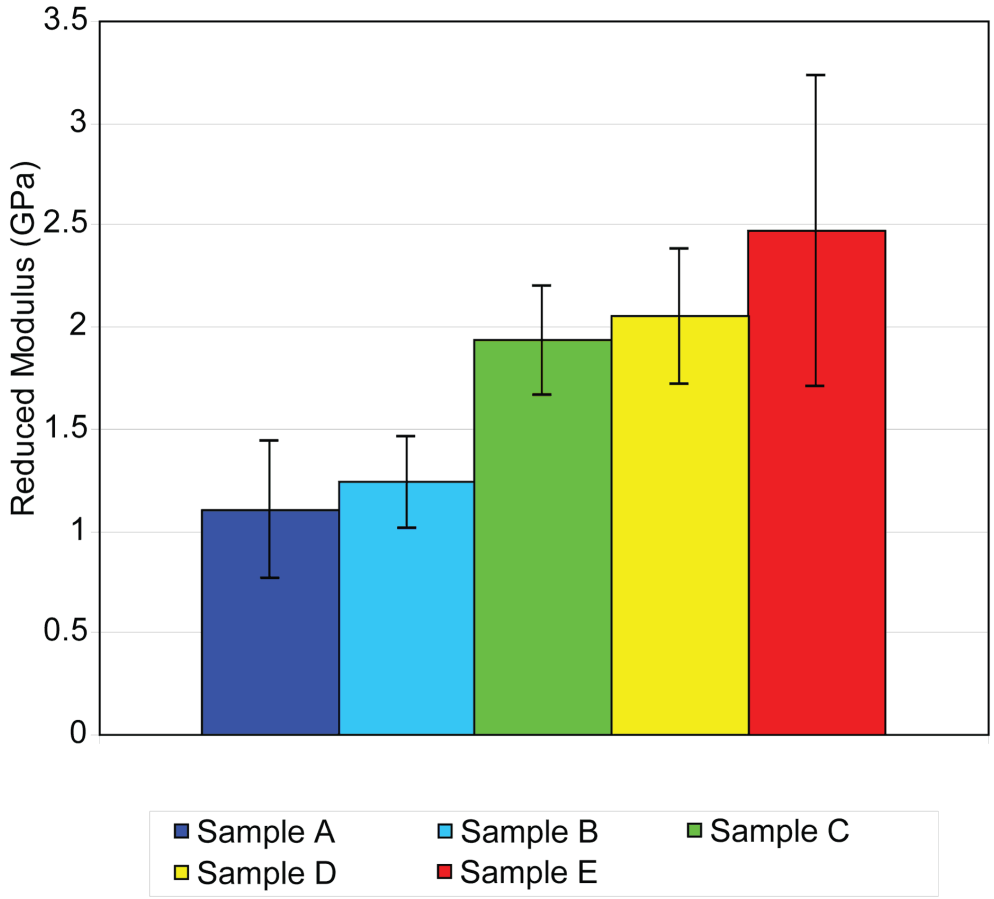

Figure 4.6: Reduced modulus of ion implanted and coated substrates at a depth of 250nm

4.3 Discussion

The CoCr interlayer coating initially had a hardness similar ($p>0.05$) to the Graphit-iC^{TM} coating which had a similar substrate bias, however at 150nm there was a significant difference ($p<0.05$). This continued until 300nm with the exception of the indentation at 210nm where an outlier caused an increased hardness of the Graphit-iC^{TM} coating. Other coatings with a constant bias remained constant at a depth of 30nm there was no significant difference between from Sample 2 which had a bias of 60V. The coatings differ by the addition of the CoCr interlayer which is therefore the likely cause of the increased hardness.

Yang *et al.* (2000) report that over the bias range used in this thesis, increased bias leads to increased hardness; this is reflected in the results seen here and suggests why Sample 4, the 60 to 40V transition bias coating, increases in hardness from a level similar to that of Sample 1 (40V bias) at the surface to Sample 2 (60V bias) at a depth of 300nm.

It is commonly understood that the hardness of a material relates to it's wear property, increased hardness usually equating to reduced wear (Archard, 1953). Lancaster (1963) also relates wear properties to the elastic modulus of a material, suggesting that the wear rate is inversely proportional to the elastic modulus for smooth surfaces. Leyland and Matthews (2000) however proposes that this relationship is because materials with a high elastic modulus also exhibit a high hardness. It has been noted by Oberle (1951) that increasing wear resistance correlates well with the rank order of the hardness-modulus ratio (H/E). This

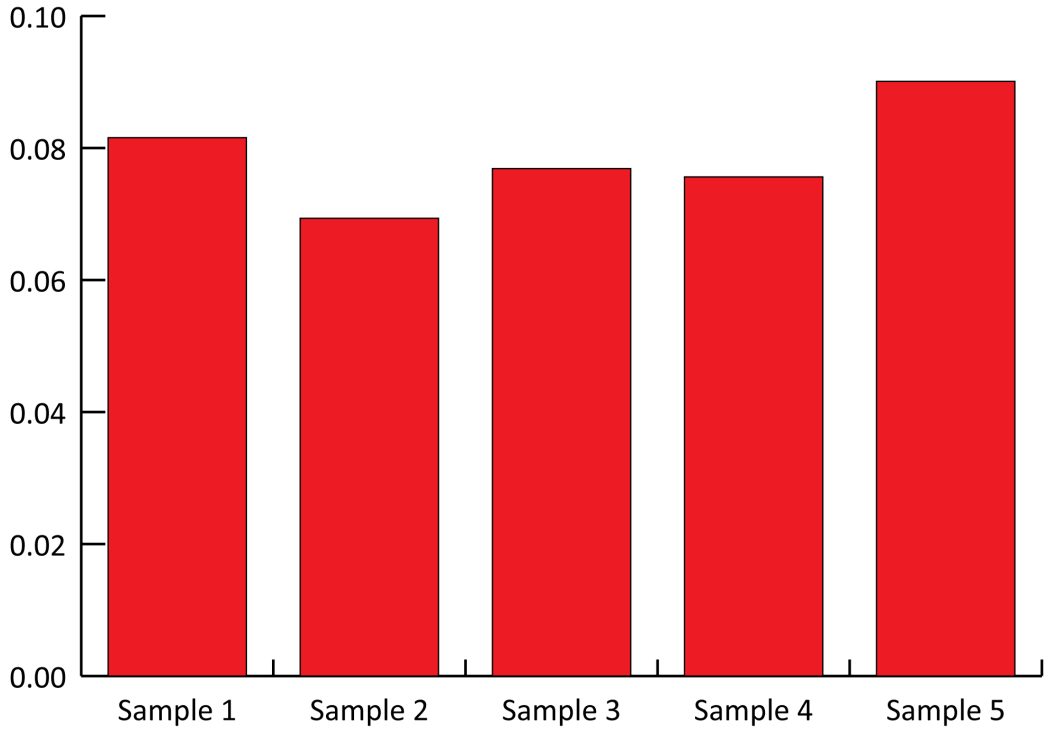

Figure 4.7: Comparison of H/E ratio for coatings deposited onto CoCr

has been investigated further by Leyland and Matthews (2000) who supports the theory, but highlights the fact that there is no conclusive evidence to suggest a need to reduce the modulus of elasticity to improve wear.

Considering this, the H/E ratio for the coatings deposited onto CoCr suggest that Sample 5, the coating with a CoCr interlayer, will have the lowest wear factor, followed by the 40V bias coating (Figure 4.7). This opposes what would be predicted if ranking only hardness, which shows the 40V bias coating with the lowest hardness.

The effect of nitrogen ion implantation was not as expected. The process was intended to increase the hardness of UHMWPE at the substrate coating boundary, however it appears that the effect of ion implantation used at the levels in this

study was to reduce the hardness of the polymer; this may be due to the ion bombardment disrupting the polymer chains, breaking them into shorter fragments; shorter polymer chains would reduce the material hardness and cause the results observed here.

Hardness of the samples with a 40nm chromium layer do not vary significantly from the unmodified UHMWPE. This can possibly be attributed to the nitrogen implantation disrupting the polymer chains and softening the surface as shown in the samples that were not initially coated with chromium. The chromium layer on the surface however disguises the softening with a hard top layer.

With regards to the H/E ratio, the coating deposited onto UHMWPE which was implanted with nitrogen at 15KeV and a dose of 5×10^{15}particles/cm^2 is ranked first, ranked last is the coated UHMWPE which had not been ion implanted (Figure 4.8), suggesting that the ion implantation will offer some benefit to the wear properties. If hardness was the main factor contributing to wear resistance, it would suggest that ion implantation will have a detrimental effect on the wear. The implantation has however had the effect of reducing the reduced modulus of the UHMWPE samples, thereby making them more resistant to plastic deformation for the same strain.

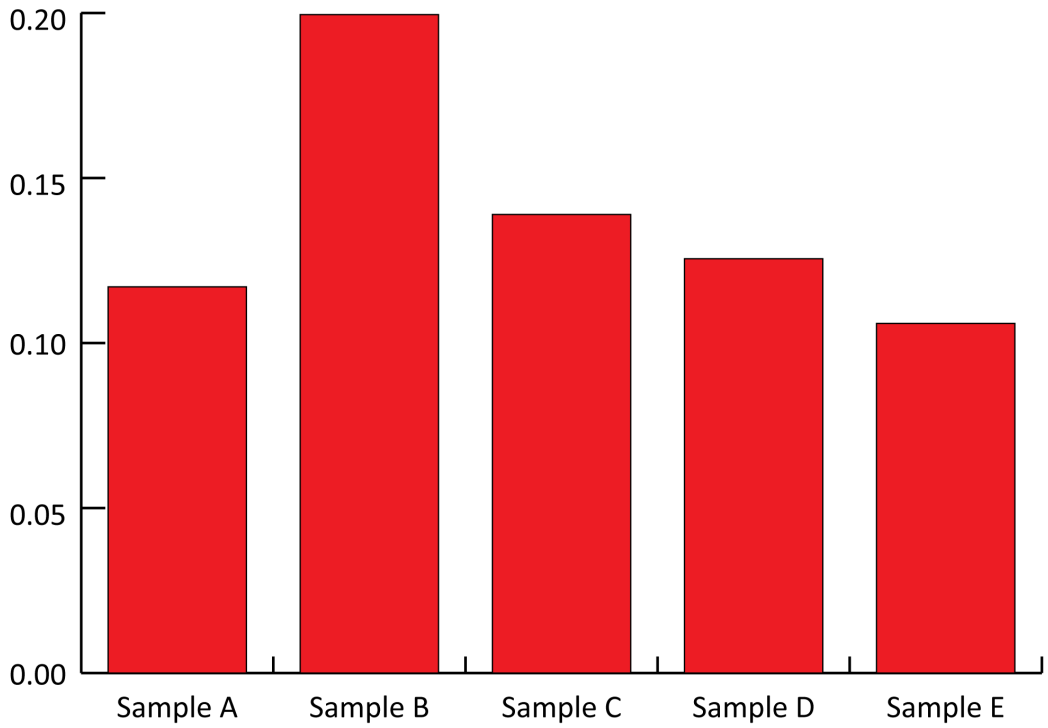

Figure 4.8: Comparison of H/E ratio for coatings deposited onto modified UHMWPE

4.4 Summary

Reported in this chapter is hardness of the coatings deposited for this study. It was shown that the substrate bias contributes to the hardness of a coating and that increasing the bias leads to a harder coating. The ion implantation carried out in this study has softened the UHMWPE substrate.

Calculation of the H/E ratio would suggest that the CoCr interlayer coating and 40V bias will have the lowest wear factors; on the UHMWPE substrates, the UHMWPE modified with nitrogen at 15KeV and a dose of 5×10^{15}particles/cm^2 may have the lowest wear factor.

5. Coating Adhesion

5.1 Introduction

It has been identified in the literature that adhesion of coatings is a problem when they are deposited onto hip joint prostheses (Section 2.5). Improved adhesion to the substrate should reduce the incidence of this, this can be measured by a number of methods including: scratch testing, pull off tests and Daimler-Benz tests (Morshed *et al.*, 2003; Randall *et al.*, 2001; Heinke *et al.*, 1995).

The Daimler Benz test involves loading a Rockwell C indentor onto the coating and observed the resulting indent. The test is qualitative in nature, the adhesion being graded from HF1 to HF6 dependent on the level of cracking and delamination around the edge of the indent (Heinke *et al.*, 1995). This method is most suited to rapid quality control checks of production coatings.

Both scratch testing and pull off tests are quantitative in nature. With scratch testing a stylus (typically a Rockwell diamond tip) is drawn across the coated substrate with a controlled increasing load. Performance of the coating can be determined by examination of the resulting scar under a microscope to observe points of initial failure, edge cracking, initial failure and total failure. The position of the feature on the scar can be related to the load. Alternatively acoustic emissions or friction can be recorded as the scratch test is being formed (Randall *et al.*, 2001; Zhang *et al.*, 2008; Yatsuzuka *et al.*, 2009). Pull off tests involve applying a stud, fixed with an epoxy adhesive to the coating. The force required

to pull the stud and coating from the substrate indicates the adhesion (Morshed *et al.*, 2003).

Similar to wear testing, parameters for scratch tests vary between research groups and papers. Randall *et al.* (2001) examined the effect of indentor size, scratch speed and loading rate and established that increasing the indentor size and loading rate increased the critical load, while the critical load decreased for increasing scratch speed.

This chapter examines the adhesion of the coatings deposited onto CoCr and UHMWPE using the scratch test method.

5.2 Method

5.2.1 CoCr Substrates

During this study the Teer Coatings Ltd. ST3001 Scratch tester was used at Teer Coatings Ltd. (2007). An initial load of 10N was applied and increased at a rate of 100N/min ($1.67 Ns^{-1}$), the drag speed was 10mm/min ($1.67 \times 10^{-4} ms^{-1}$). These parameters were selected due to their routine use at Teer Coatings Ltd., thereby enabling comparison with similar coatings if necessary in the future.

The adhesion of the coating was quantified by locating points of initial chipping and total failure under the microscope (Figure 5.1) and determining the associated load at these points on the scar using equation 5.1.

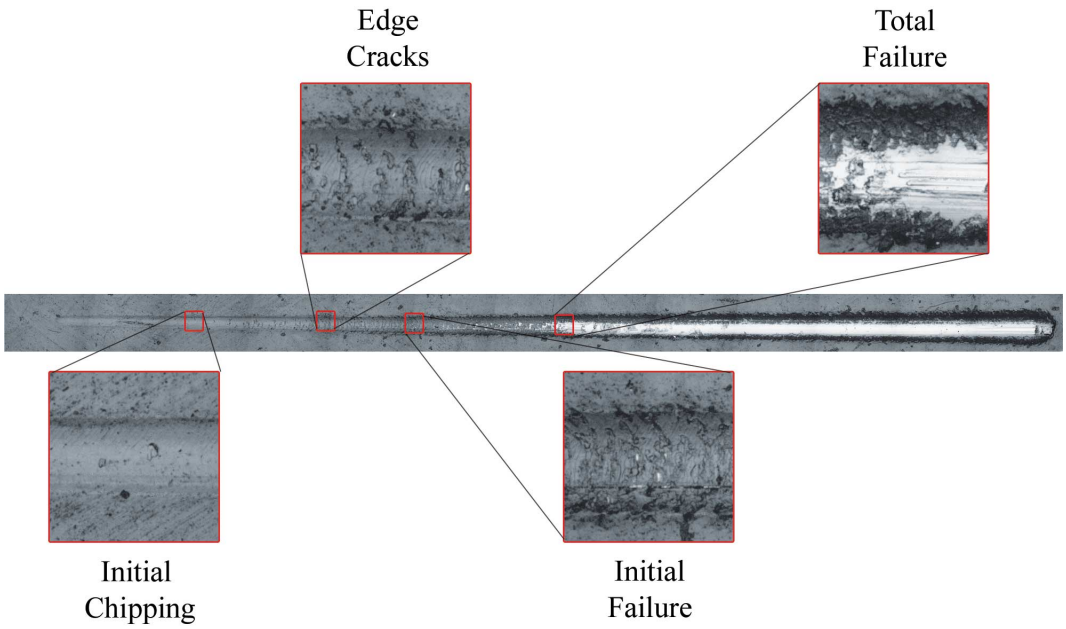

Figure 5.1: Points of interest on a scratch test micrograph

$$Load\ at\ measured\ point = (\frac{load\ rate}{drag\ speed}) \times\ distance\ along\ scar\ + initial\ load \tag{5.1}$$

One CoCr disc from each coating run was scratch tested; three repeats were carried out on the disc.

5.2.2 UHMWPE Substrates

In the case of scratch tests against UHMWPE, the discs deformed due to the load it was placed under; the tip holder came into contact with the test disc thereby preventing a complete scratch from being recorded. The effect of deformation was mitigated by using a 1.5mm tungsten carbide ball bearing instead of the

rockwell diamond, decreasing the initial load to 5N; the final load was 80N. This reduced the contact pressure but prevented comparison with any of the coatings deposited onto metal substrates, it did enable subjective comparison between the other coated UHMWPE substrates.

Similar to the CoCr samples, one disc of each of the various ion implantation samples was tested with three repeats.

5.3 Results

5.3.1 CoCr Substrates

The points of chipping and total failure for all of the coatings can be found in Table 5.1 and are illustrated in Figure 5.2. The coating with the greatest resistance to chipping and total coating failure was Sample 5: Graphit-iC^{TM} with a CoCr interlayer (52N and 58N respectively). Different coatings had the lowest resistance to chipping and total coating failure, these were Sample 4: 60 to 40V transition bias coating (39N) and Sample 3: 80V bias coating (49N) respectively. Analysis of Variance (ANOVA) indicates that there is a statistical difference between the coatings ($p<0.05$). Analysis suggests that coating variation causes a difference in the point of chipping and total failure (ANOVA $p<0.05$).

Table 5.1: Scratch test results of coatings deposited onto CoCr

Coating	Description	Track Chipping (N)		Total Failure (N)	
		Mean	Standard Deviation	Mean	Standard Deviation
Sample 1	40V Bias	45	1.6	54	1.5
Sample 2	Graphit-iC™	45	4.3	52	1.5
Sample 3	80V Bias	42	2.6	49	2.3
Sample 4	60 to 40V Transition Bias	39	2.9	50	5.3
Sample 5	CoCr Interlayer	52	1.8	58	1.7

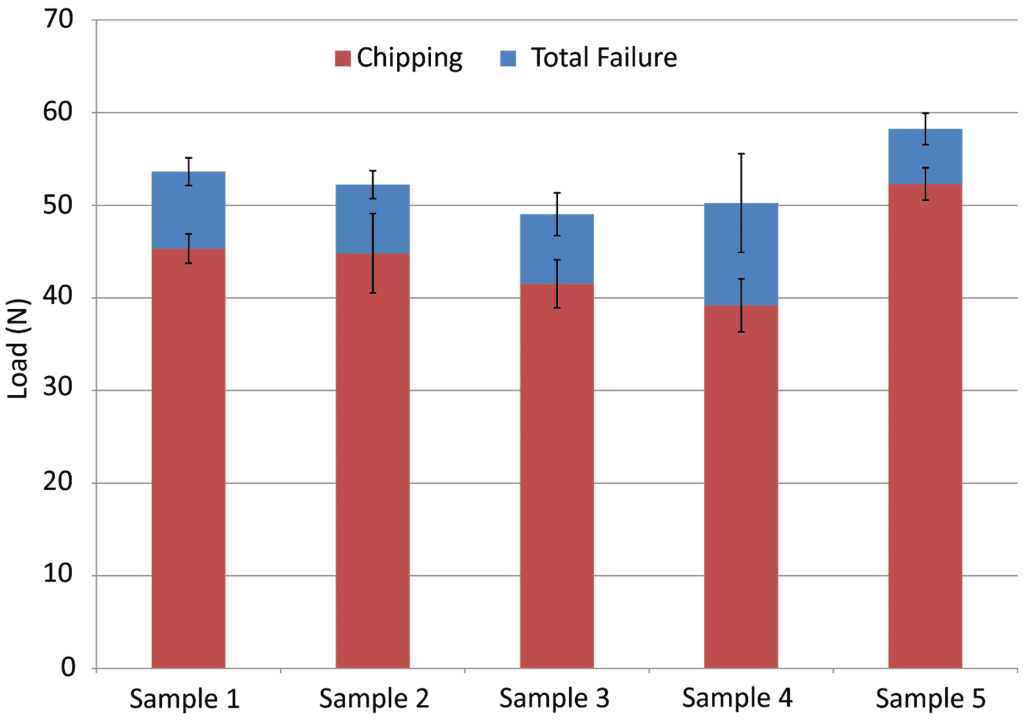

Figure 5.2: Chart illustrating scratch test results from coatings deposited onto CoCr

5.3.2 UHMWPE Substrates

Scratches in the UHMWPE produced deep grooves within the substrate and coating, confocal micrographs were obtained to overcome the depth of field problems that arose. Visual inspection of the micrographs (Figures 5.3 through 5.7) enable a subjective interpretation of the results. There was crazing across the surface of the coatings even outside of the areas being scratch tested; this was most pronounced on the coatings ion implanted at 45KeV and is indicative of cohesive failure. Despite this none of the coatings exhibited total adhesive failure (i.e. delamination) on the scratch tests. However, Samples D and E, initially coated with chromium and then ion implanted with a 45 KeV beam showed characteristic signs of starting to fail as the higher test loads were reached.

Figure 5.3: Micrograph of scratch on Sample A - amorphous carbon coated UHMWPE substrate ion implanted with nitrogen at 15KeV and a dose of 1×10^{15} particles/cm^2

Figure 5.4: Micrograph of scratch on Sample B - amorphous carbon coated UHMWPE substrate ion implanted with nitrogen at 15KeV and a dose of 5×10^{15} particles/cm^2

Figure 5.5: Micrograph of scratch on Sample C - amorphous carbon coated UHMWPE substrate ion implanted with nitrogen at 45KeV and a dose of 1×10^{15} particles/cm^2

Figure 5.6: Micrograph of scratch on Sample D - amorphous carbon coated UHMWPE substrate ion implanted with nitrogen at 45KeV and a dose of 5×10^{15} particles/cm^2

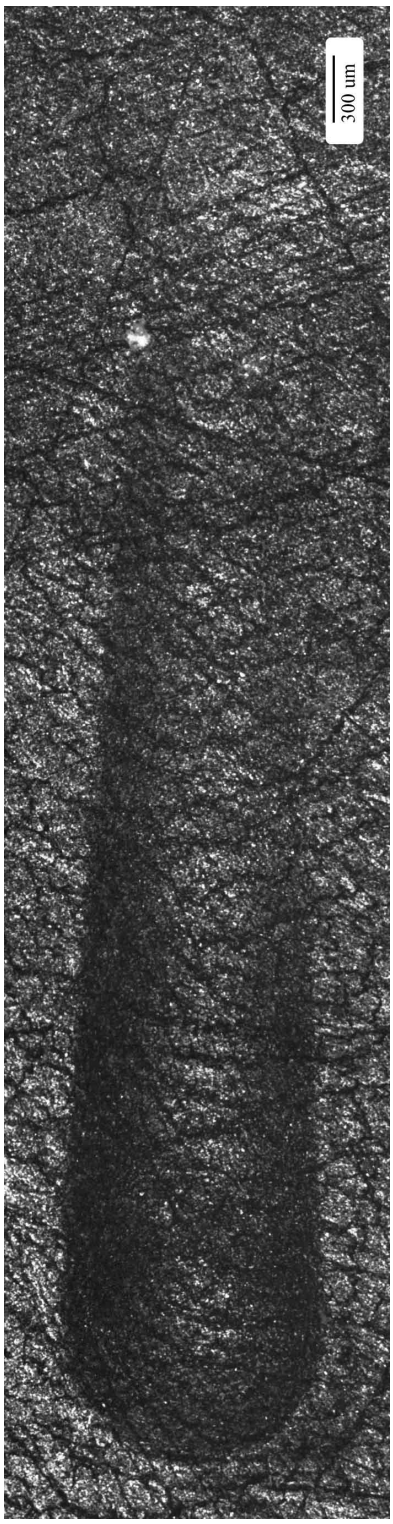

Figure 5.7: Micrograph of scratch on Sample E -amorphous carbon coated unmodified UHMWPE

5.4 Discussion

Adhesion of the 40, 60 and 80V bias coatings to CoCr (Samples 1-3) worsened with increasing bias; this has been reported on other substrates (Yang *et al.*, 2000). As discussed in Section 2.5.1 is caused by the higher bias increasing coating stress, which reduces the adhesive performance of the coating. Increased coating thickness can also lead to increased stress and it was noted in Chapter 3 that the 40V bias coating (Sample 1, Table 3.8) was 2.2μm thick, 0.2μm more than the other coatings; this could have increased the coating stress and reduced the adhesive performance, although if this was the case it was not sufficient to reduce the adhesion to a level less than the Graphit-iC^{TM} (Sample 2, Table 3.8), which uses a 60V substrate bias.

If the substrate bias were the main factor that affects the adhesion of the coating, then it would be expected that Sample 4, the 60 to 40V transition bias coating, would have similar adhesive properties to the 40V bias coating and Graphit-iC^{TM} coating. This however was not the case as it exhibited total failure at 50N compared to 54N and 52N for the 40V bias and Graphit-iC^{TM} coatings respectively. Similarly chipping occurred at 39N for Sample 4 compared to 45 for the 40V bias and Graphit-iC^{TM} coatings. It is not clear why the 60 to 40V transition bias coating performed as it did; the reduction in adhesion is linked to an increased intrinsic stress within the coating (Donnet and Erdemir, 2008) which was most likely caused by the transitional bias.

As discussed in Section 2.5.1, multilayers can reduce the intrinsic stress within a

coating (Sheeja *et al.*, 2003; Zhang *et al.*, 2005b), this appears to have been the case with the CoCr interlayer coating which had the strongest adhesion out of the tested coatings. This coating comprises a layer of CoCr followed by chromium and then carbon. A factor which could also have contributed is the transition from the substrate into the coating. Lyubimov *et al.* (1992) reported that gradient coatings prevent distinct boundaries for cracks to propagate along. The deposition of CoCr in Sample 5 onto the CoCr substrate may have been advantageous for this reason.

It was not possible to quantify the adhesion of the coatings deposited onto UHMWPE, Samples A-E, this and the use of a different indentor prevents comparison with the CoCr substrates. It was the intention of the ion implantation to increase the hardness of the UHMWPE substrate so the difference in hardness between the UHMWPE and coating was reduced. It was anticipated that this would improve adhesion, however Chapter 3 showed that the effect of ion implantation was to reduce the hardness of the substrate and therefore increase the difference in hardness between the UHMWPE and coating, it would therefore be expected that the ion implanted samples will not adhere as well as unmodified UHMWPE.

This is true for the samples initially coated with chromium and subsequently ion implanted at 45KeV. Coating delamination can be seen in Figures 5.8 and 5.9. Islands of coating can be seen to remain adhering to the substrate. Such extensive delamination does not occur on the unmodified UHMWPE where the coating appears to remain mostly adhered to the substrate (Figure 5.10).

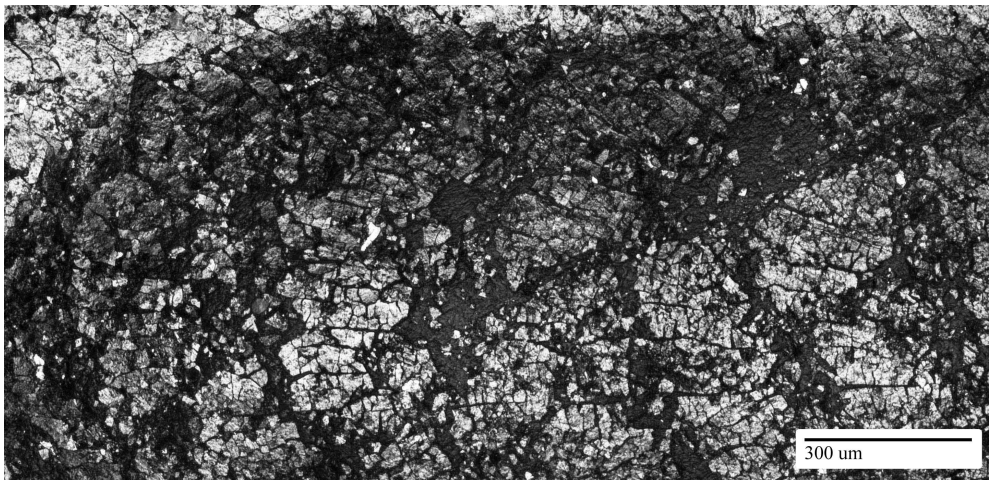

Figure 5.8: 20×magnification micrograph of scratch on Sample C, an amorphous carbon coated UHMWPE substrate ion implanted with nitrogen at 45KeV and a dose of 1×10^{15} particles/cm^2

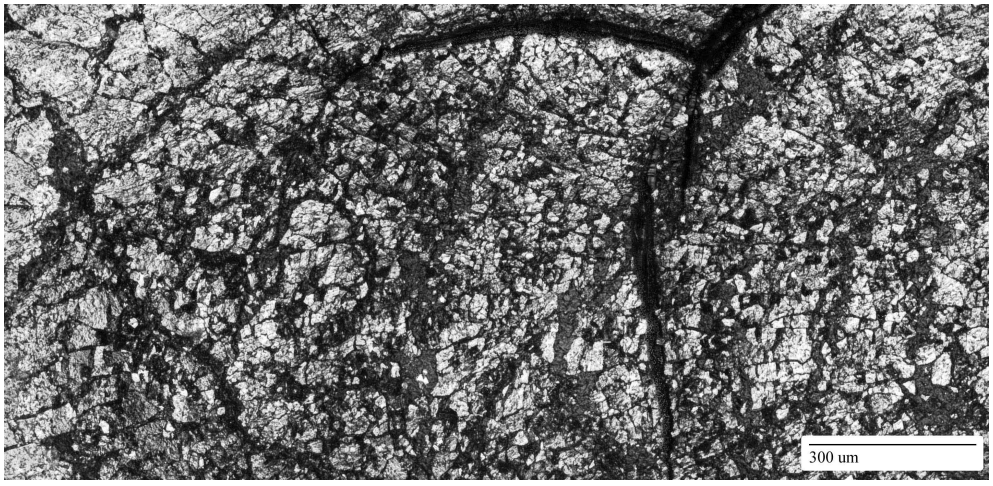

Figure 5.9: 20×magnification micrograph of scratch on Sample D, an amorphous carbon coated UHMWPE substrate ion implanted with nitrogen at 45KeV and a dose of 5×10^{15} particles/cm^2

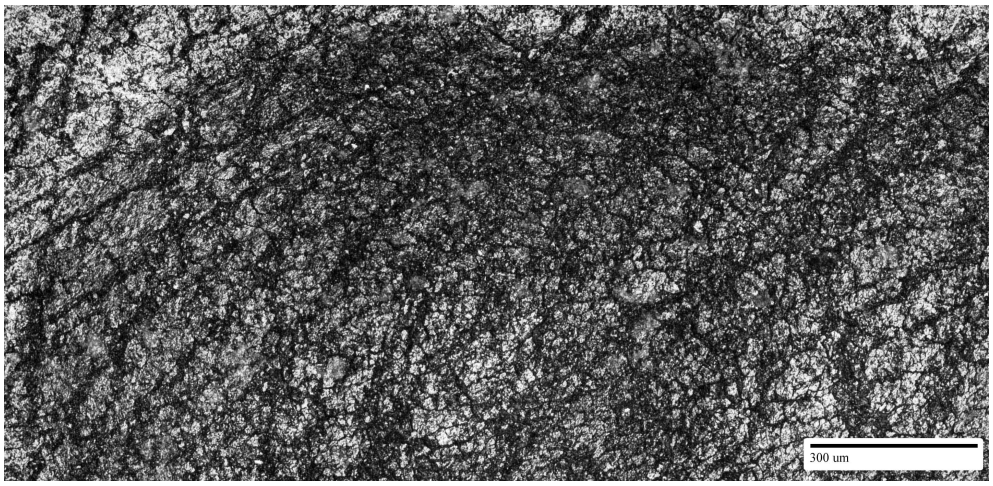

Figure 5.10: 20×magnification micrograph of scratch on Sample E, an unmodified amorphous carbon coated UHMWPE substrate

Similarly to the unmodified coated UHMWPE the micrographs of the 15KeV modified UHMWPE samples do not show large areas of delamination with small islands of adherent coating (Figures 5.11 and 5.12). In these two cases it appears that the coating has undergone massive cohesive failure, the speckled appearance suggesting microcracks all over the surface of the coating. But, this does not appear to be to the detriment of the coating adhesion.

It would appear that because there are discrete islands of coating, caused by the cohesive failure, when a load is applied which causes the UHMWPE to deform, the coating is also able to deform without being stressed such that the coating fails and delaminates. Segmentation of DLC coatings has been investigated by Aoki and Ohtake (2004). This study used a grid structure to mask the substrate and create discrete areas (1 ×1mm) of coating during deposition and found that the coating was more resistant to fracture under pin on disc testing compared to a non segmented DLC coating. Aoki and Ohtake (2004) also reported that because

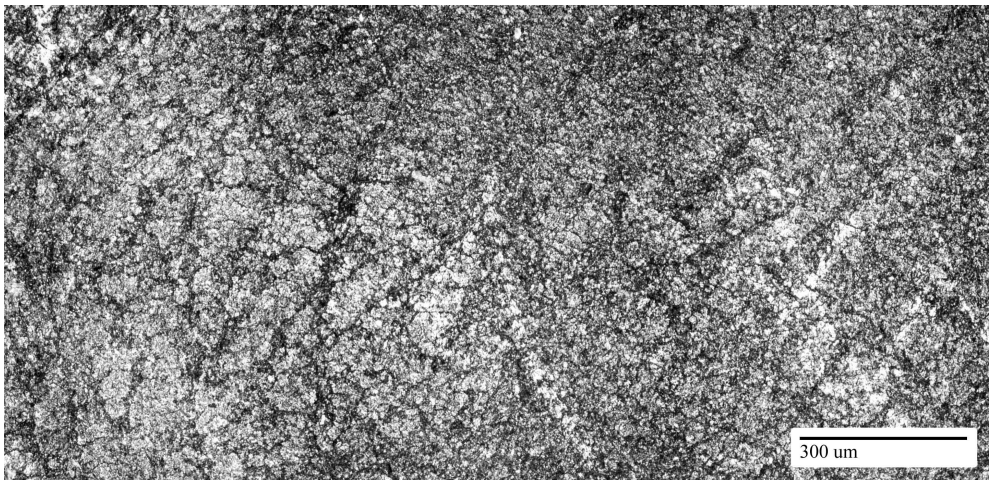

Figure 5.11: 20×magnification micrograph of scratch on Sample A, an amorphous carbon coated UHMWPE substrate ion implanted with nitrogen at 15KeV and a dose of 1×10^{15} particles/cm^2

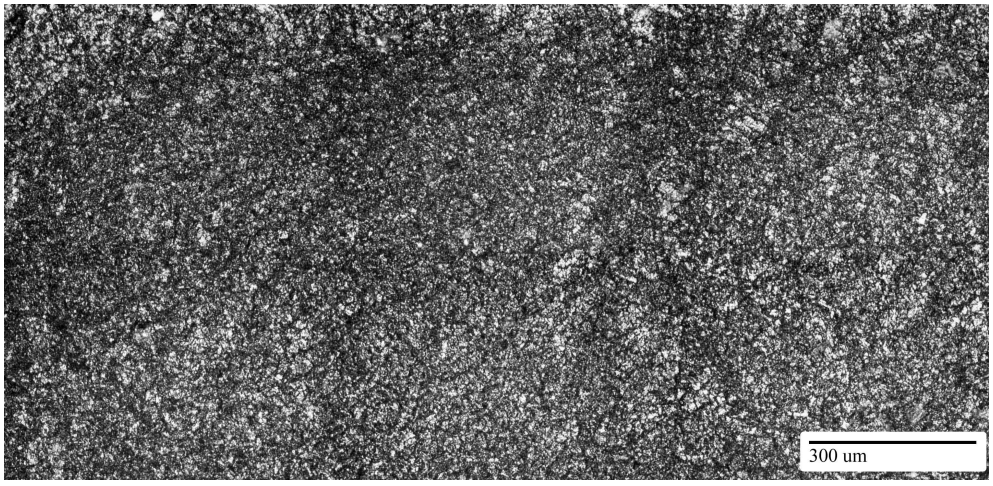

Figure 5.12: 20×magnification micrograph of scratch on Sample B, an amorphous carbon coated UHMWPE substrate ion implanted with nitrogen at 15KeV and a dose of 5×10^{15} particles/cm^2

of the high surface roughness of their Sample (1μm R_a) it was suspected that the coating was fracturing in the troughs and causing micro-segments to form; this may be occurring in the UHMWPE discs used in this study, which have a surface roughness of 0.29μm R_a.

5.5 Summary

Within this chapter the adhesion characteristics of the coatings deposited for this study have been discussed. Scratch testing was used to determine this and found that of the coatings deposited onto CoCr, the coating with the CoCr interlayer (Sample 5) was the most adherent and resistant to the scratch test. The 80V bias coating (Sample 3) and 60 to 40V transition bias (Sample 4) coating were the least adherent.

It was not possible to quantify the adhesion of the coatings deposited onto UHMWPE as substrate deformation prevented this. It was however established that Samples C and D, which were precoated with chromium and then ion implanted with nitrogen did not have particularly good adhesion compared with Samples A, B and E. In all of the UHMWPE samples, the deposited coating exhibited signs of cohesive failure, cracks being observed across the surface.

6. Coating Toughness

6.1 Introduction

During the gait cycle, loading is applied cyclically to the hip joint and separation between the femoral head and acetabular cup occurs. Some wear simulators tests consider this by inducing micro-separation (Nevelos *et al.*, 2000; Mak *et al.*, 2002). Fatigue and toughness of a coating deposited onto hip joints is therefore going to play a role in it's overall performance.

Micro-impact testing is a technique which can be used for low cycle, accelerated fatigue testing of coatings (Beake *et al.*, 2001b, 2004). Before this technique, toughness was commonly gauged by the length of cracks formed from the corner of a Vickers indentation; this technique however is prone to significant uncertainty (Anstis *et al.*, 1981).

The micro-impact test typically causes an initial plastic deformation which leads to the formation of subsurface cracks; subsequent impacts cause crack growth until there is a fracture which causes a sudden change in depth. As the test continues further cracks and fractures occur. These effects can be measured by (Beake *et al.*, 2004):

1. The final depth of the probe at the end of the test
2. The presence of fractures
3. The time to first fracture

4. Probability of fracture within a given time

6.2 Method

A Nanotest device previously described in Section 4 was used at the Micro Materials Ltd. site (2009). The device had been modified by placing a solenoid at the bottom the pendulum (Figure 6.1). A cube corner indentor was used instead of a Berkovich tip.

The solenoid enabled the indentor to be lifted from the surface of the test piece by 9μm and subsequently accelerated back to the sample with a force of 5, 25 or 50mN. These impacts occurred every 4 seconds over a 300 second test duration.

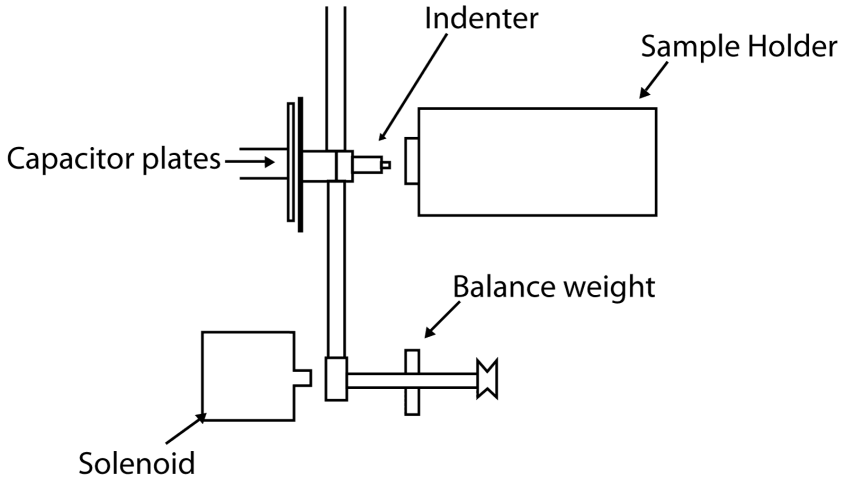

Figure 6.1: Micromaterials NanoTest schematic with solenoid

6.3 Results

6.3.1 CoCr Substrates

The response of the coatings to initial impact was similar in all cases; the initial impact (the depth of the first impact) deformed the coating and substrate resulting in a depth of 389-777nm for a load of 25mN (Sample 5 and 3 respectively) and 776-1,352 for a load of 50mN (Sample 5 and 3 respectively); this can be seen in Table 6.1. The following impact resulted in failure of the coating and larger depths being recorded.

Table 6.1: Indentation depth into coated CoCr substrates

	Initial indent depth (nm)		Final Depth (nm)	
	25mN	50mN	25mN	50mN
Sample 1	440	794	3,187	5,047
Sample 2	671	1,028	3,049	4,980
Sample 3	777	1,352	4,128	5,487
Sample 4	690	1,028	3,021	4,679
Sample 5	389	776	2,645	4,692

Table 6.2: Rank order of coated CoCr substrates by indentation depth

	Initial indent depth (nm)		Final Depth (nm)	
	25mN	50mN	25mN	50mN
1	CoCr Interlayer	CoCr Interlayer	CoCr Interlayer	60-40V Bias
2	40V Bias	40V Bias	60-40V Bias	CoCr Interlayer
3	60V Bias	60V Bias =	60V Bias	60V Bias
4	60-40V Bias	60-40V Bias =	40V Bias	40V Bias
5	80V Bias	80V Bias	80V Bias	80V Bias

Subsequent impacts resulted in a gradual increase in depth, in the case of Sample 1, 4 and 5 this was a relatively slow increase which were followed after a series of impacts with a step change in depth associated with the fracture and delamination of the coating. In the case of Sample 3 - the 80V coating, fracture and failure occurred on the third impact in both 25mN and 50mN tests (Figure 6.2 and 6.3). The final indentor depth, measured at the last impact, for each coating is recorded in Table 6.1; similar to the initial impact depth, Sample 5, with the CoCr interlayer, performs well relative to the other coatings; while Sample 3, 80V bias, performs badly.

In light of this data on initial indent depth and final depth, it is possible to rank the performance of the coatings Table 6.2. Sample 5, the CoCr interlayer coating, consistently performs well relative to the other coatings, conversely Sample 3, the 80V bias coating is consistently the worst coating tested for toughness and fatigue resistance.

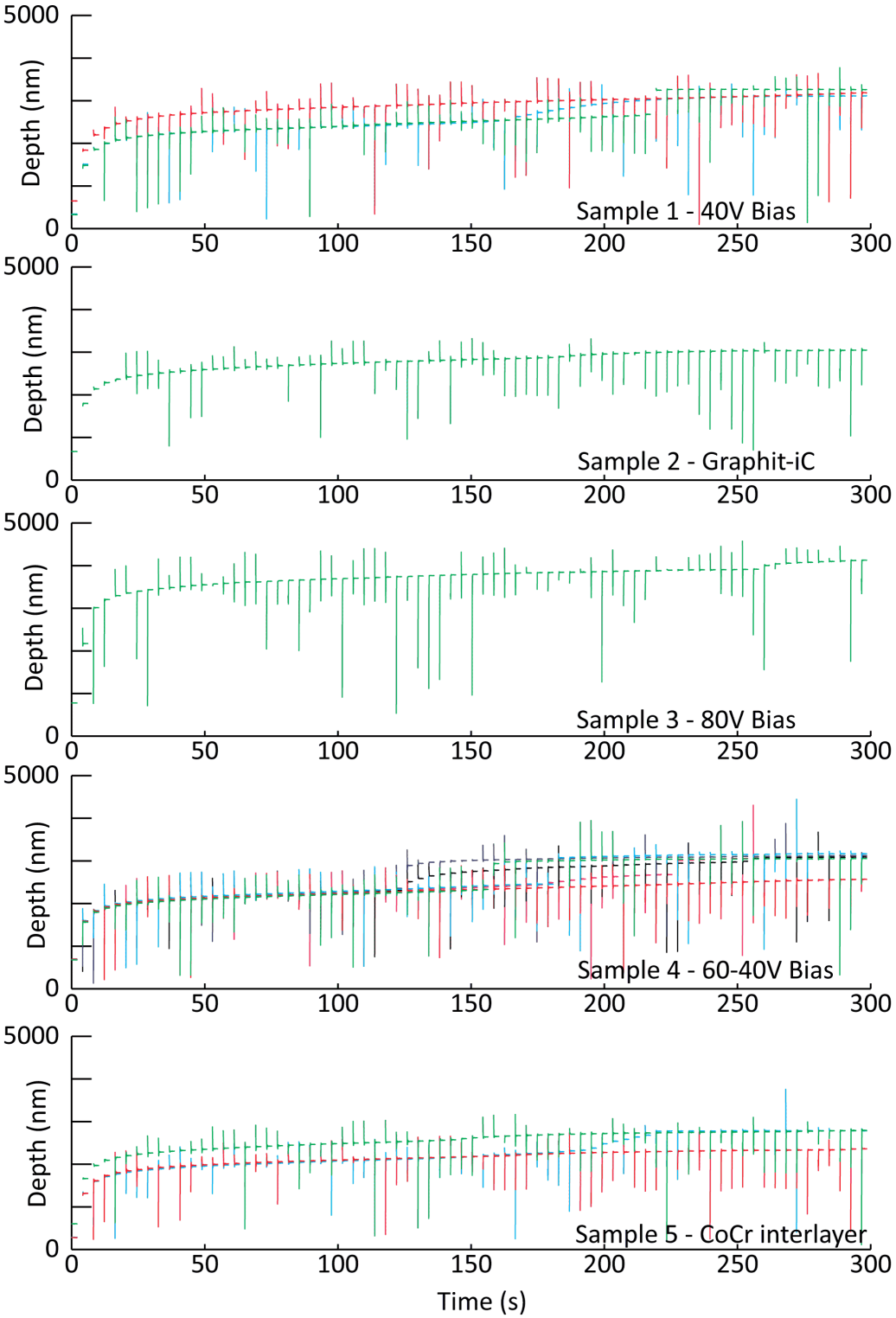

Figure 6.2: Depth-time profile of coatings when impacted with a force of 25mN

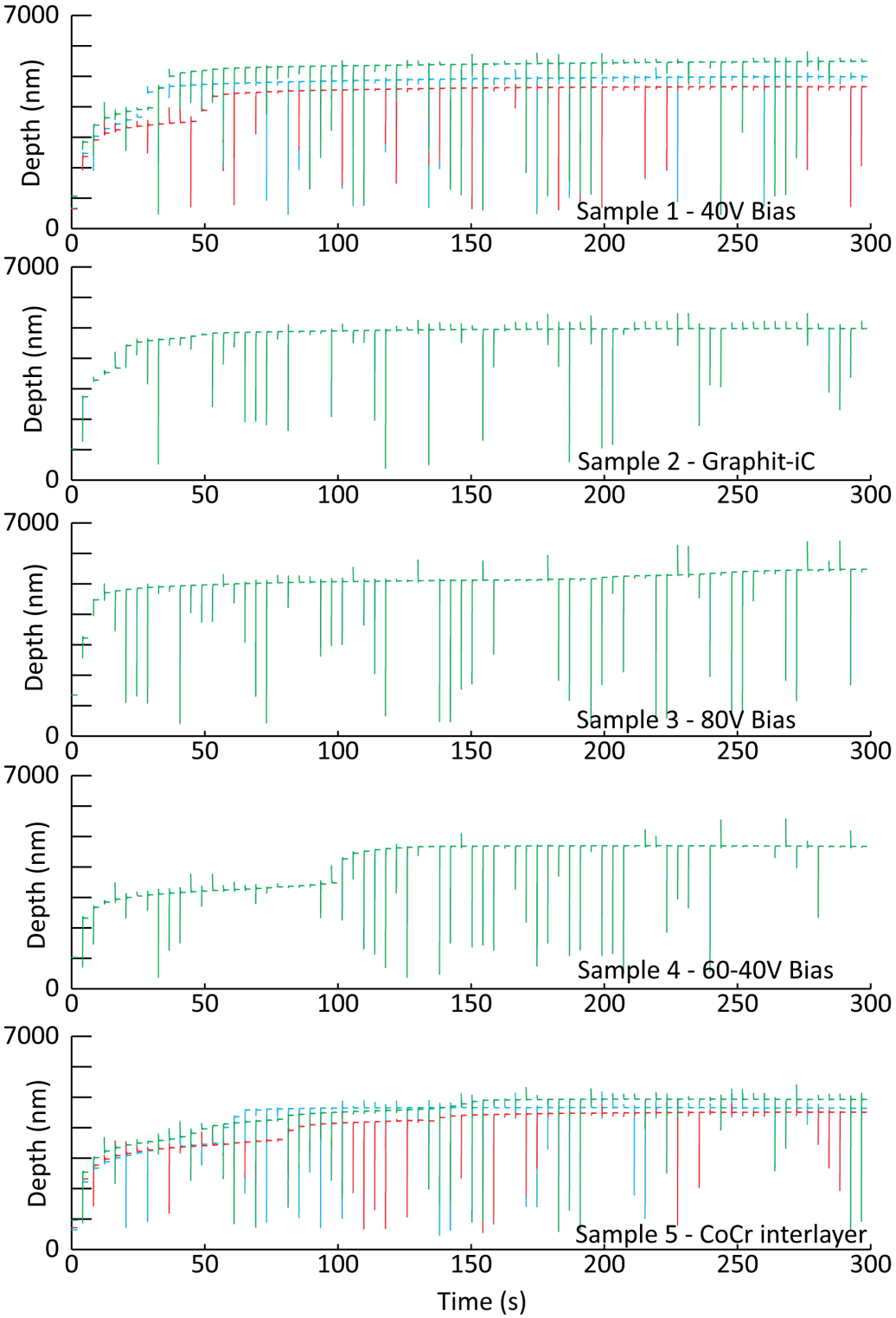

Figure 6.3: Depth-time profile of coatings when impacted with a force of 50mN

6.3.2 UHMWPE Substrates

Testing was carried out on Sample A, the UHMWPE substrate modified by nitrogen ion implantation with 15KeV energy and a dose of 1×10^{15}particles/cm^2. The indentor was accelerated with a force of 5mN and 25mN. In both cases the coating failed after the first impact because the substrate was unable to support the coating. This can be seen in Figure 6.4 (for clarity only the first 50 seconds are shown in the figure, for the remainder of the 300 second test there was a steadily increasing depth) with the initial impact achieving a depth of 939 and 11,908nm at 5mN and 25mN respectively, jumping to 6,608 and 15,446nm at the second impact and final depths of 9,894 and 15,997nm. No further tests were carried out on UHMWPE substrates because the effect of the UHMWPE will dominate with these test parameters.

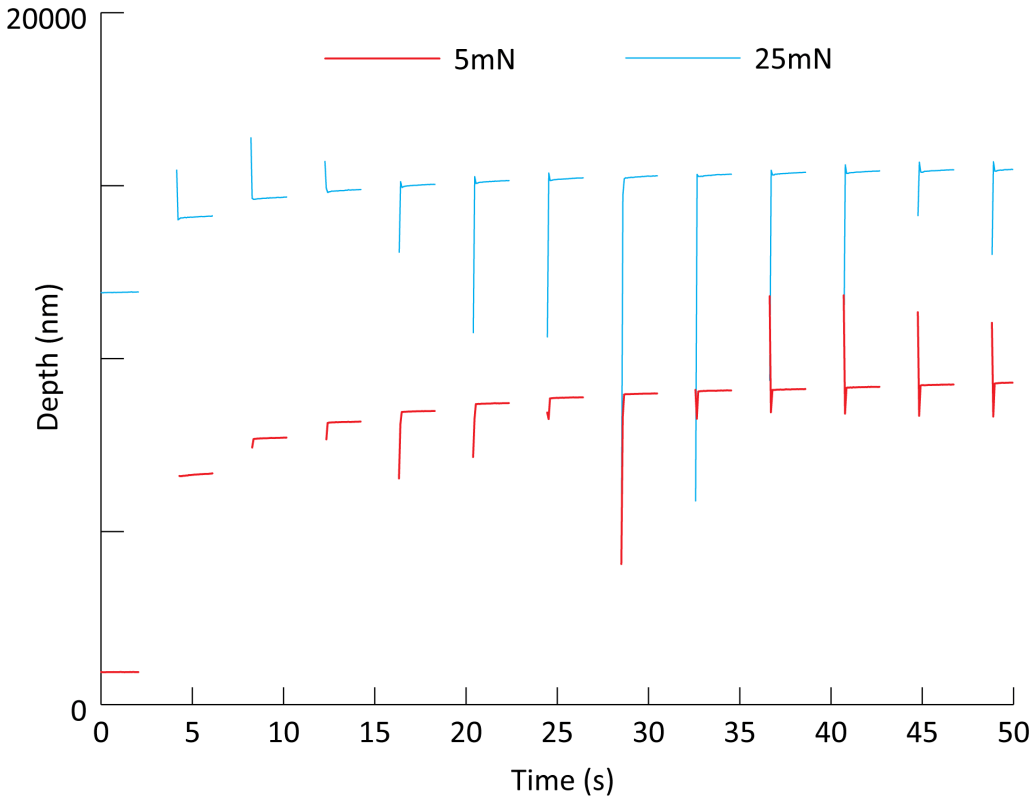

Figure 6.4: Depth-time profile for UHMWPE impacted with a force of 5mN and 25mN

6.4 Discussion

In order for statistically valid quantitative data to be obtained it is necessary to obtain repeats of tests carried out; time factors prevented repeats being taken on all tests in this series however trends can be seen within the data; the results correlate well when comparing the 25 and 50mN forces suggesting that the tests without repeats are not anomalous. By ranking the coatings they can be compared relative to each other. The rank order of initial penetration and final penetration (Table 6.2) compares the relative toughness of the coatings (Beake *et al.*, 2001a).

To date, there has been relatively little investigation into the fracture toughness of coatings deposited onto substrate materials; this is in part due to the difficulty of adequately quantifying the data; Zhang *et al.* (2005a) has reviewed the various methodologies and highlighted the difficulties associated with not having a standard procedure. Consequently there is little data available to draw a comparison with.

The technique used here has been used previously on the Graphit-iC^{TM} coating (Beake *et al.*, 2004). Different test parameters were used, although there does appear to be similarities within the data, lower impact forces were used and this resulted in lower penetration depths as well as a longer period to coating fracture. The article suggests that intrinsic stress and adhesion may be more important characteristics than hardness for resistance to impacts. Data collected here would lend support to this theory.

The two coatings developed here with the highest hardness, the CoCr interlayer coating and the coating with an 80V bias (Section 4) rank at the opposite extremes when it comes to their fracture resistance, the CoCr interlayer coating performing consistently well, while the 80V bias coating performs consistently badly (Table 6.2).

The adhesion, which has been related to the intrinsic stresses of the coating (Section 5.4), correlates when compared with the initial penetration, but this is not the case when comparing the final depths, which results in the 40V bias coating and 60-40V transition bias coatings swapping 2nd and 4th positions. This could be attributed to the effect of fatigue on the coating.

Fatigue of the coating can be interpreted by the presence of steps in the depth-time graphs. The presence of a sudden change in depth was indicative of delamination or failure of the coating, which can be seen by examination under microscope (40x). Figure 6.5 illustrates this delamination on Sample 4. The first repeat does not delaminate, which can be seen in the micrograph image and is reflected in the depth-time profile with no sudden change in depth. Repeats 2 and 3 delaminate; this is can be observed in their micrograph images and by the sudden change in depth in their associated depth time profiles. These delaminations and fractures result from the coalescence of subsurface cracks that develop from the cyclic action of the impacts and is indicative of fatigue (Beake *et al.*, 2004). Considering this, Samples 4 and 5 demonstrate the most fatigue resistance at 50mN; at 25mN Samples 4 and 5 performed similarly well. At 25mN the Graphit-iC^{TM} also performed well, although there were no repeats, the single

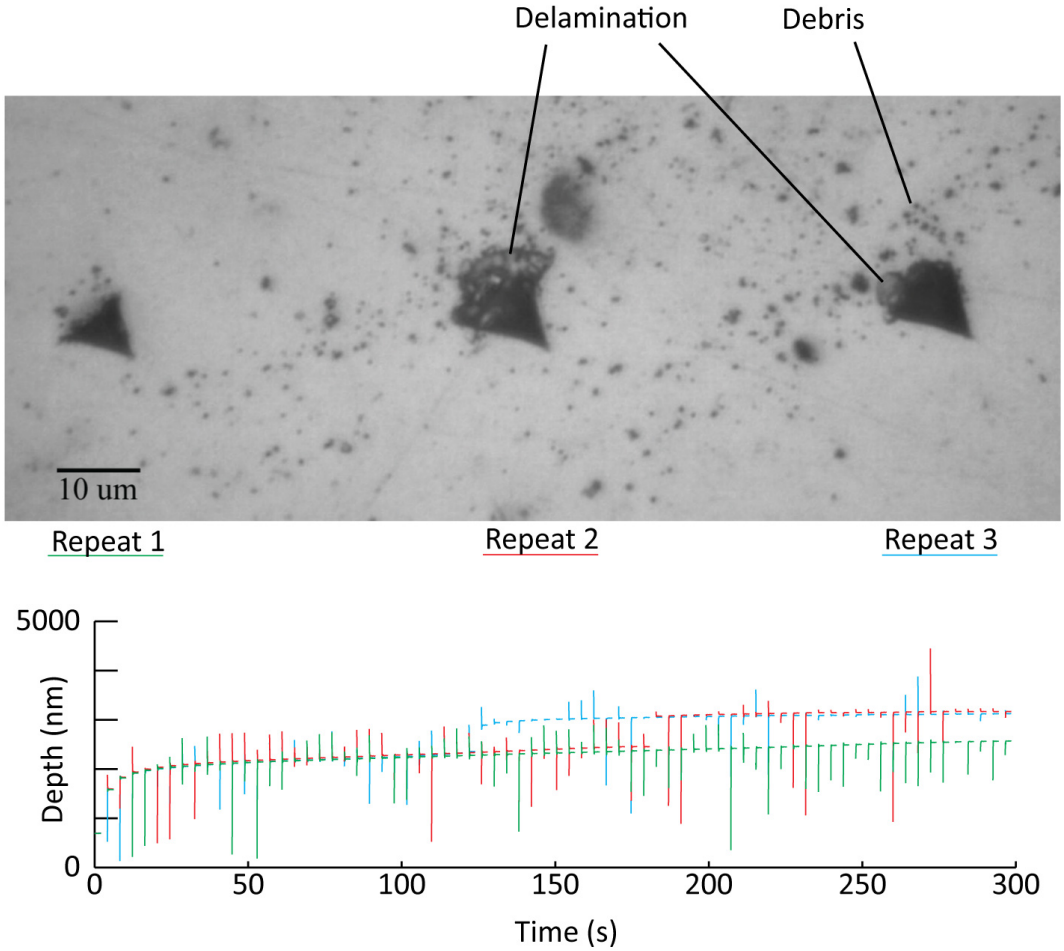

Figure 6.5: Comparison of depth-time profile with micrograph of resulting indents on Sample 4 - 60-40V transition bias, force 25mN

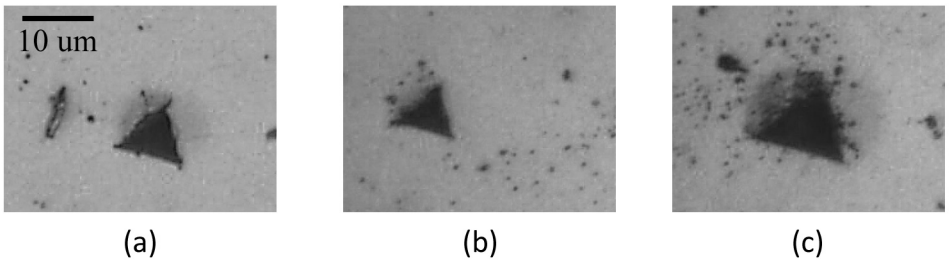

Figure 6.6: Micrograph of indents showing no fracture (a) Sample 2 - Graphit-iC, (b) Sample 4 - 60-40V transition bias (c) Sample 5 - CoCr interlayer

test did not exhibit signs of fracture (Figure 6.2 and 6.6).

6.5 Summary

The toughness and fatigue properties of the coatings deposited for this study are reported in this chapter. It was found that the coating with a CoCr interlayer ranked highest in all toughness criteria and the coating deposited with an 80V ranked last in all criteria.

It is likely that difference between rank order for the initial and final indentation depths is related to the fatigue properties of the coating. This resulted in the 60-40V transition bias coating moving up the rank order to 2nd place.

Low cycle impact testing on the coated UHMWPE substrate resulted in failure of the coating due to the substrate being unable to support the load.

7. Coating Wear And Friction

7.1 Introduction

Wear performance is one of the critical factors for any hip prosthesis. Hip joint wear simulators attempt to fully simulate the wear seen in a natural joint in both load and motion as well as lubrication. Gait varies from person to person within a range of normality. The range of motion and loading of the joint depends on many factors including the person's weight, muscle strength, height and the speed at which the person is moving. Consequently, the loading and motion used in a simulator can only approximate the natural gait. Numerous studies have been carried out examining the gait cycle, using both indirect (Paul, 1967) and direct (Rydell, 1966; Bergmann *et al.*, 2001) methods. The gait and loading cycles used in simulators are simplified and the majority of simulators use different cycles, including the Durham simulators (Smith and Unsworth, 2001), Leeds simulator (Dowson and Jobbins, 1988; Barbour *et al.*, 1999) and HUT simulator (Saikko, 1996; Saikko and Ahlroos, 1999). An international standard exists (Technical Committee ISO/TC 150, Subcommittee 4, 2002) which specifies a loading and gait cycle.

Bovine serum is commonly used as a lubricant for hip simulation; Ahlroos and Saikko (1997) reports that the serum sufficiently replicates in-vivo conditions. The International standard (Technical Committee ISO/TC 150, Subcommittee 4, 2002) specifies that 25% bovine calf serum is used for lubricating the joint. However, debate continues over the required concentration, with the ASTM standard

Table 7.1: Parameters of various pin on disc studies in the literature

Paper	Rotational Speed (ms^{-1})	Contact Pressure	Distance (m)
Saikko (1998)	0.0204	10MPa	60,000 approx
Joyce *et al.* (2000)	0.052	2.04MPa	172,400
Platon *et al.* (2001)	0.1	pin: 0.25MPa; ball: ϕ10 or 26mm: 3.7N	1,080
Serra *et al.* (2002)	0.3-1.0	33.47N (ϕ5.0mm hemisphere)	3,000
Gispert *et al.* (2006)	0.046	0.39-1.53MPa	1,000
Hoseini *et al.* (2008)	0.1	9MPa	17,200

F732-00 allowing for a range from 25% to 100% (American Society for Testing and Materials, 2006). The ISO standard also suggests, but does not require a minimum protein mass concentration of 17g/l, this is due to the increasing wear that has been observed with increased protein concentration (Wang *et al.*, 1999b).

Full simulation of a joint is time consuming and prohibitive in most cases. Early trials can use pin on disc techniques, which are cheaper and faster than full simulation while still producing wear and tribological data.

The contact pressure, speed and sliding path between pin and disc can all be varied; it is also possible for the pin to oscillate against the disc. These parameters vary largely between different studies (Table 7.1).

The influence of these parameters on the wear factor varies, load and distance of travel having the largest impact, this is reflected in the Lancaster equation (Lancaster, 1973) which states: $V = kLx$ where V is the volume of wear, x is the sliding distance and k is the wear factor.

The Lancaster equation does not consider other factors such as sliding velocity

and contact stress although their contribution to the wear is debated. Sliding velocity has been considered in work by Fisher *et al.* (1994), who demonstrated that when varying the velocity from 0.035 to 0.240ms^{-1} there was no significant difference between wear rates. Other fields, which have used pin on disc methods have found that varying speeds does have an effect on wear (Ravikiran and Surappa, 1997; Gomes *et al.*, 2001) however, these studies are not representative of parameters used in orthopaedics, having different speeds, lubricating regimes, temperatures and other factors which will confound the influence of sliding speed.

The effect of contact stress is a more contentious issue. Rose *et al.* (1983); Barbour *et al.* (1995); Mazzucco and Spector (2003); Vassiliou and Unsworth (2004) and Saikko (2006) have all considered the effect. Barbour *et al.* (1995); Vassiliou and Unsworth (2004) and Saikko (2006) all found that as contact stress increases the wear factor decreases and that the effect is more pronounced when the stress is lower - if the stress is high, increasing it further will have less of an effect. This does not correlate with results published by Mazzucco and Spector (2003) who found that neither the load or the stress had an impact on the wear rate, instead their data suggested that the contact area impacted the wear rate. Rose *et al.* (1983) also found only the load impacted the wear rate, as suggested by the Lancaster equation. It is not clear why these studies are not in agreement; the area requires further study before an understanding of the mechanisms involved can be reached.

The track which the pin follows on the disc is also of importance, particularly when investigating UHMWPE (Bragdon *et al.*, 1996; Wang *et al.*, 1996; Saikko,

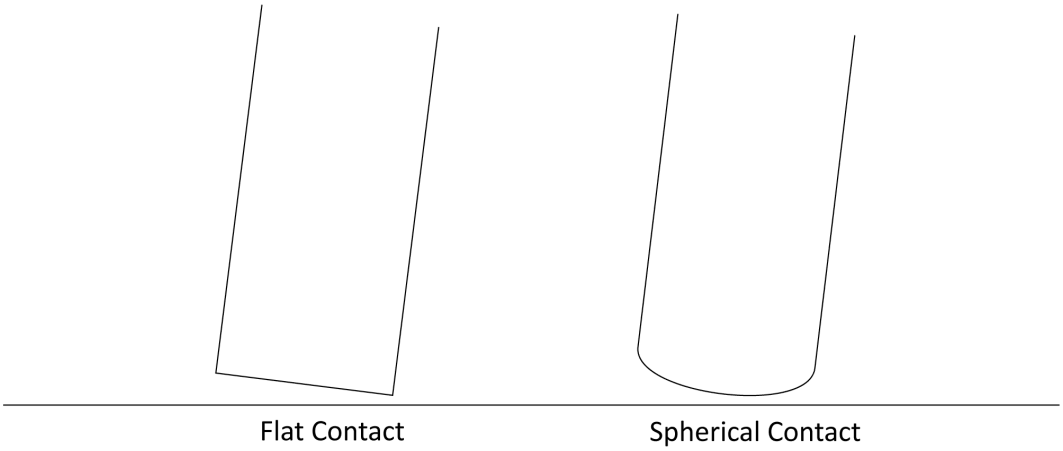

Figure 7.1: Drawing of poorly aligned pin geometries

1998); the wear of UHMWPE when tested using a unidirectional pin on disc method exhibits a level of wear orders of magnitude lower than that seen in vivo. This is because the material undergoes strain hardening in the direction of loading as the polymer chains realign (Wang *et al.*, 1997). Multidirectional pin on disc methods cause the UHMWPE to undergo strain softening and consequently produce more realistic wear levels (Joyce *et al.*, 2000; Saikko, 1998). A similar effect is seen when testing metal on metal combinations, pin on disc studies have shown an increase in wear with unidirectional tracks as opposed to multidirectional tracks (Tipper *et al.*, 1999; Scholes and Unsworth, 2001); it is thought that the multidirectional sliding polishes the components thereby reducing wear.

In addition to the parameters such as load, pressure, speed and time, as well as the wear track; pin on disc test configuration geometries can also vary: loads can be applied through a rounded end onto a flat disc or a flat pin onto a disc (Figure 7.1). The rounded contact is most forgiving to any misalignment although the contact area will progressively increase as wear occurs (Garcia-Prieto *et al.*, 2004;

Besong *et al.*, 2001). The flat pin will present a constant contact area as it wears, although in the event of any misalignment there will be an increase in contact pressure and uneven wear. This is particularly problematic for coated materials as the pressure could damage the coating and cause early failure (Besong *et al.*, 2001).

Studies attempt to use parameters which obtain wear rates which correlate with those found in-vivo. This is possible for standard orthopaedic materials such as UHMWPE, steel, CoCr and titanium alloys which have a wealth of in-vivo data available, but innovative materials pose a problem; particularly coatings, for which the author has been unable to obtain any quantitative in-vivo wear data from literature.

Wear factors relating to DLC coatings deposited for an orthopaedic application are predominantly from pin on disc studies as opposed to wear simulators. Sheeja *et al.* (2004) have examined the wear of DLC coatings deposited on CoCr sliding against similarly coated CoCr using unidirectional pin on disc tests and report a wear factor of between 6.8×10^{-17}m^3/Nm and 2.59×10^{-18}m^3/Nm. Platon *et al.* (2001) also use unidirectional pin on disc to report wear factors an order of magnitude lower than Sheeja *et al.* (2004), 3.7×10^{-19}m^3/Nm for DLC coated stainless steel components and 8.5×10^{-19}m^3/Nm for DLC coated titanium alloy components. Tiainen (2001) reports wear factors of less than 1×10^{-16}m^3/Nm for CoCr coated with DLC sliding against similarly coated CoCr.

Osterle *et al.* (2008) have used a reciprocating pin on disc method which recorded

a larger wear for DLC coatings on Ti6Al4V, they investigated amorphous carbons, hydrogenated amorphous carbons and TiN obtaining wear factors of 8.4×10^{-17}-1.2×10^{-16}m^3/Nm, 0.8-4.3$\times10^{-16}$m^3/Nm and 2.4×10^{-15}m^3/Nm respectively. This study was carried out using a droplet of water for lubrication which was refreshed every 12 hours. Osterle *et al.* (2008) acknowledge that bovine serum was not used and this could have an impact on the wear rate however, they do not consider that a single droplet as opposed to full immersion may also have an impact; this may have affected the result for the hydrogenated carbon coating as others (Field *et al.*, 2004; Meunier *et al.*, 2005) report that hydrogenated DLC films do not perform as well as unhydrogenated carbon films under wet conditions. Another reciprocating pin on disc study has been carried out by Williams *et al.* (2003) who report a wear factor of approximately 8×10^{-15}m^3/Nm for TiN coated CoCr components.

In this chapter the wear of coatings deposited for this study is discussed, having been determined using a pin on disc method.

7.2 Method

7.2.1 Pin on Disc Configuration

The pin on disc test device used was the Teer Coatings Ltd POD-2 test device (Figure 7.2). The device is limited to producing unidirectional motion by rotating the disc underneath a static pin.

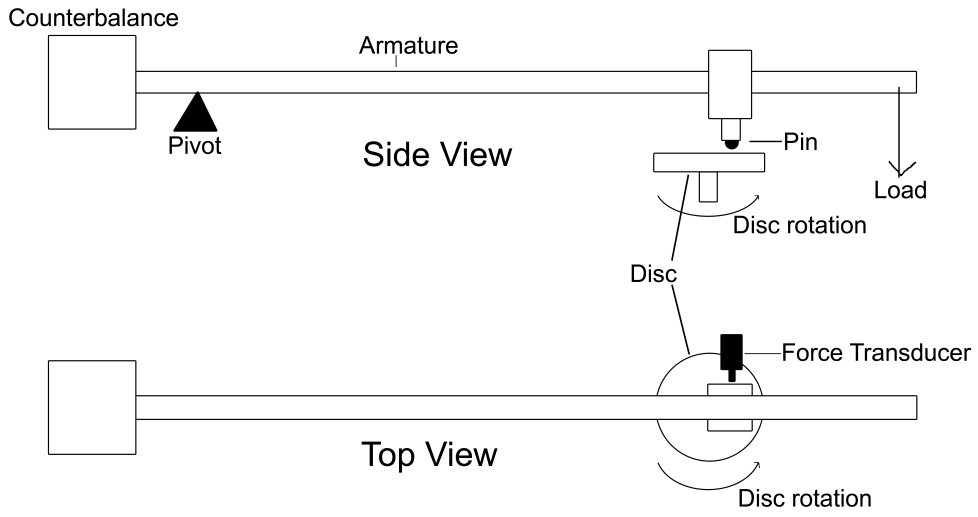

Figure 7.2: Schematic of Teer Coatings Ltd. pin on disc tester

The armature (Figure 7.2) loads the pin onto the disc. By offsetting the armature so that the pin is not central to the disc a circular wear track will be formed. The friction between the disc and pin generates a tangential force in the armature which rests against a secured force transducer. The transducer is linked to a computer which records the force. Because the applied load is known it is possible to calculate the friction.

The Teer Coatings Ltd. POD-2 is configured to use a spherical contact from a ball bearing however, they are difficult to obtain if made from orthopaedic materials. To obtain a spherical contact a pin with a hemispherical end is easier to produce. The pin could be re-machined and polished however, this would take time; destroy any previous wear scars thereby preventing further investigation and would make the pin shorter which, due to the design of the pin on disc device, would alter the loading.

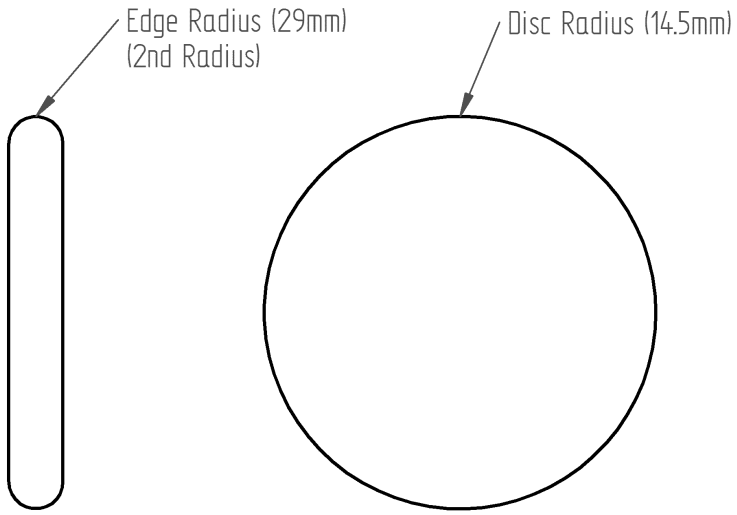

Figure 7.3: Orthographic projection of double radius "pin" (not to scale)

The edge of a disc can be used as the pin to obtain the required spherical contact, by machining a second radius onto the edge. By introducing a second radius to the edge of the disc it is possible to remove the risk of an edge contact (Figure 7.3). If the edge radius and disc edge are equal it would result in a spherical contact. By increasing or decreasing the edge radius, different contact pressures can be achieved although the contact is no longer spherical in nature.

For clarification, throughout this study, this "disc edge pin" will be referred to as the "pin"; the pin edge radius and disc radius are shown in Figure 7.3.

The pins used in this study had a disc radius of 14.5mm, constrained by material supply and ability to modify the test machine to accommodate a larger pin; the edge radius was decided to be 29mm (Figure 7.3). A larger edge radius is more prone to form error during machining due to the increased tolerance required. Form error being the deviation best fit radius arc.

7.2.2 Disc Manufacture

The discs used for all testing in this thesis were made from either CoCr or UHMWPE. The discs of CoCr were cut with a 4mm thickness using wire electro-discharge machining from a single 29mm diameter bar of CoCr supplied by Firth Rixon Ltd (2005); the bar conformed to ASTM F75 (American Society for Testing and Materials, 2007), a low carbon, cast composition. The surface finish of the CoCr disc was reduced to between 4 and 10nm R_a by lapping. Discs of UHMWPE were cut to the same thickness from a bar 45mm in diameter by Perplas Ltd (2005); the parts had an average surface finish of 0.29μm R_a, within the 2μm R_a specified by ISO7206-2 (Technical Committee ISO/TC 150, Subcommittee 4, 1996).

These roughness, and all future roughness measurements, were made using a contact profilometry technique. By drawing a stylus over the surface of a material, it is possible to measure the surface roughness and form. The vertical deflection, as it is drawn across the surface can be recorded with a resolution of up to 1nm. Contact profilometry is more suited to 2D datasets as the stylus only has to pass over the sample once. It is possible to build 3D datasets by passing the stylus over the sample multiple times, offsetting each new pass, however this is extremely time consuming and more suited to interferometric techniques described and used later in this study (Section 7.2.5).

The primary advantage of contact techniques over white-light interferometry is the large scan size. Laterally this is can be in the region of 100mm and verti-

cal upward of 10mm compared to approximately 5mm lateral and sub millimetre vertical ranges for an interferometer. When measuring form and roughness, particularly on femoral head, the range available with the contact profilometry technique can be useful.

The profilometer used in this study was a Form Talysurf PGI 1200 manufactured by Taylor Hobson Ltd.

7.2.3 Pin Manufacture

Pins used in testing were manufactured from CoCr. They were cut from the same bar as the discs (Section 7.2.2), to the same dimensions. The pin was given it's edge radius by turning on a lathe using a forming tool; this obtained an average surface finish of 0.317μm Ra (standard deviation 0.068) and radius of 28.560mm (standard deviation 4.669).

Polishing was carried out using a 7 axis CNC Zeeko Ltd polishing machine. The Zeeko machine was able to maintain the radius giving repeatable form and surface finish. A Polishing pad of 12cm diameter was rotated in the F axis (Figure 7.4) and was able to move in the x, y and z axes, the pin to be polished was positioned at the virtual pivot point of the A, B and C axes.

During the polishing process, axis A was rocked through the arc of the pin edge radius while axis B was held in the position shown in Figure 7.4; this maintained the disc edge radius. It also required that the z axis be varied to maintain the distance of the polishing pad from the disc edge being polished; therefore because

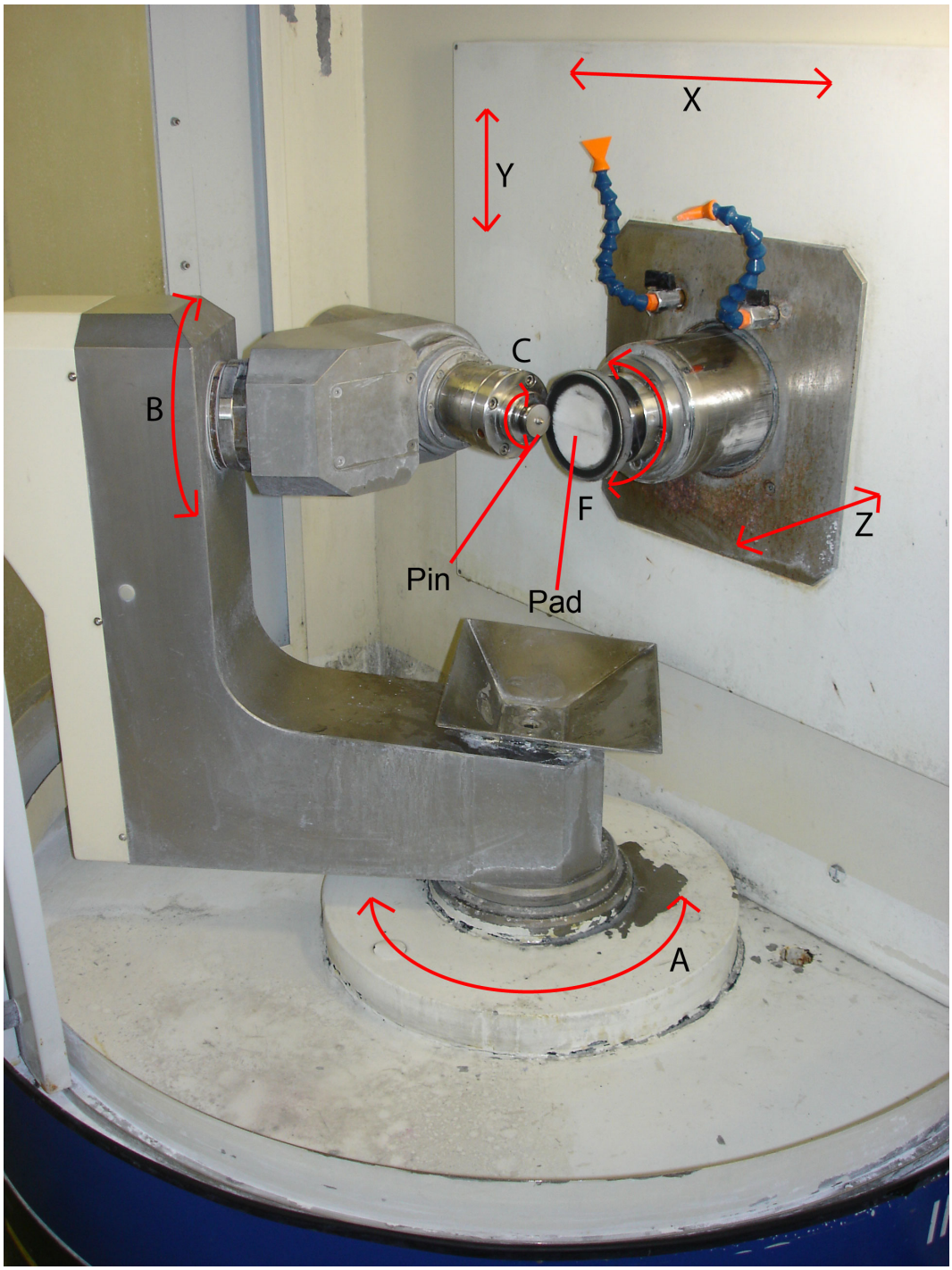

Figure 7.4: The 7 axes of the Zeeko CNC polishing machine

axis A was driven, z had to be calculated using Equation 7.1 . The derivation of Equation 7.1 can be seen in Appendix C.1, with a schematic being shown in Figure C.1.

$$z = \sqrt{(R_d - R_e)^2 + R_e^2 - (2(R_d - R_e)R_e\cos(\pi - \theta))}$$
$$\cos\left(\theta - \arcsin\left(\frac{\theta - (R_e\sin(\pi - \theta))}{\sqrt{(R_d - R_e)^2 + R_e^2 - (2(R_d - R_e)R_e\cos(\pi - \theta))}}\right)\right)$$
$$\mathrm{R_d} = \text{disc radius},\ \mathrm{R_e} = \text{radius at edge},\ \theta = \text{angle (radians) offset} \quad (7.1)$$

17 pins were polished using grit papers and diamond paste. When the polishing medium was changed the surface roughness and form was measured using a Taylor Hobson Form Talysurf PGI 1200. Realignment of the sample after measurement was not a critical factor. The initial surface roughness from turning of the lathe was 317nm (standard deviation 4nm) with a form of 28.56mm (standard deviation 3.41) and form error of 0.66μm (SD 0.32μm) . Initially 400 grit SiC paper was used followed by 600, 1,500 grit and finally 6μm diamond paste, which progressively improved the surface roughness (Figure 7.5). This achieved an average surface finish of 14nm (standard deviation 4nm), form of 30.58mm (standard deviation 4.88mm) and form error not exceeding 1μm with an average of 0.31μm (SD 0.27μm).

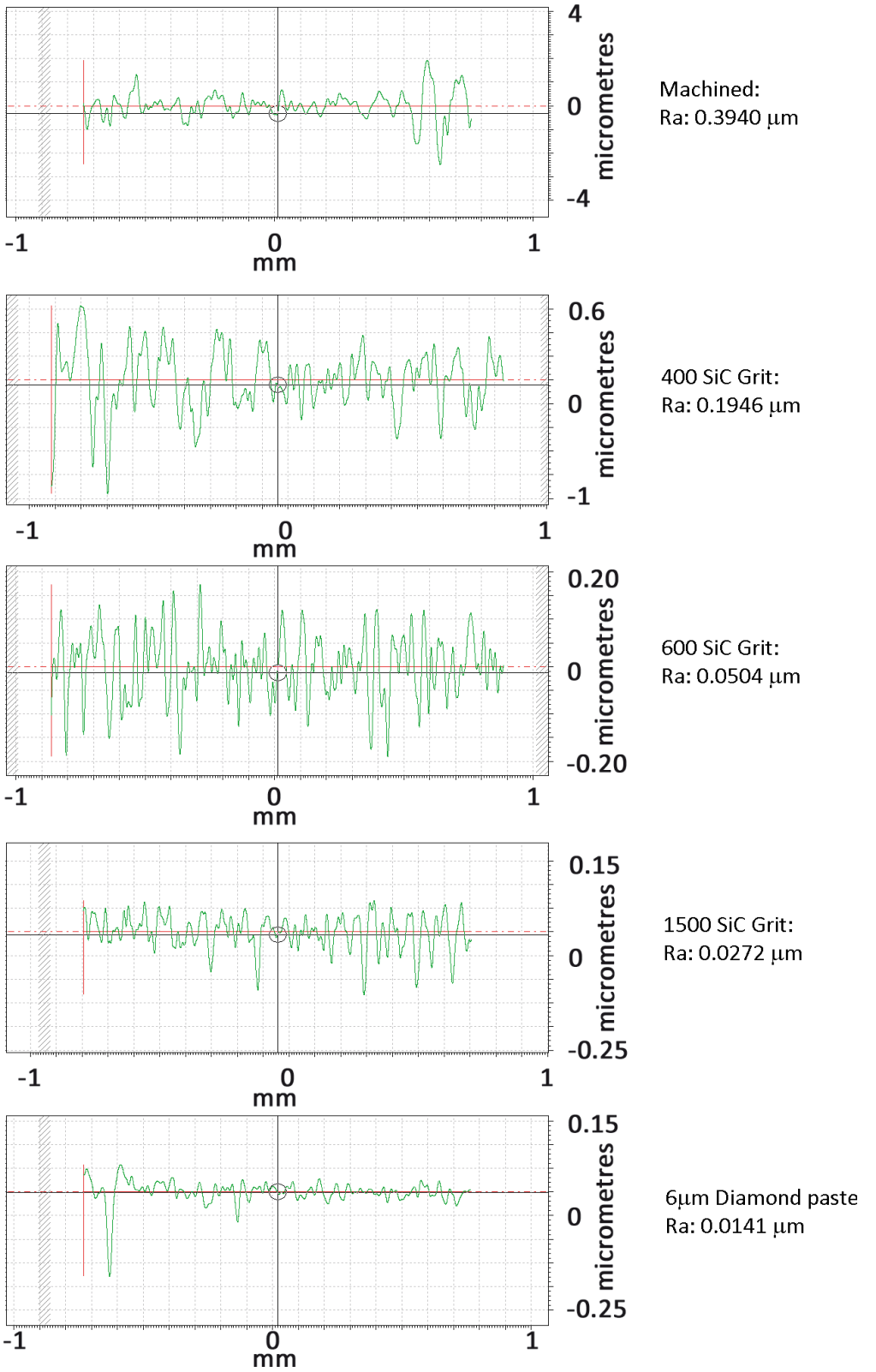

Figure 7.5: An example of the progressive improvement of surface finish on CoCr disc edges during polishing

7.2.4 Pin on Disc Testing Parameters

The testing was separated into two groups dependent on the substrate the coating had been applied to - either CoCr or UHMWPE. The tests were carried out in 25% bovine serum although protein concentration was not measured as it was believed that due to the loads being used, a boundary lubrication regime would be present; controlling the protein concentration would not affect this case because the load was the dominant factor. The linear velocity was chosen to be 100mms^{-1}, similar speeds have been used by Platon *et al.* (2001); Hoseini *et al.* (2008); Serra *et al.* (2002) which ranged from 100-1000mms^{-1}.

A load of 20N was applied which results in a mean contact pressure of 370MPa, peak 560MPa, for CoCr-CoCr contact and 30-40MPa for CoCr-UHMWPE contact. These values are higher than those used in studies utilising a flat pin, such as Saikko (1998); Joyce *et al.* (2000) who used pressures of 10MPa and 2.04MPa respectively (Table 7.1); studies using spherical contacts however are closer, Platon *et al.* (2001) obtaining pressures of 181-668MPa for MOM contacts and 12-23MPa for POM contacts. Serra *et al.* (2002) also tested with mean contact pressures ranging from 1.05-1.26GPa.

7.2.4.1 CoCr Substrates

A CoCr pin, coated with one of the coatings described in Chapter 3, Table 3.8 was tested while sliding against both an identically coated CoCr disc, or an uncoated CoCr disc (Table 7.2).

Table 7.2: CoCr substrates test matrix

	Pin Coating (Sample number)					
Plate Coating	1	2	3	4	5	uncoated
1	x					x
2		x				x
3			x			x
4				x		x
5					x	x
uncoated						x

The tests were run for 1 hour which resulted in travelling distance of 360m. This is shorter than other tests, Platon *et al.* (2001); Gispert *et al.* (2006) having used a sliding distance of 1,000m and 1,080m respectively, other longer tests by Saikko (1998); Joyce *et al.* (2000) have been run for 60,000m and 172,400m respectively.

The longer tests take into consideration the fact that MOM contacts have higher rates of wear during the first 500,000 cycles (Medley *et al.*, 1996; Scholes *et al.*, 2001; Streicher *et al.*, 1996), which is known as "run-in wear", after this period the wear reduces to a steady state. To reach this number of cycles using parameters here, each test would take 3 days.

These tests along with those of Platon *et al.* (2001); Gispert *et al.* (2006) do not reach the point of steady state wear and will therefore overestimate the wear for the metal on metal contacts. Considering that the tests will not exceed 500,000 cycles, it is necessary to run them only as long as is necessary to measure the wear, in the case of the CoCr substrates this will be measured from the pin (Section 7.2.5) and not from the plates. Because wear on the plates is spread over a larger area, a more significant depth change has to occur to be measurable; this makes the test prohibitively long.

Each pin and disc combination was tested 3 times with a different disc and with an unworn area of the pin.

7.2.4.2 UHMWPE Substrates

The Graphit-iC^{TM} coated UHMWPE discs (Samples A-E) were tested against both a Graphit-iC^{TM} (Sample 2) coated CoCr pin and an uncoated CoCr pin (Table 7.3).

Table 7.3: UHMWPE substrates test matrix

	Pin Coating (Sample number)					
Plate substrate	1	2	3	4	5	uncoated
A		x				x
B		x				x
C		x				x
D		x				x
E		x				x

The wear was measured from both the pin and the disc using techniques described in Sections 7.2.5 and 7.2.6 respectively. The pin on disc test for this group lasted for 3 hours and resulted in a sliding distance of 900m. This is also shorter than other published work, but in the case of POM combinations there is no initial run in wear.

Each pin and disc combination was tested 3 times with a different disc and with an unworn area of the pin.

7.2.5 Measuring Pin Wear

The wear scar which formed on the pin is elliptical (Figure 7.6). Wear was

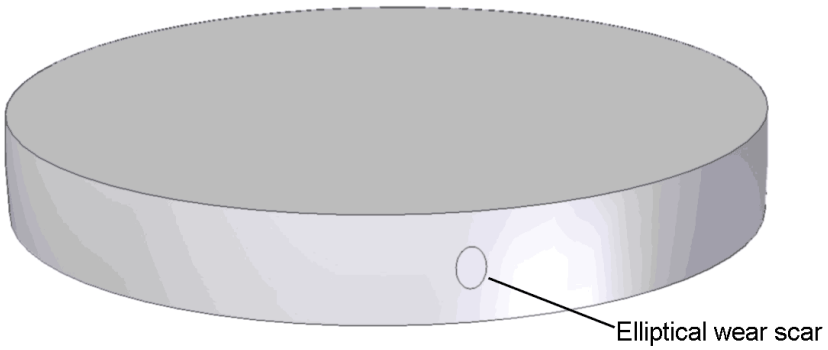

Figure 7.6: CAD image illustrating typical location of wear scar

calculated from the pin by examination under an optical microscope (10x magnification). The wear scar (Figure 7.7) diameter was measured so that volume loss could be calculated using Equation 7.2. The derivation of the equation can be found in Appendix C.2.

$$V = \pi \int_{R_d}^{\sqrt{R_d^2 - X^2}} \sqrt{R_d^2 - x^2}\sqrt{R_e^2 - (x + (R_e - R_d))^2}dx \tag{7.2}$$

R_d = disc radius (Figure 7.3) ,

R_e = disc edge radius (Figure 7.3),

x = radius of scar with respect to disc "edge" radius

To confirm the technique 6 of the pin on disc wear tests were also measured using white-light interferometry so that a comparison of the two techniques could be made. White-light optical interferometry can give sub-nanometre vertical resolution over a two dimensional surface. Interferometry typically uses a single light source which is split into two beams (Figure 7.8). One beam path is to the sample and reflects back to a camera. Simultaneously the second path is directed

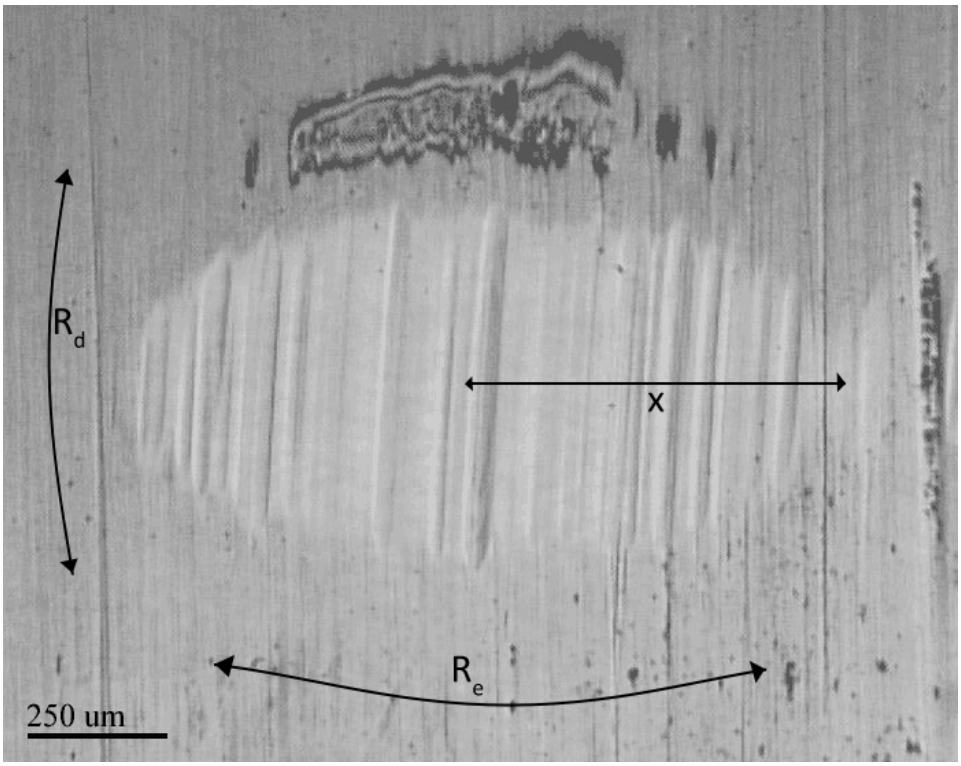

Figure 7.7: Typical wear scar on pin after pin on disc testing

to the same camera, but avoiding the sample. The camera combines the beams; any difference in path length causes a phase difference to be detected. The phase difference can be measured and used to identify the difference in path lengths. The interferometer used in this study was a Talysurf CCI 6000, manufactured by Talyor Hobson, UK.

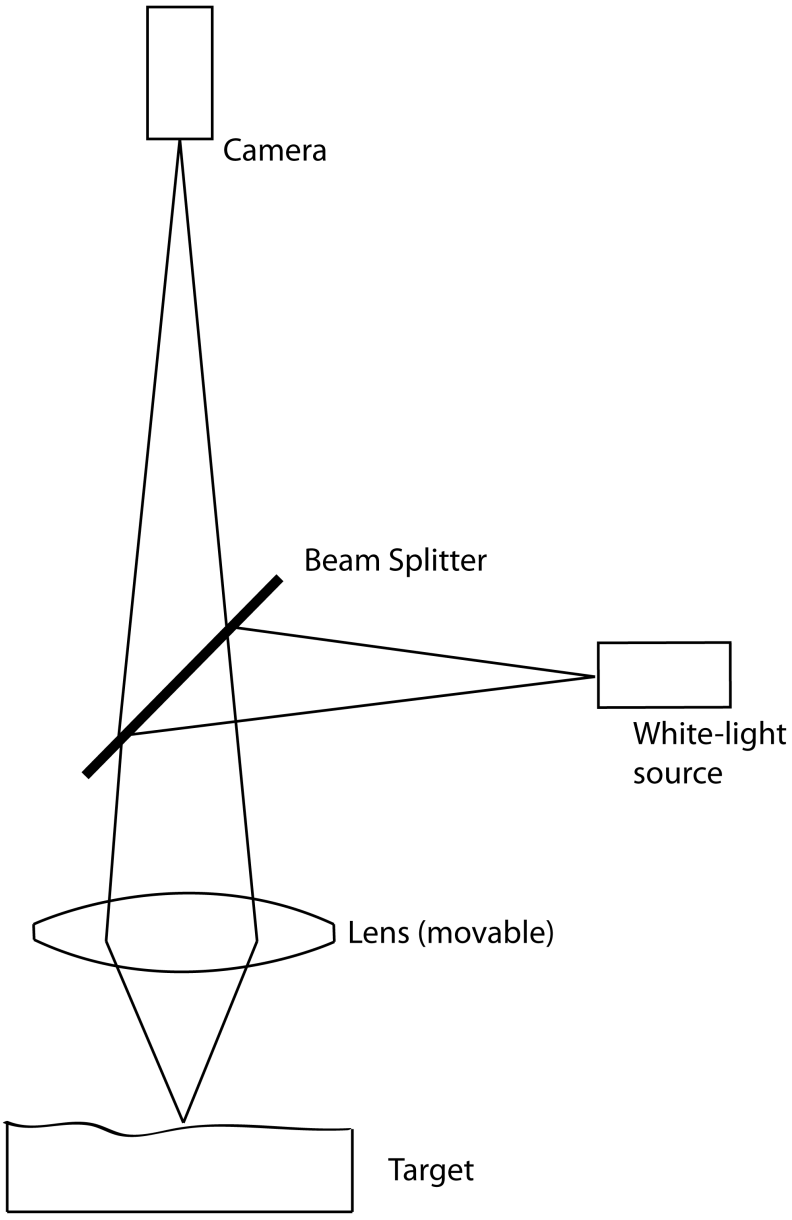

Figure 7.8: White-light interferometer

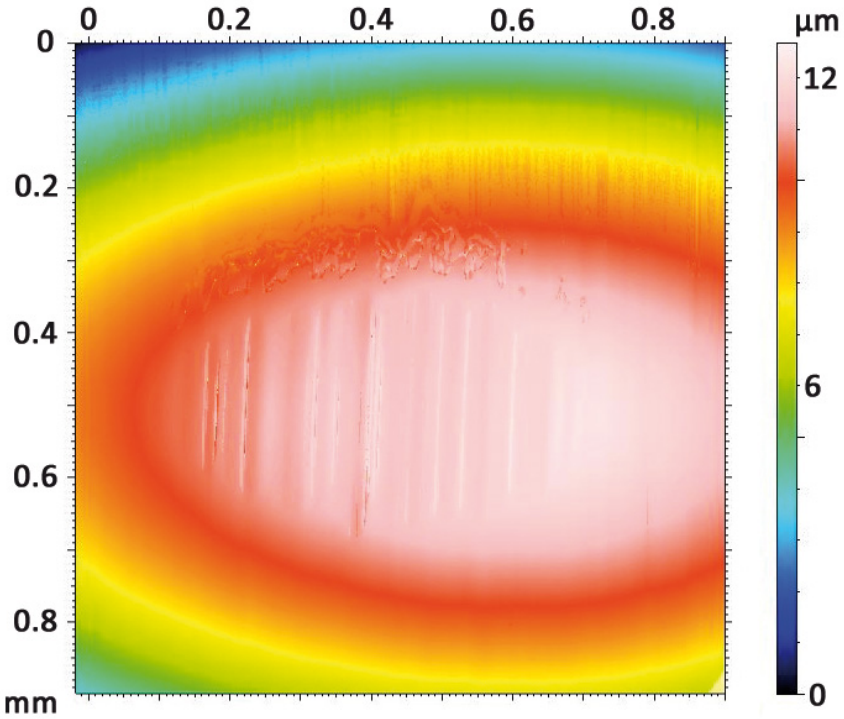

Figure 7.9: Scan of worn pin surface

A typical interferometric image of the wear scar can be seen in Figure 7.9; this illustrates the x y position in space and z position by colour. The equipment is able to remove the form from the scan (Figure 7.10). In effect this flattens out the disc and causes the wear scar to appear as a dip in the surface, this can be seen more clearly in a 3D representation (Figure 7.11). Once the form has been removed the volume of the hole can be calculated.

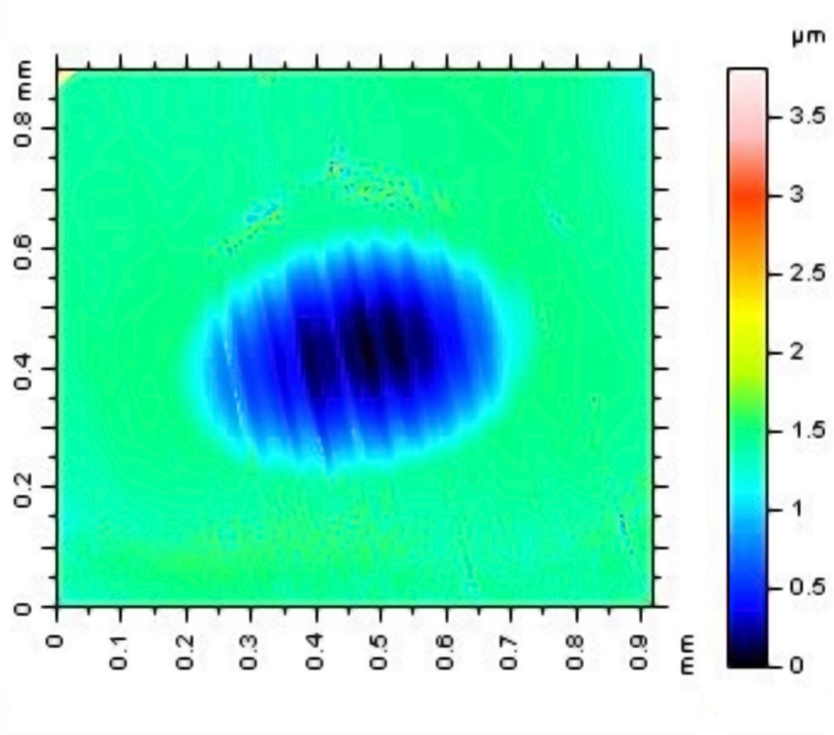

Figure 7.10: Form removal of worn pin

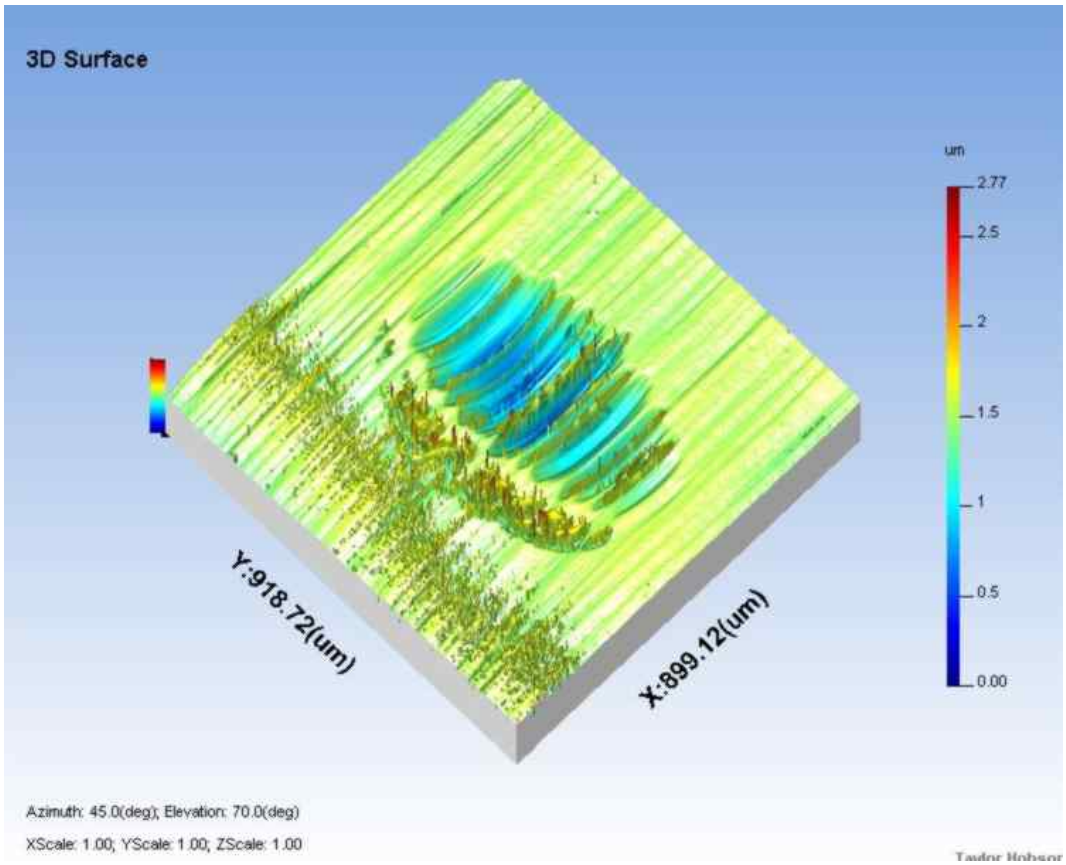

Figure 7.11: 3D representation of pin with form removed

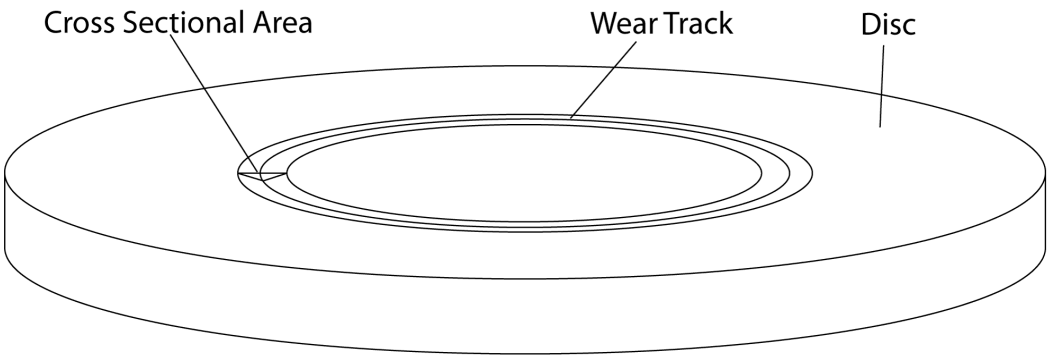

Figure 7.12: Diagram of disc wear track

A paired t-test was used to compare the wear calculated from the optical microscope measurements (4.45×10^{-5}mm^3, standard deviation 3.21×10^{-5}) and the wear calculated using the interferometer (3.17×10^{-5}mm^3, standard deviation 2.24×10^{-5}). It was found that the values were not significantly different ($p>0.05$), thereby validating the use of optical measurement.

7.2.6 Measuring Disc Wear

The volume of wear from the wear track can be calculated by measuring the cross sectional area of the wear track and multiplying by track length (Figure 7.12). The cross section can be approximated to be triangular and the area being the half the track width multiplied by the deepest part of the wear track (Stallard, 2005).

Measurement of the track depth can typically be measured using a optical microscope, however in this case there were two problems with this method: the wear was too small to measure a change, but more significantly there was a high

risk that the substrate would deform underneath the coating and therefore the measurement would include the deformation as wear. Consequently it was necessary to measure the thickness of the coating as opposed to the depth of the wear track. This was achieved by Rutherford Backscattering (RBS).

RBS obtains a spectrum by accelerating a positive ion, typically an alpha particle, at the material to be analysed. If it passes close to the nucleus of a substrate atom it will be deflected and backscattered. Detection and measurement of the energy of this backscattered ion at a given angle can be used to determine the atom that caused the backscatter and the depth within the sample.

At it's most simplistic an incident ion will be backscattered by a single substrate atom and be measured by the detector, the energy of the scattered ion can be related to the other factors by Equation 7.3 (M_1 = Mass of incident ion; M_2 = Mass of substrate atom; θ=scattering angle).

$$\frac{E_{scattered}}{E_{incident}} = \left(\frac{\sqrt{(1 - (\frac{M_1 \sin\theta}{M_2})^2)} + \frac{M_1 \cos\theta}{M_2}}{1 + \frac{M_1}{M_2}} \right)^2 \tag{7.3}$$

As the ion penetrates into the substrate it becomes more probable that any backscattered ion will be involved in additional collisions within the substrate, this is illustrated in Figure 7.13. Each collision decreases the energy of the backscattered ion, therefore a range of energies will be detected; decreasing from the maximum energy that is detected when there is only one collision; the range of energies is a function of the material thickness. The material density can also be calculated from the number of backscattered ions detected.

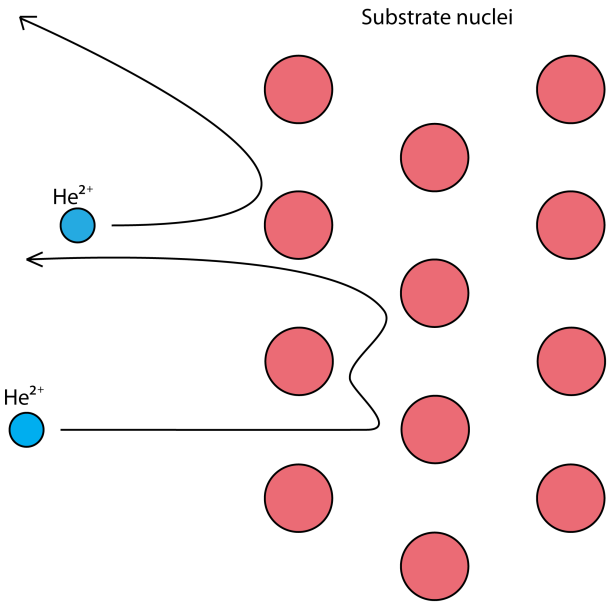

Figure 7.13: Backscattering of He^{2+}

Samples that contain multiple elements complicate analysis. The range of energies acquired from specific elements can superimpose making direct interpretation of the data impossible. Assumptions have to be made about the composition of the material to characterise the substrate. These assumptions are then used to mathematically model the RBS spectra, from the computational model the assumptions are refined in an iterative cycle until the measured spectra and the computed spectra match. Despite the difficulties in interpreting data the technique is extremely powerful, able to carry out depth profiling non destructively.

RBS analysis used in this thesis was carried out at the Ion Beam Centre, University of Surrey, UK (2007). A Helium beam energy of 3,115KeV was obtained with a current of less than 20nA and a beam diameter of 1mm. Calibration was carried out using an Au/Ni/SiO2/Si sample described in Jeynes *et al.* (1998). Analysis was carried out using datafurnace software developed at the University of Surrey which has been discussed and validated in Barradas *et al.* (2007); Jeynes *et al.* (2006); Boudreault *et al.* (2002). For the analysis the samples were approximated to 3 discrete layers; a top layer of carbon followed by a layer of chromium and lastly carbon (RBS is unable to detect hydrogen).

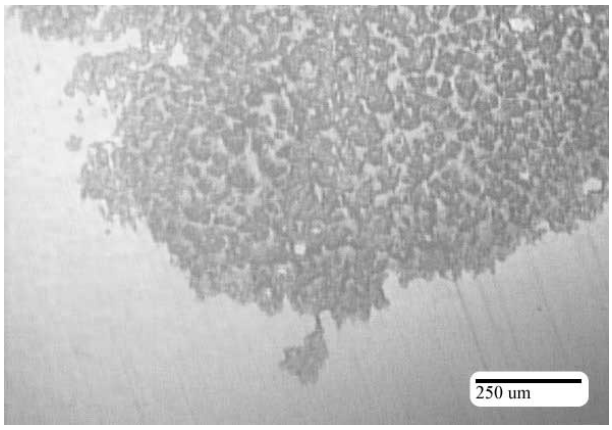

Figure 7.14: Deposit on the 40V bias coated disc edge

7.3 Results

7.3.1 CoCr Substrate

7.3.1.1 Wear

From the group of MOM tests, it was necessary to stop testing the 80V bias (Sample 3) coating when sliding against an uncoated CoCr disc because of risk of damage to the testing equipment, as the equipment was vibrating.

It was also not possible to measure the wear from any of the 40V bias (Sample 1) coated pins. This was due to a deposit building up on the surface of the coating during all of the tests; efforts to remove the deposit by cleaning with acetone were unsuccessful; additional pin on disc tests were carried out for 3 hours in order to determine wear, but the deposit remained and no wear scar was evident. The deposit can be seen in Figure 7.14.

X-ray photoelectron spectroscopy (XPS) analysis of the deposit was carried out to identify the elements within it; a breakdown of the atomic concentrations in the deposit and the coating in the immediate area can be seen in Table 7.4. Spectra from the XPS analysis can be seen in Appendix D.

Table 7.4: Atomic concentrations of a deposit on 40V bias carbon coating, determined by XPS

Element	Off Deposit At%	On Deposit At%
Carbon	45.78	46.47
Oxygen	38.91	43.11
Sodium	0.50	1.14
Chromium	10.50	4.09
Iron	0	0.58
Nitrogen	0.83	0.63
Sulphur	0	0.71
Chlorine	0	0.24
Silicon	3.25	1.47
Calcium	0.23	0.85
Potassium	0	0.72

When sliding against an identically coated disc, the 60 to 40V transition bias coating (Sample 4) followed by Teer Coatings Ltd.'s Graphit-iC^{TM} coating (Sample 2) had the lowest wear factor (3.65×10^{-18}m^3/Nm and 6.43×10^{-18}m^3/Nm respectively). When the CoCr disc remained uncoated, the Graphit-iC^{TM} coating produced the lowest wear with 9.21×10^{-18}m^3/Nm followed by the 60 to 40V coating with 1.73×10^{-17}m^3/Nm (Figures 7.15 and 7.16).

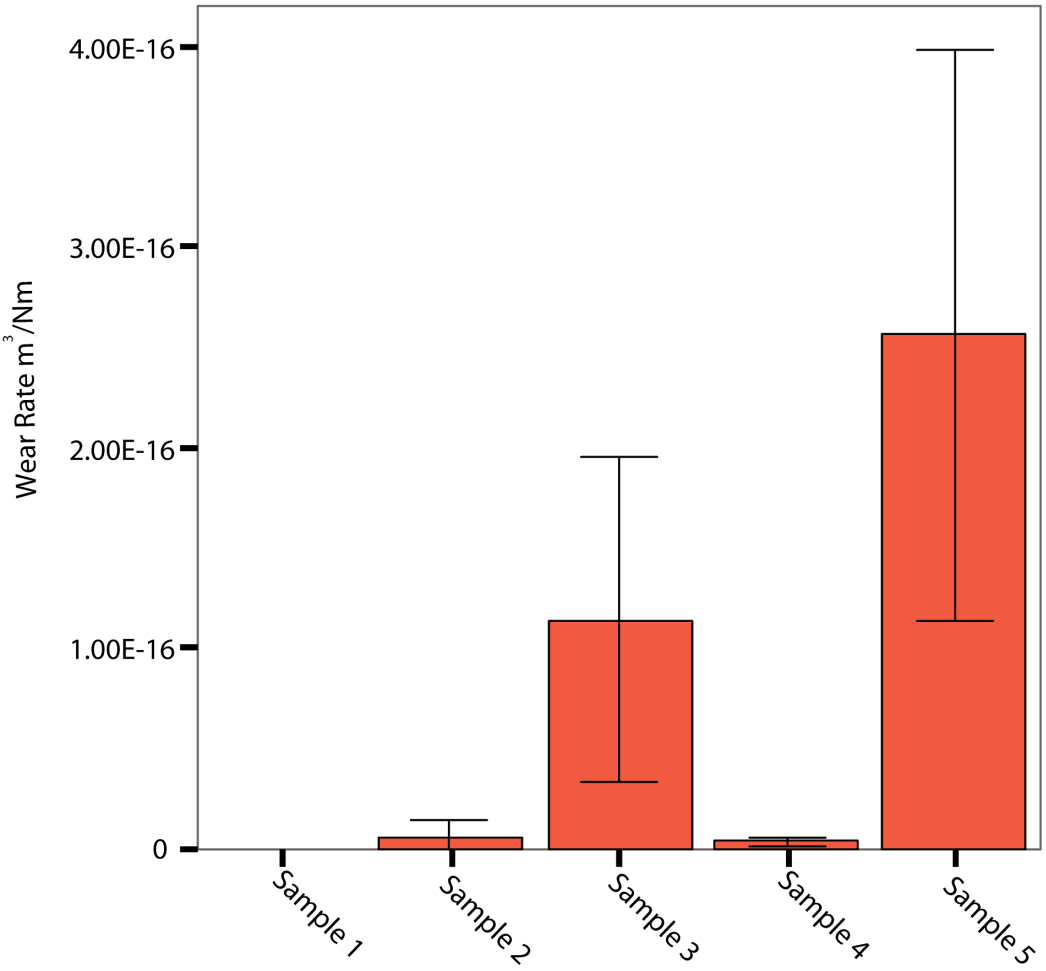

Figure 7.15: POD wear factor of a coated pin against a coated CoCr disc

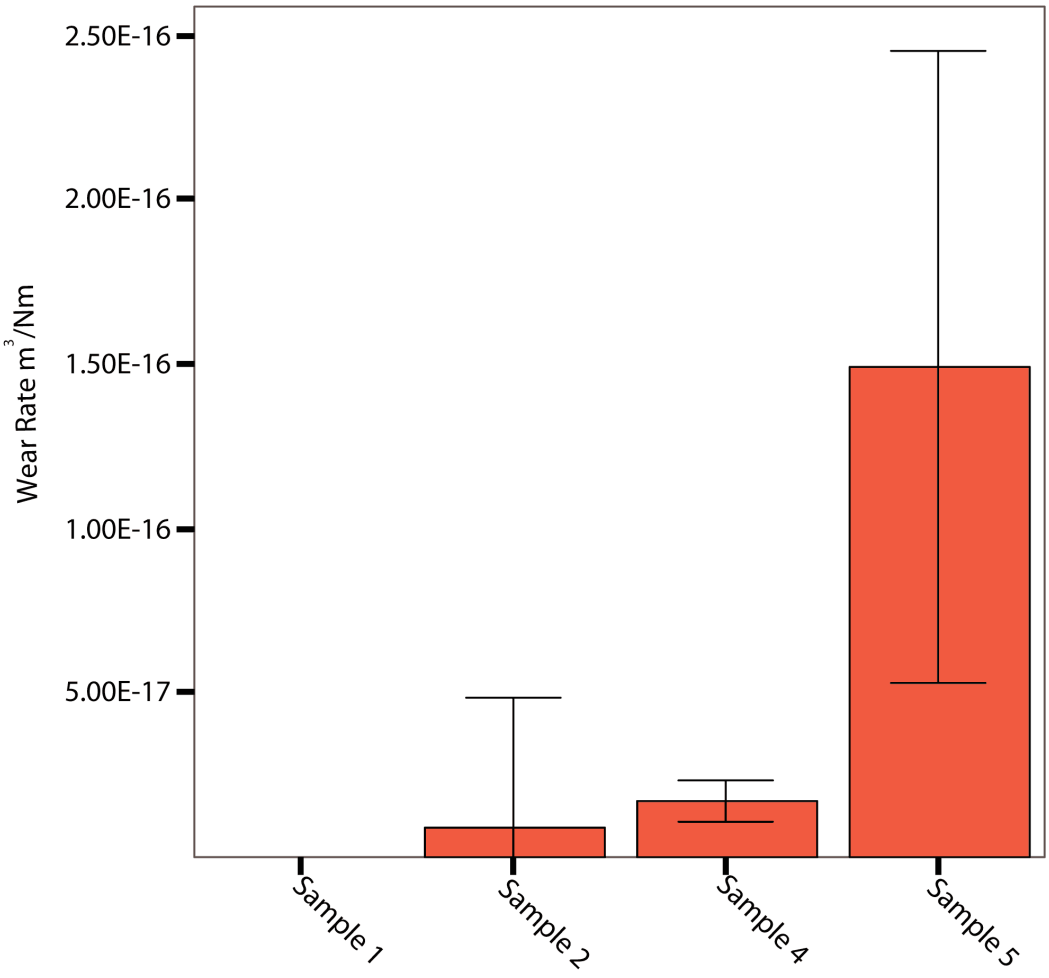

Figure 7.16: POD wear factor of a coated pin against an uncoated CoCr disc

With the exception of the CoCr interlayer coating (Sample 5); the coating wear on the pin was lower when the disc was also coated (Table 7.5).

The pin wear between coatings is statistically different (ANOVA $p<0.05$), the mean wear is detailed in Table 7.5.

Table 7.5: Wear of amorphous carbon coated CoCr from pin on disc tests

Sample	Pin Coating Description	Disc	Wear factor ($\times 10^{-18}$m^3/Nm) Mean	Standard Deviation
1	40V Bias	Coated	Unmeasurable	n/a
		None	Unmeasurable	n/a
2	Graphit-iC™	Coated	6.43	3.09
		None	9.21	4.41
3	80V Bias	Coated	114†	32.4
		None	not tested ‡	n/a
4	60 to 40V transition bias	Coated	3.65	0.725
		None	17.3	2.50
5	CoCr interlayer	Coated	256†	57.3
		None	149†	38.6

†Coating failure

‡Testing stopped due to risk of damage to equipment

It should be noted that the coating was worn through to the substrate in the case of the CoCr interlayer coating when sliding against uncoated and coating discs (Figure 7.17). The 80V bias coating sliding against a coated substrate (Figure 7.18) also wore through to the substrate. Wear factors can be calculated from these scars, however they do not reflect the wear factor of the coating itself as the wear properties of the substrate start to have an effect as soon as the coating is worn through.

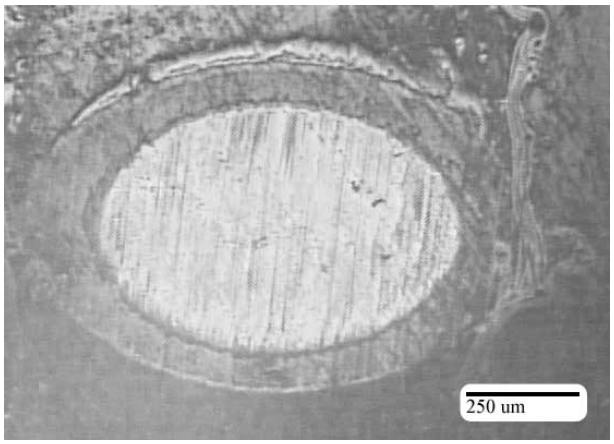

Figure 7.17: Disc edge wear scar of an amorphous carbon coating with a CoCr interlayer

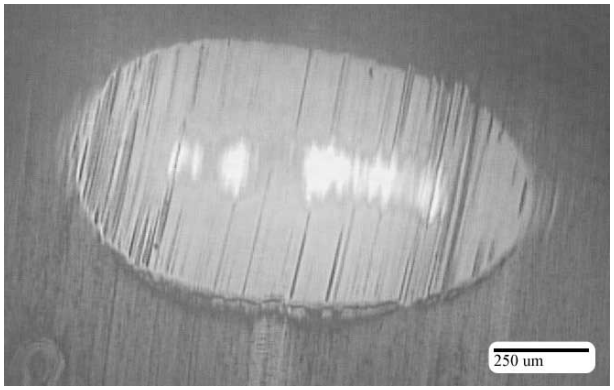

Figure 7.18: Disc edge wear scar of an 80V bias amorphous carbon coating

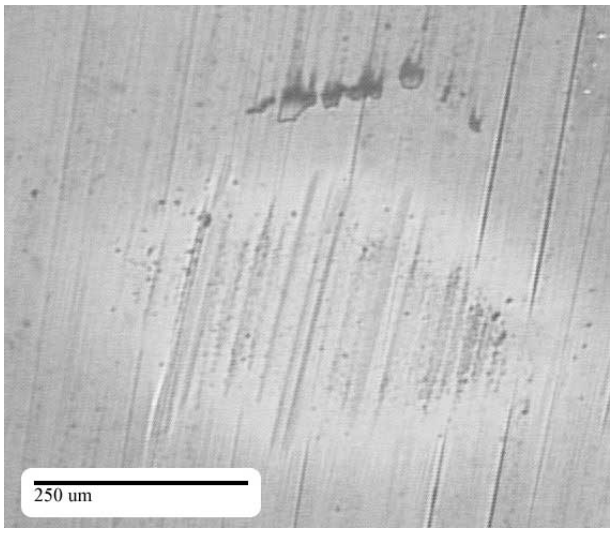

Figure 7.19: Disc edge wear scar of a Graphit-iC^{TM} coating

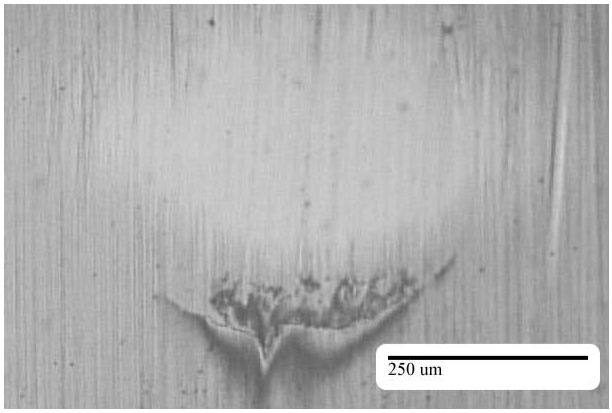

Figure 7.20: Disc edge wear scar of a 60 to 40V transition bias amorphous carbon coating

Smaller wear scars, reflecting the smaller amount of wear can be seen for the Graphit-iC^{TM} coating and the 60 to 40V transition bias coating were observed (Figures 7.19 and 7.20); evidence of a transfer layer can be seen in these two cases.

Figures 7.17 to 7.20 all show the pin wear scar when tested against a coated disc, similar images were observed when the disc was uncoated; with the exception of the CoCr interlayer coating which formed an irregular scar on the disc edge

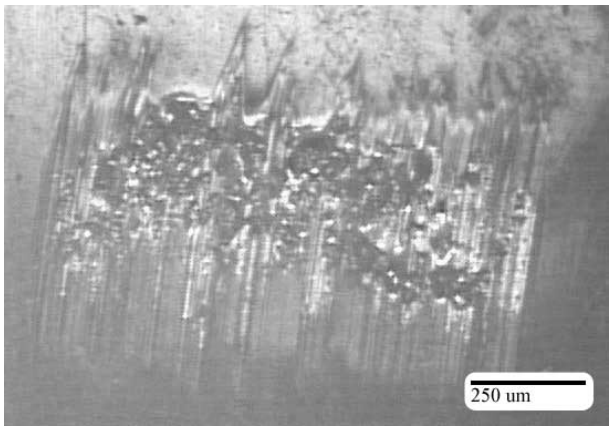

Figure 7.21: Irregular pin wear scar of an amorphous carbon coating with a CoCr interlayer sliding against an uncoated CoCr disc

(Figure 7.21).

7.3.1.2 Friction

Statistical analysis of the friction of the coatings deposited onto CoCr suggest that there is not statistical difference arising from the surface coating, or whether just one, or both of the components is coated (ANOVA $P>0.05$). The friction coefficient measured ranged between 0.12-0.18 when a coated disc was sliding against an uncoated CoCr pin, while it ranged between 0.14-0.19 when both the pin and disc were coated. This compares to 0.25 (standard deviation 0.024) for an uncoated CoCr pin and disc (Figure 7.22, Table 7.6). Application of a coating to one or both of the components resulted in a significant difference from when the components were both uncoated ($p<0.05$).

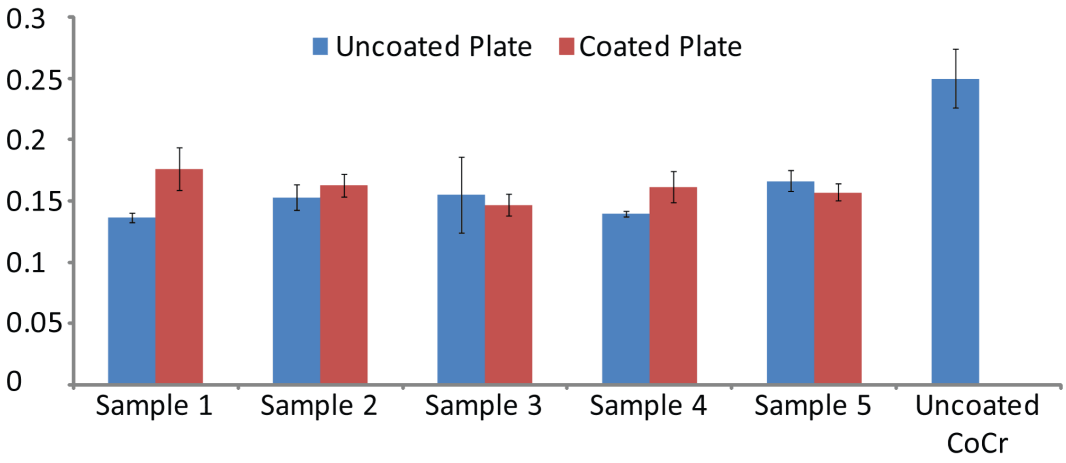

Figure 7.22: Friction coefficient of coated pins sliding against a CoCr disc

Table 7.6: Friction data from pin on disc tested amorphous carbon coatings on CoCr

Sample	Coating Description	Disc	Friction Coefficient Mean	Friction Coefficient Standard Deviation
1	40V Bias	Coated	0.18	0.02
		None	0.13	0.01
2	Graphit-iC^{TM}	Coated	0.16	0.01
		None	0.15	0.03
3	80V Bias	Coated	0.15	0.01
		None	0.16	0.03
4	60 to 40V transition bias	Coated	0.16	0.01
		None	0.14	0.00
5	CoCr interlayer	Coated	0.16	0.01
		None	0.17	0.00

7.3.2 UHMWPE Substrate

7.3.2.1 Wear

The wear factors of all the tested combinations is detailed in Table 7.7. The ion implantation of the UHMWPE discs did not have any statistical difference in wear of the CoCr pins ($p>0.05$), their wear factor ranging from 1.18×10^{-16} to 1.38×10^{-15}m^3/Nm when they were coated with Graphit-iC^{TM} and from 1.07×10^{-15} to 1.25×10^{-15}m^3/Nm when the pin was uncoated. There was a statistical difference in means between the wear of the coated and uncoated pins ($p<0.05$); this is illustrated in Figure 7.23.

It was not possible to accurately determine the wear of the coatings deposited onto any of the UHMWPE discs. The wear was too small to measure as the resolution

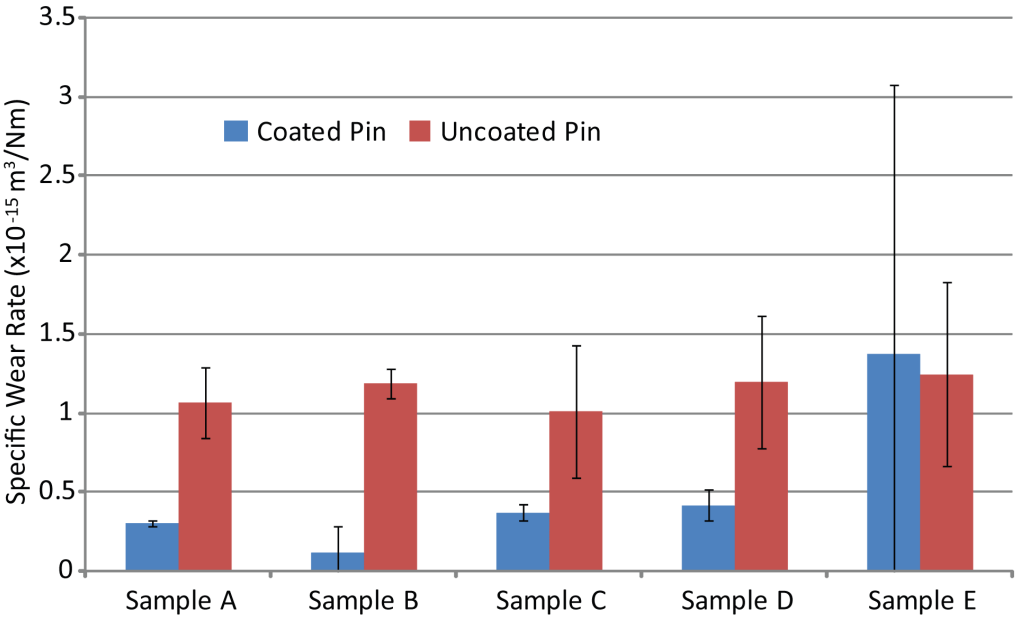

Figure 7.23: Wear factor of a CoCr counter-face pin when sliding against nitrogen implanted UHMWPE with a carbon coating

Table 7.7: Wear factor of a CoCr counter-face pin when sliding against nitrogen implanted UHMWPE with a carbon coating

Substrate sample	Coated CoCr pin ($\times 10^{-18}$m^3/Nm)		Uncoated CoCr pin ($\times 10^{-18}$m^3/Nm)	
	Mean	Standard Deviation	Mean	Standard Deviation
A	306	18.4	1,070	226
B	118	167	1,190	90.3
C	370	51.5	1,010	419
D	423	96.2	1,200	419
E	1,380	1,700	1,250	582

of the RBS measurement technique was not high enough to differentiate a change in thickness of the coating on the wear track and off the track.

The resolution of the RBS technique was calculated to be 24nm. The fitting of the analysis curve is the limiting factor in this technique, it is from this that the error was calculated. The sample with the best analytical fit was used and the difference in thickness of the chromium layer both on and off the wear track was used as a point of reference. Because the measured points are on the same disc, in close proximity it can be assumed the chromium layer thickness is identical at each measured point. A difference of 1.6% was measured, 380nm off the wear track and 374nm on the wear track; this can be attributed to error in the analysis. The thickness of the carbon layer on this sample was calculated to be 1,505nm; assuming the worst case error (1.6% as previously stated), wear could amount to 24nm and not be measurable. This would account for a factor of $9.6\times10^{-17}\mathrm{m}^3/\mathrm{Nm}$.

7.3.2.2 Friction

Similar to the coatings deposited onto CoCr substrates, the coatings deposited onto UHMWPE substrates failed to show any significant difference in friction resulting from the surface modification (ANOVA $p>0.05$). There was however significant difference in friction when comparing coated pins (0.15-0.20) against uncoated pins sliding against the coated UHMWPE substrate (0.27-0.32) ($p<0.05$). In addition, application of a coating to the UHMWPE substrate in an UHMWPE-CoCr couple results in a statistically significant increase in friction ($p<0.05$); when

tested uncoated samples had a friction value of 0.07 (standard deviation 0.01).

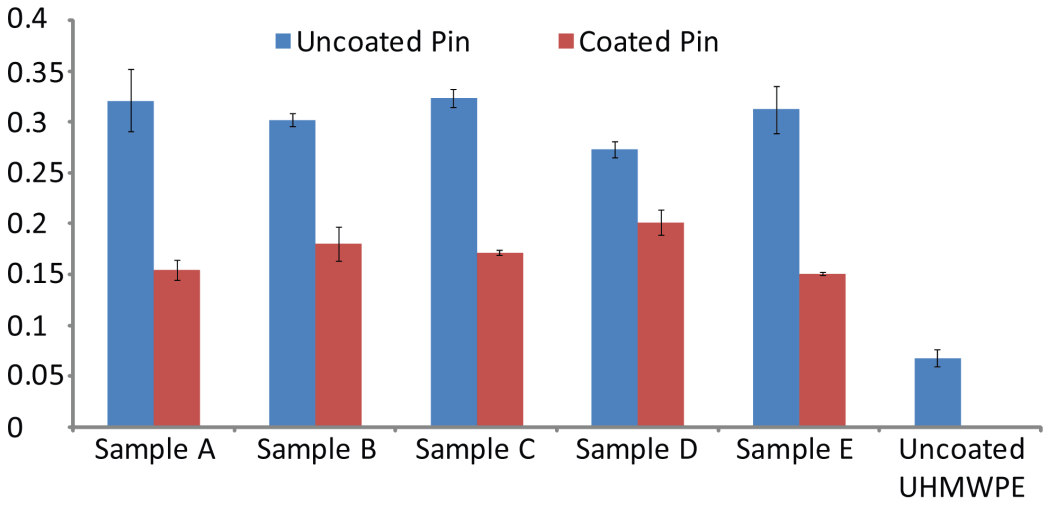

Figure 7.24: Pin on disc friction coefficient during testing of ion implanted UHMWPE with a CoCr counter-face pin

Table 7.8: Friction from pin on disc tested ion implanted UHMWPE

Sample	Pin Material	Friction Coefficient Mean	Friction Coefficient Standard Deviation
A	Coated CoCr	0.15	0.01
	CoCr	0.32	0.03
B	Coated CoCr	0.18	0.02
	CoCr	0.30	0.01
C	Coated CoCr	0.17	0.00
	CoCr	0.32	0.01
D	Coated CoCr	0.20	0.01
	CoCr	0.27	0.01
E	Coated CoCr	0.15	0.00
	CoCr	0.31	0.02

7.4 Discussion

In addition to the testing of coated components, uncoated CoCr was tested for wear performance while sliding against another uncoated CoCr component. These tests produced a wear factor of 3.53×10^{-15}m^3/Nm (standard deviation 1.04×10^{-15}). Scholes and Unsworth (2001) report wear factors of low carbon CoCr with linear sliding to be 1.9×10^{-15}m^3/Nm for the pin and 4.5×10^{-15}m^3/Nm for the disc.

Although it was found that the CoCr interlayer coating has superior adhesion over that of the other coatings (Chapter 5) and that it had the best impact resistance and toughness (Chapter 6), its wear performance is by far the worst, achieving a wear factor of only 2.56×10^{-16} and 1.49×10^{-16}m^3/Nm when sliding against a coated and uncoated discs respectively. In both cases the coating failed and wore through to the substrate, therefore leading to this wear factor being a composite of the coating wear factor and the wear factor of CoCr. Examination of the wear scar shows an irregular and scored scar which is suggestive of third body wear. The finding in Chapter 4 that this coating increased in hardness after a depth of 150nm to a level greater than any of the others would suggest that the coating debris is the cause. Also contributory to the high wear is the lack of transfer layer, which is known to be one of the reasons why Graphit-iC^{TM} type coatings have a low wear rate(Erdemir *et al.*, 1995; Camino *et al.*, 1999).

The 40V bias coating however had unmeasurable wear due to a deposit forming on the surface at location where the wear scar is expected (Figure 7.25). The

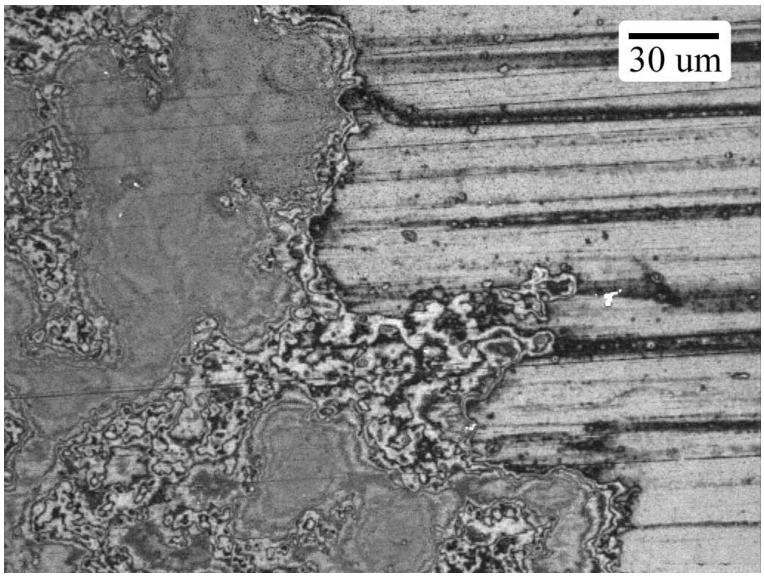

Figure 7.25: Confocal image of deposit on 40V bias coating. A surface deposit can be seen on the left

deposit is too extensive to have formed from the coating and so cannot be a transfer layer. It has most likely formed from the bovine serum and bonded onto the coating surface, this assumption is supported by the XPS analysis which found elements typically found in organic material in the deposit but not on the surrounding coating. It is not clear what caused or enabled the formation of this layer; if the bias voltage was the cause then a similar deposit should have been observed on the transition bias layer coating which had a 40V bias top layer, however this was not the case.

It is not possible to state that there was no wear on the 40V bias coating as it was not possible to remove the deposit, however there is a possibility that the layer acted as a protective layer and prevented, or at least reduced the coating wear.

Application of the coating to CoCr did not just reduce the wear when tested

against another CoCr substrate, wear was also reduced in the CoCr when sliding against a UHMWPE substrate, but it was unfortunate that the wear factor of the coated UHMWPE could not be accurately determined due to the insufficient resolution of the analysis technique. The resolution was limited primarily by the poor fitting of the curve to the collected data. Visual inspection of the curves does not indicate any wear in the track. Calculation of the resolution of the technique indicates that if wear had been measurable then it would have been at least $9.6\times10^{-17}m^3$/Nm, this is an order of magnitude lower than the wear factors reported in the literature. Pin on disc testing by Saikko *et al.* (2001a) and Chanda *et al.* (1997) obtained wear factors of 0.29-1.27$\times10^{-15}m^3$/Nm and 3.1-5.5$\times10^{-16}m^3$/Nm respectively. This compares with a simulator study on the wear of UHMWPE which calculates the wear factor to be 1.51-1.80$\times10^{-15}m^3$/Nm (Saikko and Ahlroos, 1999). These wear factors would account for a track depth of 85-500nm and would be easily measured. By running the tests for longer wear would have been increased and may have been measurable. In this study the tests were run for three hours, unfortunately limited access to the equipment prevented tests being run for longer.

Friction readings for the uncoated CoCr MOM tests (0.25) and uncoated POM tests (0.07) are at the higher end of ranges quoted for similar tests in the literature (Scholes *et al.*, 2000; Hall *et al.*, 1994; Unsworth, 1978). The testing used here has not attempted to replicate the environment of the hip joint; the loading is not dynamic and the speeds are not representative. In addition due to the contact pressures and speeds involved, there will be a boundary lubricating regime

during the test; the lubricating regime in hip joints has been shown to be a mixed regime (Unsworth, 1978) with some tests of large diameter resurfacing joints fluid suggesting that film lubrication may be possible (Vassiliou *et al.*, 2006).

As detailed in Section 2.3.3, Charnley was concerned that the friction of a joint contributed to loosening. Hall *et al.* (1997, 1994) have since suggested that this may not be entirely the case; they found that there was little evidence of raised friction in the Charnley implant contributing to the loosening of joints however. Although, they suggest that further investigation is necessary as it is not clear the role of the thick walled socket which could be reducing the frictional torque at the bone interface.

It is beneficial that deposition of the coatings on CoCr in MOM joints reduces the friction, however it is a concern that the friction increased when coatings were deposited onto UHMWPE. Friction coefficients when only the UHMWPE is coated and the CoCr pin is uncoated are above levels typically seen in any hip joint material combination; when both components are coated the friction reduces to levels similar to those seen in MOM joints.

7.5 Summary

This chapter has described the wear and friction performance of the coatings deposited for this study. The pin on disc technique used here established that when deposited onto CoCr the coatings reduce the wear factors by orders of

magnitude over that of uncoated CoCr as well as the friction. When tested using components that were both coated, the wear was reduced further still.

It was also found that there was significant difference between the deposited coatings. Despite having stronger adhesion than other coatings (Chapter 5) the CoCr interlayer coating had the highest rate of wear. It was suspected that the 40V coating had no wear due to a surface deposit that formed during the tested which provided a protective layer.

It was not possible to measure the wear of coatings deposited onto UHMWPE, however the resolution of the technique used to measure the wear was 24nm, which equates to a wear factor of 9.6×10^{-17}m^3/Nm. The deposition of Graphit-iC^{TM} onto ion implanted UHMWPE resulted in a change in friction over an uncoated POM combination although in this case the result was increased friction. Modification of the UHMWPE by ion implantation had no affect when compared with unmodified coated UHMWPE. This increased friction was less pronounced when both the CoCr and UHMWPE were coated with Graphit-iC^{TM}.

8. Conclusions

It was hypothesised that the application of amorphous carbon coatings, to orthopaedic materials, could reduce the level of wear and therefore extend the life of hip joints replacements that had been implanted into patients.

It was found in the literature that the primarily cause of failure was due to aseptic loosening; an event which can be caused by osteolysis, an immunological condition caused by the presence of wear particles.

To date, use of surface coatings to reduce the wear of hip joint prosthesis is limited; where surface coatings are used the most common is TiN. Use of amorphous carbon coatings in the field have not been reported on extensively; papers which refer to carbon coatings typically refer to DLC coatings which have significantly higher sp^3 ratios. Only two publications have been found describing the in vivo performance of a DLC joint (Taeger *et al.*, 2003; Joyce, 2007). Little information is available on these coatings, such as their sp^3 ratios, additional metal elements included in the coating structure and interlayers or gradient layers.

Of work reported on from in-vitro studies, coatings are typically deposited onto metal components; deposition onto UHMWPE, a material which wears significantly more than metals, is not discussed; only a single publication describing the deposition of a DLC onto UHMWPE for in-vitro testing could be found (Sheeja *et al.*, 2005).

Of papers which have been published on TiN and DLC coatings deposited onto

hip joint prostheses or other orthopaedic implants, it is frequently reported that coating adhesion is a problem.

An amorphous carbon coating, Graphit-iC^{TM}, has been developed by Teer Coatings Ltd. coatings which has been demonstrated to have low wear and friction properties as well as good adhesion (Camino *et al.*, 1999) in various environments (Stallard *et al.*, 2004) and applications (Coldwell *et al.*, 2004). It was thought that the coating would have the potential to perform well in an orthopaedic application.

Variations on the Graphit-iC^{TM} coating were deposited onto CoCr substrates; in light of reviewing the literature, attempts were made to improve adhesion of the coating to the substrate, this was through varying the deposition process bias; introducing graduations within the coating and by using a CoCr interlayer.

A Graphit-iC^{TM} type coating was also deposited onto UHMWPE. It was a concern that depositing a hard coating onto a substrate would cause adhesion problems because of the difference in hardness, nitrogen ion implantation was therefore used to harden the substrate.

Subsequent to deposition the coatings were characterised for hardness, adhesion, toughness, fatigue, wear and friction.

It was found that ion implantation led to a reduction in coating hardness; the nitrogen ion bombardment disrupted the polymer chains and softened the polymeric structure from an unimplanted nano-hardness of 0.26GPa to 0.13GPa when

nitrogen implanted at 15KeV and a dose of 1×10^{15}particles/cm^2. Despite this, adhesion of the coatings was similar to the unmodified UHMWPE. Application of a 50nm layer of chromium prior to ion implantation did not have a positive effect on adhesion. It is thought that the subsequent implantation not only weakened the underlying polymer, but also bonded with the chromium layer to form a hard layer of chromium nitride. This caused a larger hardness differential which had a negative effect on coating adhesion.

Despite the findings regarding adhesion and hardness of the coating onto UHMWPE, wear was found to be unmeasurable following pin on disc testing. The RBS technique used was calculated to have a resolution of 9.6×10^{-17}m^3/Nm; this is an order of magnitude better than published wear factors for uncoated UHMWPE. It was noticed during the scratch testing that there was crazing on the coatings deposited onto UHMWPE, suggestive of cohesive failure. It is thought that this enabled the coating to deform with the substrate and not fail adhesively.

Modification of the coating was investigated to improve performance over Graphit-iC^{TM} when deposited onto CoCr. The literature identifies intrinsic stresses as a significant factor in a coatings adhesion and that the stresses can be reduced by the use of gradient coatings and lower deposition energies. Scratch testing found that the lower 40V bias voltage of Sample 1 led to an improved adhesion over that of Graphit-iC^{TM} which was deposited at 60V. It was also found that the use of a CoCr interlayer (Sample 5) led to better adhesion. The use of a gradient coating (Sample 4) with a varying bias led to reduced adhesion performance. nano impact testing also identified the 40V bias and CoCr interlayer coating as having

the best impact resistance relative to the other coatings that were modified. The 80V bias coating had the lowest adhesion and impact resistance compared to the other coatings deposited.

Although the CoCr interlayer coating had good adhesion, it performed the worst when tested for wear resistance. Examination of the wear scar led to the conclusion that the coating was susceptible to third body wear. This was attributed to the hardness of the coating, which increased with depth. The 40V bias coating had an unmeasurable rate of wear due to a deposit from the bovine serum lubricant developing at the wear point. It is unclear what caused this deposit to form and it was noted that the 60 to 40V transition bias coating (Sample 4), which had a similar 40V bias surface layer did not have a similar deposit. When comparing all of the coatings relative to uncoated CoCr, the coating with the greatest wear without failure was the Sample 4, the 60 to 40V transition bias, when sliding against and uncoated CoCr; for this test a wear factor of $1.7\times10^{-17}\mathrm{m}^3/\mathrm{Nm}$ was obtained. This is compared to uncoated CoCr which obtained a wear factor of $3.53\times10^{-15}\mathrm{m}^3/\mathrm{Nm}$.

8.1 Original Contribution to the Body of Knowledge

The following original contributions to the body of knowledge have been made by this thesis.

8.1.1 A Novel Pin on Disc Test Method

The addition of a second radius onto the edge of a disc has not previously been reported, it has been presented at the Laser Metrology and Machine Performance VIII conference (Appendix E.1.1). This method offered three benefits over that of the traditional pin on disc method.

1. By rotating the disc a new area could be presented for testing. This prevents the need for re-machining of the pin and repolishing and re-coating of the pin when stock is in short supply. Rotating the disc is quick and easy.

2. Use of the same disc for multiple runs improves consistency. There is less variation in the coating and the form and roughness remain the same.

3. The second radius prevents edge contact between the pin and disc thereby preventing high stress points and likely coating failure. By controlling the radius different contact pressures can be achieved.

8.1.2 Deposition of Substrate Tailored Coatings for CoCr Alloys

Amorphous carbon coatings were deposited onto CoCr and tested for suitability in hip joint replacement applications. Based off of Graphit-iC^{TM}, modifications were made to the coating bias and inter-layers to improve tribological performance in a biological environment and to improve the coating adhesion to CoCr. Application of these coatings has reduced the wear factor from 3.53×10^{-15}m^3/Nm

for uncoated CoCr to 1.7×10^{-17}m^3/Nm. This is comparable to the wear factors of other DLC coatings reported in the literature, but goes further to address the adhesions issues reported with DLC coatings.

The coatings hardness, toughness, wear, friction and adhesion were characterised, posters have been presented at the UK Society of Biomaterials 2006 (Appendix E.2.2) and Materials Congress 2006 (Appendix E.2.1).

8.1.3 Deposition of Amorphous Carbon Coatings onto UHMWPE for Orthopaedic Applications

An amorphous carbon coating was deposited onto UHMWPE to improve the wear performance of hip joint replacements. The UHMWPE had been ion implanted with nitrogen prior to coating deposition to improve adhesion characteristics. This is the first study to detail the tribological performance of coated UHMWPE in an orthopaedic environment.

Attempts were made to determine the coating wear performance on the UHMWPE substrates by RBS. This was in addition to friction performance, adhesion and hardness of the coating. It was not possible to directly measure the wear of the coated UHMWPE, however the resolution of the technique would suggest that the wear factor was less than 9.6×10^{-17}m^3/Nm. This compares favourably with the wear factors of uncoated UHMWPE reported in the literature.

8.2 Further Work

Wear testing in this study has been limited to a pin on disc method. It has been identified from work in the literature that the method used is unlikely to accurately replicate the hip joint environment and can only be used as a guide to the potential of the coatings relative to each other. In order to fully determine the potential of the coatings deposited it is necessary to use a wear simulator; the wear of the coating will be determined and it will also be able to infer the adhesion of the coating in an appropriate environment.

To improve upon the coating itself, it will be necessary to further investigate the interface between coating and substrate. This study examined deposition onto UHMWPE which is a particularly soft substrate in comparison to the metallic CoCr. Surface modification will be necessary to achieve maximum performance. By matching hardness at the interface and depositing a transition coating to avoid a differential at which stress concentrations can occur adhesion and wear should be improved.

References

Abadias, G. Stress and preferred orientation in nitride-based pvd coatings. *Surface and Coatings Technology*, **202**, pp. 2223–2235 (2008).

Ahlroos, T. and Saikko, V. Wear of prosthetic joint materials in various lubricants. *Wear*, **211**, pp. 113–119 (1997).

Aisenberg, S. and Chabot, R. Ion-beam deposition of thin films of diamondlike carbon. *Journal of Applied Physics*, **42**, pp. 2953–2958 (1971).

American Society for Testing and Materials. Standard specification for tool steel high speed. Technical Report A600-92a, American Society for Testing and Materials (2004).

American Society for Testing and Materials. Standard test method for wear testing of polymeric materials used in total joint prostheses. Technical Report F732-00, American Society for Testing and Materials (2006).

American Society for Testing and Materials. Standard specification for cobalt-28 chromium-6 molybdenum alloy castings and casting alloy for surgical implants. Technical Report F75-07, American Society for Testing and Materials (2007).

Amstutz, H. C. and Grigoris, P. Metal on metal bearings in hip arthroplasty. *Clinical Orthopaedics and Related Research*, **329S**, pp. S11–S34 (1996).

Anon. Burma veteran still hip after 60 years. The Times (UK), 31st August (2007).

Anstis, G. R., Chantikul, P., Lawn, B. R. and Marshall, D. B. A critical evaluation of indentation techniques for measuring fracture toughness: I, direct crack measurements. *Journal of the american ceramic society*, **64(9)**, pp. 533–538 (1981).

Aoki, Y. and Ohtake, N. Tribological properties of segment-structured diamond-like carbon films. *Tribology International*, **37**, pp. 941–947 (2004).

Archard, J. F. Contact and rubbing of flat surfaces. *Journal of Applied Physics*, **24(8)**, pp. 981–988 (1953).

Arnell, R. D., Colligon, J. S., Minnebaev, K. F. and Yurasova, V. E. The effect of nitrogen content on the structure and mechanical properties of TiN films produced by magnetron sputtering. *Vacuum*, **47(5)**, pp. 425–431 (1996).

Aston University. Surface Science Research Group, School of Engineering and Applied Science, Aston Triangle, Birmingham, B4 7ET, UK (2006).
URL: *http://www.aston.ac.uk Last Accessed 26th April 2009*

Azushima, A., Tanno, Y., Iwata, H. and Aoki, K. Coefficients of friction of TiN coatings with preferred grain orientations under dry condition. *Wear*, **265**, pp. 1017–1022 (2008).

Barbour, P. S. M., Barton, D. C. and Fisher, J. The influence of contact stress on the wear of uhmwpe for total replacement hip prostheses. *Wear*, **181**, pp. 250–257 (1995).

Barbour, P. S. M., Stone, M. H. and Fisher, J. A hip joint simulator study using

simplified loading and motion cycles generating physiological wear paths and rates. *Proceedings of the Institute of Mechanical Engineers Part H: Journal of Engineering in Medicine*, **213**, pp. 455–467 (1999).

Barradas, N. P., Arstila, K., Battistig, G., Bianconi, M., Dytlewski, N., Jeynes, C., Kótai, E., Lulli, G., Mayer, M., Rauhala, E., Szilágyi, E. and Thompson, M. International atomic energy agency intercomparison of ion beam analysis software. *Nuclear Instruments and Methods in Physics Research B*, **262**, pp. 281–303 (2007).

Batchelor, A. W. and Chandrasekaran, M. *Series on Biomaterials and Bioengineering - Vol. 3: Service characteristics of biomedical materials and implants*. Imperial College Press (2004).

Batista, J., Joseph, M., Godoy, C. and Matthews, A. Micro-abrasion wear testing of pvd tin coatings on untreated and plasma nitrided aisi h13 steel. *Wear*, **249**, pp. 971–979 (2002).

Beake, B. D., Garcia, M. J. I. and Smith, J. F. Micro-impact testing: A new technique for investigating fracture toughness. *Thin Solid Films*, **398-399**, pp. 438–443 (2001a).

Beake, B. D., Goodes, S. R. and Smith, J. F. Micro-impact testing: A new technique for investigating thin film toughness, adhesion, erosive wear resistance, and dynamic hardness. *Surface Engineering*, **17(3)**, pp. 187–192 (2001b).

Beake, B. D., Lau, S. P. and Smith, J. F. Evaluating the fracture properties and

fatigue wear of tetrahedral amorphous carbon films on silicon by nano-impact testing. *Surface and Coatings Technology*, **177-178**, pp. 611–615 (2004).

Bell, R. S., Schatzker, J., Fornasier, V. L. and Goodman, S. B. A study of implant failure in the wagner resurfacing arthroplasty. *Journal of Bone and Joint Surgery*, **67**, pp. 1165–1175 (1985).

Bergmann, G., Deuretzbacher, G., Heller, M., Graichena, F., Rohlmanna, A., Straussb, J. and Dudac, G. N. Hip contact forces and ait patterns from routine activities. *Journal of Biomechanics*, **34(7)**, pp. 859–871 (2001).

Besong, A. A., Jin, Z. M. and Fisher, J. Importance of pin geometry on pin-on-plate wear testing of hard-on-hard bearing materials for artificial hip joints. *Proceedings of the Institute of Mechanical Engineers Part H: Journal of Engineering in Medicine*, **215**, pp. 605–610 (2001).

Boudreault, G., Jeynes, C., Wendler, E., Nejim, A., Webb, R. P. and Watjen, U. Accurate rbs measurement of ion implant doses in a-si. *Surface and Interface Analysis*, **33**, pp. 478–486 (2002).

Boutin, P., Christel, P., Dorlot, J.-M., Meunier, A., de Roquancourt, A., Blanquaert, D., Herman, S., Sedel, L. and Witvoet, J. The use of dense alumina-alumina ceramic combination in total hip replacement. *Journal of Biomedical Materials Research*, **22**, pp. 1203–1232 (1988).

Bowsher, J. G., Hussain, A., Williams, P., Nevelos, J. and Shelton, J. C. Effect of ion implantation on the tribology of metal-on-metal hip prostheses. *Journal of Arthroplasty*, **19(8 Suppl 3)**, pp. 107–111 (2004).

Bragdon, C. R., O'Connor, D. O., Lowenstein, J. D., Jasty, M. and Syniuta, W. D. The importance of multidirectional motion on the wear of polyethylene. *Proceedings of the Institute of Mechanical Engineers Part H: Journal of Engineering in Medicine*, **210(3)**, pp. 157–165 (1996).

Burnett, P. J. and Rickerby, D. S. The erosion behaviour of tin coatings on steels. *Journal of materials science*, **23**, pp. 2429–2443 (1988).

Camino, D., Jones, A. H. S., Mercs, D. and Teer, D. G. High performance sputtered carbon coatings for wear resistant applications. *Vacuum*, **52**, pp. 125–131 (1999).

Cawley, J., Metcalf, J. E. P., Jones, A. H., Band, T. H. and Skupien, D. S. A tribological study of cobalt chromium molybdenum alloys used in metal-on-metal resurfacing hip arthroplasty. *wear*, **255**, pp. 999–1006 (2003).

Chanda, A., Mukhopadhyay, A. K., Basu, D. and Chatterjee, S. Wear and friction behaviour of uhmwpe - alumina combination for total hip replacement. *Ceramics International*, **23(5)**, pp. 437–447 (1997).

Charnley, J. Total hip replacement by low friction arthroplasty. *Clinical Orthopaedics and Related Research*, **72**, pp. 7–21 (1970).

Charnley, J. C. Tissue reactions to polytetrafluoroethylene. *Lancet*, **285(7400)**, p. 1379 (1963).

Chen, C.-C. and Hong, F. C.-N. Interfacial studies for improving the adhesion of

diamond-like carbon films on steel. *Applied surface science*, **243**, pp. 296–303 (2005).

Chevallier, J. and Chabert, J. P. Microhardness of TiN_x coatings obtained by reactive cathodic sputtering. *Thin Solid Films*, **80**, p. 263 (1981).

Chiba, A., Kumagai, K., Nomura, N. and Miyakawa, S. Pin-on-disk wear behaviour in a like-on-like configuration in a biological environment of high carbon cast and low carbon forged co29cr6mo alloys. *Acta Materialia*, **55**, pp. 1309–1318 (2007).

Chou, W.-J., Yu, G.-P. and Huang, J.-H. Mechanical properties of tin thin film coatings on 304 stainless steel substrates. *Surface and Coatings Technology*, **149**, pp. 7–13 (2002).

Coldwell, H. L., Dewes, R. C., Aspinwall, D. K., Renevier, N. M. and Teer, D. G. The use of soft/lubricating coatings when dry drilling BS L168 aluminium alloy. *Surface and Coatings Technology*, **177-178**, pp. 716–726 (2004).

Coleman, R. F., Herrington, J. and Scales, J. T. Concentration of wear products in hair, blood, and urine after total hip replacement. *British Medical Journal*, **1**, pp. 527–529 (1973).

Collier, J. P., Surprenant, V. A., Jensen, R. E., Mayor, M. B. and Surprenant, H. P. Corrosion between the components of modular femoral hip prostheses. *Journal of Bone and Joint Surgery*, **74B**, pp. 511–7 (1992).

Daley, B., Doherty, A. T., Fairman, B. and Case, C. P. Wear debris from hip or

knee replacements causes chromosomal damage in human cells in tissue culture. *Journal of Bone and Joint Surgery*, **86B(4)**, pp. 598–606 (2004).

Davis, C. A. A simple model for the formation of compressive stress in thin films by ion bombardment. *Thin Solid Films*, **226**, pp. 30–34 (1993).

Davis, J. R., editor. *Handbook of Materials for Medical Devices*. ASM International (2003).

Department of Health. Hospital episode statistics (2006).

URL: *http://www.hesonline.nhs.uk/ Last Accessed 26th April 2009*

Dobrzanski, L., Kwasny, W., Shishkov, R. and Madejski, J. Effect of the deposition parameters on the properties of the two-layer surface coatings obtained using magnetron sputtering. *Journal of Materials Processing Technology*, **113**, pp. 493–501 (2001).

Donnet, C. and Erdemir, A., editors. *Tribology of Diamond-like Carbon Films Fundamentals and Applications*. Springer (2008).

Doorn, P. F., Campbell, P. A., Worrall, J., Benya, P. D., McKellop, H. A. and Amstutz, H. C. Metal wear particle characterisation from metal-on-metal total hip replacements: transmission electron microscopy study of periprosthetic tissues and isolated particles. *Journal of Biomedical Materials Research*, **42**, pp. 103–111 (1998).

Dowson, D. and Jobbins, B. Design and development of a versatile hip joint

simulator and a preliminary assessment of wear and creep in charnley total replacement hip joints. *Engineering in Medicine*, **17**, pp. 111–117 (1988).

Duckworth, T. *Lecture Notes on Orthopaedics and Fractures*. Blackwell Science, 3rd edition (1995).

Dumbleton, J. H. *Tribology of natural and artificial joints*. Elsevier (1981).

Echigoya, J., Liu, Z.-T., Imamura, A. and Takatsu, S. Transmission electron microscopy studies of growth and interface structure of chemically vapour deposited tic and tin films on wc-co alloy substrates. *Thin Solid Films*, **198**, pp. 293–300 (1991).

Edison, T. A. Art of plating one material with another. US Patent No. 526,147 (1884).

Endotec. 20 Valley Street, South Orange, New Jersey, 07079, United States (2009).

URL: *http://www.endotec.com/ Last Accessed 26th April 2009*

Erdemir, A., Bindal, C., Pagan, J. and Wilbur, P. Characterization of transfer layers on steel surfaces sliding against diamond-like hydrocarbon films in dry nitrogen. *Surface and Coatings Technology*, **76-77**, pp. 559–563 (1995).

Eskildsen, S. S., Mathiasen, C. and Foss, M. Plasma cvd: process capabilities and economic aspects. *Surface and Coatings Technology*, **116-119**, pp. 18–24 (1999).

Fallon, P. J., Veerasamy, V. S., Davis, C. A., Robertson, J., Amaratunga, G. A. J. and Koskinen, J. Properties of filtered-ion-beam-deposited diamondlike carbon as a function of ion energy. *Physical Review B*, **48(7)**, pp. 4777–4782 (1993).

Faulkner, A., Kennedy, L. G., Baxter, K., Donovan, J., Wilkinson, M. and Bevan, G. Effectiveness of hip prostheses in primary total hip replacement: a critical review of evidence and an economic model. *Health Technology Assessment*, **2(6)** (1998).

Field, S. K. (2009). Private Communication.

Field, S. K., Jarratt, M. and Teer, D. G. Tribological properties of graphite-like and diamond-like carbon coatings. *Tribology International*, **37**, pp. 949–956 (2004).

Firth Rixon Ltd. Firth House, Meadowhall Road, Sheffield, S9 1JD, UK (2005).
URL: *http://www.firthrixson.com Last Accessed 26th April 2009*

Fisher, J., Dowson, D., Hamdzah, H. and Lee, H. L. The effect of sliding velocity on the friction and wear of uhmwpe for use in total artificial joints. *Wear*, **175**, pp. 219–225 (1994).

Food and Drug Administration. 10903 New Hampshire Ave, Silver Spring, MD 20903, United States (2009).
URL: *http://www.fda.gov/ Last Accessed 26th April 2009*

Garcia-Prieto, I., Faulkner, M. D. and Alcock, J. R. The influence of specimen

misalignment on wear in conforming pin on disk tests. *Wear*, **257**, pp. 157–166 (2004).

Genda, E., Iwasaki, N., Li, G., MacWilliams, B. A., Barrance, P. J. and Chao, E. Y. S. Normal hip joint contact pressure distribution in single-leg standing-effect of gender and anatomic parameters. *Journal of Biomechanics*, **34**, pp. 895–905 (2001).

Gillespie, W., Frampton, C., Henderson, R. and Ryon, P. The incidence of cancer following total hip replacements. *Journal of Bone and Joint Surgery*, **70B(4)**, pp. 539–542 (1988).

Gispert, M. P., Serro, A. P., Colaco, R. and Saramango, B. Friction and wear mechanisms in hip prosthesis: Comparison of joint materials behaviour in several lubricants. *Wear*, **260**, pp. 149–158 (2006).

Glück, T. Referat über die durch das moderne chirurgische experiment gewonnen positiven resultate, betreffend die naht und den ersatz von defekten hoherer gewebe, sowie über die verwertung resorbirbarer und lebendiger tampons in der chirurgie. *Arch. Klin. Chir.*, **41**, p. 187 (1891).

Gomes, J. R., Silva, O. M., Silva, C. M., Pardini, L. C. and Silva, R. F. The effect of sliding speed and temperature on the tribological behaviour of carbon-carbon composites. *Wear*, **249**, pp. 240–245 (2001).

Gray, H. *Anatomy Descriptive and Surgical*. John W Parker and Son, West Strand, London (1858).

Green, T. R., Fisher, J., Stone, M., Wroblewski, B. M. and Ingham, E. Polyethylene particles of a "critical size" are necessary for the induction of cytokines by macrophages in vitro. *Biomaterials*, **19**, pp. 2297–2303 (1998).

Greenwood, J. A. and Williamson, J. B. P. Contact of nominally flat surfaces. *Proceedings of the Royal Society of London. Series A, Mathematical and Physical Sciences*, **295(1442)**, pp. 300–319 (1966).

Grobbelaar, C. J., Plessis, T. A. D. and Marais, F. The radiation improvement of polyethylene prostheses. *Journal of Bone and Joint Surgery*, **60B**, pp. 370–374 (1978).

Habermann, B., Ewald, W., Rauschmann, M., Zichner, L. and Kurth, A. A. Fracture of ceramic heads in total hip replacement. *Archives of Orthopaedics and Trauma Surgery*, **126(7)**, pp. 464–470 (2006).

Hall, R. M., Siney, P., Unsworth, A. and Wroblewski, B. M. The association between rates of wear in retrieved acetabular components and the radius of the femoral head. *Proceedings of the Institute of Mechanical Engineers Part H: Journal of Engineering in Medicine*, **212**, pp. 321–326 (1998).

Hall, R. M., Unsworth, A., Siney, P. and Wroblewski, B. M. Wear in retrieved charnley acetabular sockets. *Proceedings of the Institute of Mechanical Engineers Part H: Journal of Engineering in Medicine*, **210**, pp. 197–207 (1996).

Hall, R. M., Unsworth, A., Wroblewski, B. M. and Burgess, I. C. Frictional characterisation of explanted charnley hip prostheses. *Wear*, **175**, pp. 159–166 (1994).

Hall, R. M., Unsworth, A., Wroblewski, B. M. and Siney, P. The friction of explanted hip prostheses. *British Journal of Rheumatology*, **36**, pp. 20–26 (1997).

Hamadouche, M. and Sedel, L. Ceramics in orthopaedics. *Journal of Bone and Joint Surgery*, **82B(8)**, pp. 1095–1099 (2000).

Harman, M. K., Banks, S. A. and Hodge, W. A. Wear analysis of a retrieved hip implant with titanium nitride coating. *Journal of Arthroplasty*, **12(8)**, pp. 938–945 (1997).

Hauert, R. A review of modified DLC coatings for biological applications. *Diamond and Related Materials*, **12**, pp. 583–589 (2003).

Hauert, R. An overview on the tribological behaviour of diamond-like carbon in technical and medical applications. *Tribology International*, **37**, pp. 991–1003 (2004).

Heinke, W., Leyland, A., Matthews, A., Berg, G., Friedrich, C. and Broszeit, E. Evaluation of pvd nitride coatings, using impact, scratch and rockwell-c adhesion tests. *Thin Solid Films*, **270**, pp. 431–438 (1995).

Holmberg, K., Ronkainen, H. and Matthews, A. Tribology of thin coatings. *Ceramics International*, **26**, pp. 787–795 (2000).

Hoseini, M., Jedenmalm, A. and Boldizar, A. Tribological investigation of coatings for artificial joints. *Wear*, **264**, pp. 958–966 (2008).

Huang, J.-H., Ma, C.-H. and Chen, H. Effect of ti interlayer on the residual stress and texture development of tin thin films deposited by unbalanced magnetron sputtering. *Surface and Coatings Technology*, **201(6)**, pp. 3199–3204 (2006).

Jeynes, C., Barradas, N. P., Blewett, M. J. and Webb, R. P. Improved ion beam analysis facilities at the university of surrey. *Nuclear Instruments and Methods in Physics Research B*, **136-138**, pp. 1229–1234 (1998).

Jeynes, C., Peng, N., Barradas, N. P. and Gwilliam, R. M. Quality assurance in an implantation laboratory by high accuracy rbs. *Nuclear Instruments and Methods in Physics Research B*, **249**, pp. 482–485 (2006).

Johnson, K. L., Greenwood, J. A. and Poon, S. Y. A simple theory of asperity contact in elastohydrodynamic lubrication. *Wear*, **19**, pp. 91–108 (1972).

Joyce, T. J. First report of dlc against dlc biomaterial combination in an explanted joint replacement. Bath Biomechanics Symposium: Biomaterials for Reconstruction of the Musculoskeletal System, University of Bath (2007).

Joyce, T. J., Monk, D., Scholes, S. C. and Unsworth, A. A multi-directional wear screening device and preliminary results of uhmwpe articulating against stainless steel. *Bio-Medical Materials and Engineering*, **10**, pp. 241–249 (2000).

Kabo, J. M., Gebhard, J. S., Loren, G. and Amstutz, H. C. In vivo wear of polyethylene acetabular components. *Journal of Bone and Joint Surgery*, **75B**, pp. 254–258 (1993).

Kaukonen, M. and Nieminen, R. M. Atomic-scale modelling of the ion-beam-

induced growth of amorphous carbon. *Physical Review B*, **61(4)**, pp. 2806–2811 (2000).

Kelly, P. J. and Arnell, R. D. Magnetron sputtering: a review of recent developments and applications. *Vacuum*, **56**, pp. 159–172 (2000).

Knotek, O., Elsing, R., Kramer, G. and Jungblut, F. On the origin of compressive stress in pvd coatings an explicative model. *Surface and Coatings Technology*, **46(3)**, pp. 265–274 (1991).

Kohary, K. and Kugler, S. Growth of amorphous carbon: Low-energy molecular dynamics simulation of atomic bombardment. *Physical Review B*, **63**, pp. 193404–1–193404–4 (2001).

Kumar, P. and Clark, M., editors. *Clinical Medicine*. W B Saunders, 4th edition (1999).

Kummer, F. J. and Rose, R. M. Corrosion of titanium/cobalt-chromium alloy couples. *Journal of Bone and Joint Surgery*, **65B(8)**, pp. 1125–1126 (1983).

Kurtz, S. M. *The UHMWPE Handbook: Ultra-High Molecular Weight Polyethylene in Total Joint Replacement*. Academic Press (2004).

Lancaster, J. K. The relationship between the wear of carbon brush materials and their elastic moduli. *British Journal of Applied Physics*, **14**, pp. 497–505 (1963).

Lancaster, J. K. Dry bearings: A survey of materials and factors affecting their performance. *Tribology*, **6**, pp. 219–251 (1973).

Langkamer, V. G., Case, C. P., Heap, P., Taylor, A., Collins, C., Pearse, M. and Solomon, L. Systemic distribution of wear debris after hip replacement. a cause for concern? *Journal of Bone and Joint Surgery*, **74B(6)**, pp. 831–839 (1992).

Law, W. A. Late results in vitallium-mold arthroplasty of the hip. *Journal of Bone and Joint Surgery*, **44A**, pp. 1497–1517 (1962).

Leyland, A. and Matthews, A. On the significance of h/e ratio in wear control: a nanocomposite coating approach to optimised tribological behaviour. *Wear*, **246**, pp. 1–11 (2000).

Lifshitz, Y., Kasi, S. R., Rabalais, J. W. and Eckstein, W. Subplantation model for film growth from hyperthermal species. *Physics Review B*, **41**, pp. 10468–10480 (1990).

Livermore, J., Ilstrup, D. and Morrey, B. Effect of femoral head size on wear of the polyethylene acetabular component. *Journal of Bone and Joint Surgery*, **72A**, pp. 518–528 (1990).

Lodyguine, A. D. Illuminant for incandescent lamps. US Patent No. 575,002 (1897).

Lyubimov, V. V., Voevodin, A. A., Spassky, S. E. and Yerokhin, A. L. Stress analysis and failure possibility assessment of multilayer physically vapour deposited coatings. *Thin Solid Films*, **207**, pp. 117–125 (1992).

Machunze, R. and Janssen, G. C. A. M. Stress gradients in titanium nitride thin films. *Surface and Coatings Technology*, **203**, pp. 550–553 (2008).

Mahoney, O. M. and Dimon, J. H. Unsatisfactory results with a ceramic total hip prosthesis. *Journal of Bone and Joint Surgery*, **72A**, pp. 663–671 (1990).

Mak, M. M., Besong, A. A., Jin, Z. M. and Fisher, J. Effect of microseparation on contact mechanics in ceramic-on-ceramic hip joint replacements. *Proceedings of the Institute of Mechanical Engineers Part H: Journal of Engineering in Medicine*, **216**, pp. 403–408 (2002).

Marcondes, A. R., Ueda, M., Kostov, K. G., Beloto, A. F., Leite, N. F., Gomes, G. F. and Lepienski, C. M. Improvements of ultra-high molecular weight polyethylene mechanical properties by nitrogen plasma immersion ion implantation. *Brazilian Journal of Physics*, **34(4B)**, pp. 1667–1672 (2004).

Maroudas, A. Distribution and diffusion of solutes in articular cartilage. *Biophysical Journal*, **10(5)**, pp. 365–379 (1970).

Maroudas, A. Transport of solutes through cartilage: permeability to large molecules. *Journal of Anatomy*, **122(2)**, pp. 335–347 (1976).

Mazzucco, D. and Spector, M. Effects of contact area and stress on the volumetric wear of ultrahigh molecular weight polyethylene. *Wear*, **254**, pp. 514–522 (2003).

McKee, G. K. and Watson-Farrar, J. Replacement of arthritic hips by the mckee-farrar prosthesis. *Journal of Bone and Joint Surgery*, **48B(2)**, pp. 245–259 (1966).

McMinn, D. J. W. Development of metal/metal hip resurfacing. *Hip International*, **13**, pp. 41–53 (2003).

Medley, J. B., chan, F. W., Krygier, J. J. and Bobyn, J. D. Comparison of alloys and designs in a hip simulator study of metal on metal implants. *Clinical Orthopaedics and Related Research*, **329S**, pp. 148–159 (1996).

Meunier, C., Alers, P., Marot, L., an N Randall, J. S. and Mikhailov, S. Friction properties of ta-c and a-c:h coatings under high vacuum. *Surface and Coatings Technology*, **200**, pp. 1976–1981 (2005).

Micro Materials Ltd. Willow House, Yale Business Village, Ellice Way, Wrexham, LL13 7YL, UK (2009).

URL: *http://www.micromaterials.co.uk Last Accessed 26th April 2009*

Mittelmeier, H. and Heisel, J. Sixteen-years experience with ceramic hip prostheses. *Clinical Orthopaedics and Related Research*, **282**, pp. 64–72 (1992).

Morlock, M., Schneider, E., Bluhm, A., Vollmer, M., Bergmann, G., Muller, V. and Honl, M. Duration and frequency of every day activities in total hip patients. *Journal of Biomechanics*, **34**, pp. 873–881 (2001).

Morshed, M. M., McNamara, B. P., Cameron, D. C. and Hashmi, M. S. J. Stress and adhesion in dlc coatings on 316l stainless steel deposited by a neutral beam source. *Journal of Materials Processing Technology*, **143-144**, pp. 922–926 (2003).

National Joint Registry for England and Wales. 3rd annual clinical report. Technical report, National Joint Registry Centre (2006).

National Joint Registry for England and Wales. 4th annual report. Technical report, National Joint Registry Centre (2007).

Nevelos, J., Ingham, E., Doyle, C., Streicher, R., Nevelos, A., Walter, W. and Fisher, J. Microseparation of the centers of alumina-alumina artificial hip joints during simulator testing produces clinically relevant wear rates and patterns. *Journal of Arthroplasty*, **15(6)**, pp. 793–795 (2000).

Nyren, O., McLaughline, J. and Gridley, G. Cancer risk after total hip replacement with metal implants a population based cohort study in sweden. *Journal of Cancer Institution*, **87(1)**, p. 33 (1995).

Oberle, T. L. Properties of influencing wear of metals. *Journal of Metals*, **3**, pp. 438–439 (1951).

Ogston, A. G. and Stanier, J. E. The physiological function of hyaluronic acid in synovial fluid; viscous, elastic and lubricant properties. *Journal of Physiology*, **119**, pp. 244–252 (1953).

O'Hern, M. E., Parrish, R. H. and Oliver, W. C. Evaluation of mechanical properties of TiN films by ultralow load indentation. *Thin Solid films*, **181**, pp. 357–363 (1989).

Oliver, W. C. and Pharr, G. M. Measurement of hardness and elastic modulus

by instrumented indentation: Advances in understanding and refinements to methodology. *Journal of Materials Research*, **19(1)**, pp. 3–20 (2004).

Onate, J., Comin, M., Braceras, I., Garcia, A., Viviente, J., Brizuela, M., Garagorri, N., Peris, J. and Alava, J. Wear reduction effect on ultra-high-molecular-weight polyethylene by application of hard coatings and ion implantation on cobalt chromium alloy, as measured in a knee wear simulation machine. *Surface and Coatings Technology*, **142-144**, pp. 1056–1062 (2001).

Oonishi, H., Takayama, Y. and Tsuji, E. Improvement of polyethylene by irradiation in artificial joints. *International Journal of Radiation Applications and Instrumentation. Part C. Radiation Physics and Chemistry*, **39(6)**, pp. 495–504 (1992).

Orthopedic Devices Branch, O. o. D. E. Guidance document for the preparation of premarket notifications for ceramic ball hip systems - draft. Technical report, Food and Drug Administration (1995).

Osterle, W., Klaffke, D., Griepentrog, M., Gross, U., Kranz, I. and Knabe, C. Potential of wear resistant coatings on ti-6al-4v for artificial hip joint bearing surfaces. *Wear*, **264**, pp. 505–517 (2008).

Ostrowski, T. and Rödel, J. Evolution of mechanical properties of porous alumina during free sintering and hot pressing. *Journal of the American Ceramic Society*, **82(11)**, pp. 3080–3086 (1999).

Paul, J. P. Forces transmitted by joints in the human body. *Proceedings of the Institution of Mechanical Engineers Part J*, **181**, pp. 8–15 (1967).

Perplas Ltd. Roechling Engineering Plastics UK Ltd, Waterwells Drive, Waterwells Business Park, Quedgeley, Gloucester, GL2 2AA, UK (2005).

URL: *http://www.perplas.co.uk Last Accessed 26th April 2009*

Piconi, C. and Maccauro, G. Zirconia as a ceramic biomaterial. *Biomaterials*, **20**, pp. 1–25 (1999).

Platon, F., Fournier, P. and Rouxel, S. Tribological behaviour of DLC coatings compared to different materials used in hip joint prostheses. *Wear*, **250**, pp. 227–236 (2001).

Raimondi, M. and Pietrabissa, R. The in-vivo wear performance of prosthetic femoral heads with titanium nitride coating. *Biomaterials*, **21**, pp. 907–913 (2000).

Randall, N. X., Favaro, G. and Frankel, C. H. The effect of intrinsic parameters on the critical load as measured with the scratch test method. *Surface and Coatings Technology*, **137**, pp. 146–151 (2001).

Ravikiran, A. and Surappa, M. K. Effect of sliding speed on wear behaviour of a356 al-30 wt. sic_p mmc. *Wear*, **206**, pp. 33–38 (1997).

Ring, P. A. Complete replacement arthroplasty of the hip by the ring prosthesis. *Journal of Bone and Joint Surgery*, **50B(4)**, pp. 720–731 (1968).

Ring, P. A. Total replacement of the hip joint: A review of a thousand operations. *Journal of Bone and Joint Surgery*, **56B(1)**, pp. 44–58 (1974).

Robertson, J. Ultrathin carbon coatings for magnetic storage technology. *Thin Solid Films*, **383**, pp. 81–88 (2001).

Rose, R. M., Goldfarb, H. V., Ellis, E. and Crugnola, A. M. On the pressure dependence of the wear of ultrahigh molecular weight polyethylene. *Wear*, **92**, pp. 99–111 (1983).

Rydell, N. W. Forces acting on the femoral head-prosthesis: A study on strain gauge supplied prostheses in living persons. *Acta Orthopaedica Scandinavica*, **37(Supp 88)**, pp. 1–132 (1966).

Safi, I. Recent aspects concerning dc reactive magnetron sputtering of thin films: a review. *Surface and Coatings Technology*, **127**, pp. 203–219 (2000).

Saikko, V. A three-axis hip joint simulator for wear and friction studies on total hip prostheses. *Proceedings of the Institute of Mechanical Engineers Part H: Journal of Engineering in Medicine*, **210**, pp. 175–185 (1996).

Saikko, V. A multidirectional motion pin-on-disk wear test method for prosthetic joint materials. *Journal of biomedical materials research*, **41(1)**, pp. 58–64 (1998).

Saikko, V. Effect of contact pressure on wear and friction of ultra-high molecular weight polyethylene in multidirectional sliding. *Proceedings of the Institute of Mechanical Engineers Part H: Journal of Engineering in Medicine*, **220**, pp. 723–731 (2006).

Saikko, V. and Ahlroos, T. Type of motion and lubricant in wear simulation

of polyethylene acetabular cup. *Proceedings of the Institute of Mechanical Engineers Part H: Journal of Engineering in Medicine*, **213(4)**, pp. 301–310 (1999).

Saikko, V., Ahlroos, T. and Calonius, O. A three-axis knee wear simulator with ball-on-flat contact. *Wear*, **249**, pp. 310–315 (2001a).

Saikko, V., Ahlroos, T., Calonius, O. and Keränen, J. Wear simulation of total hip prostheses with polyethylene against cocr, alumina and diamond-like carbon. *Biomaterials*, **22**, pp. 1507–1514 (2001b).

Schmidt, M., Weber, H. and Schön, R. Cobalt chromium molybdenum metal combination for modular hip prostheses. *Clinical Orthopaedics and Related Research*, **329S**, pp. S35–S47 (1996).

Scholes, S. C., Green, S. M. and Unsworth, A. The wear of metal on metal total hip prostheses measured in a hip simulator. *Proceedings of the Institute of Mechanical Engineers Part H: Journal of Engineering in Medicine*, **215**, pp. 523–530 (2001).

Scholes, S. C. and Unsworth, A. Pin-on-plate studies on the effect of rotation on the wear of metal-on-metal samples. *Journal of Materials Science: Materials in Medicine*, **12**, pp. 299–303 (2001).

Scholes, S. C., Unsworth, A. and Goldsmith, A. A. J. A frictional study of total hip joint replacements. *Physics in medicine and biology*, **45**, pp. 3721–3735 (2000).

Sedel, L. Evolution of alumina-on-alumina implants. *Clinical Orthopaedics and Related Research*, **379**, pp. 48–54 (2000).

Serra, E., Tucci, A., Esposito, L. and Piconi, C. Volumetric determination of the wear of ceramics for hip joints. *Biomaterials*, **23**, pp. 1131–1137 (2002).

Sheeja, D., Tay, B. K., Krishnan, S. M. and Nung, N. Tribological characterization of diamond like carbon (dlc) coatings sliding against DLC coatings. *Diamond and Related Materials*, **12**, pp. 1389–1395 (2003).

Sheeja, D., Tay, B. K. and Nung, L. N. Feasibility of diamond-like carbon coatings for orthopaedic applications. *Diamond and Related Materials*, **13**, pp. 184–190 (2004).

Sheeja, D., Tay, B. K. and Nung, L. N. Tribological characterisation of surface modified uhmwpe against dlc-coated co-cr-mo. *Surface and Coatings Technology*, **190**, pp. 231–237 (2005).

Shi, W., Li, X. Y. and Dong, H. Improved wear resistance of ultra-high molecular weight polyethylene by plasma immersion ion implantation. *Wear*, **250**, pp. 544–552 (2001).

Sieber, H. P., Rieker, C. B. and Köttig, P. Analysis of 118 second-generation metal-on-metal retrieved hip implants. *Journal of Bone and Joint Surgery*, **80B**, pp. 46–50 (1998).

Sigmund, P. Theory of sputtering. I. sputtering yield of amorphous and polycrystalline targets. *Physical Review*, **184(2)**, pp. 383–416 (1969).

Smith, S. L., Dowson, D. and Goldsmith, A. A. J. The lubrication of metal on metal total hip joints: a slide down the stribeck curve. *Proceedings of the Institution of Mechanical Engineers, Part J: Journal of Engineering Tribology*, **215(5)**, pp. 483–493 (2001).

Smith, S. L. and Unsworth, A. A five-station hip joint simulator. *Proceedings of the Institute of Mechanical Engineers Part H: Journal of Engineering in Medicine*, **215**, pp. 61–64 (2001).

Smith and Nephew plc. 15 Adam Street, London, WC2N 6LA, UK (2009). **URL:** *http://www.smithandnephew.com/ Last Accessed 26th April 2009*

Smith-Petersen, M. N. Evolution of mould arthroplasty of the hip joint. *Journal of Bone and Joint Surgery*, **30B(1)**, pp. 59–75 (1948).

Stallard, J. *The Tribological Behaviour of three Carbon-based Coatings, Tested in Air, Water and Oil Environments*. Ph.D. thesis, University of Nottingham (2005).

Stallard, J., Mercs, D., Jarratt, M., Teer, D. G. and Shipway, P. H. Study of the tribological behaviour of three carbon-based coatings, tested in air, water and oil environments at high loads. *Surface and Coatings Technology*, **177-178**, pp. 545–551 (2004).

Stanislav, J., Sikac, J. and Cermak, M. Properties of magnetron-deposited polycrystalline TiN layers. *Thin Solid Films*, **191**, pp. 255–273 (1990).

Streicher, R. M., Semlitsch, M., Schon, R., Weber, H. and Rieker, C. Metal-

on-metal articulation for artificial hip joints: laboratory studies and clinical results. *Proceedings of the Institute of Mechanical Engineers Part H: Journal of Engineering in Medicine*, **210(3)**, pp. 223–232 (1996).

Stryker Howmedica. Stryker House, Hambridge Road, Newbury, Berkshire, RG14 5EG, UK (2007).

URL: *http://www.stryker.com Last Accessed 26th April 2009*

Swedish Hip Arthroplasty Register. Annual report 2003. Technical report, Department of Orthopaedics, Sahlgrenska University Hospital (2004).

Swedish Hip Arthroplasty Register. Annual report 2005. Technical report, Department of Orthopaedics, Sahlgrenska University Hospital (2006).

Taeger, G., Podleska, L. E., Schmidt, B., Ziegler, M. and Nast-Kolb, D. Comparison of diamond-like-carbon and alumina-oxide articulating with polyethylene in total hip arthroplasty. *Materialwissenschaft und Werkstofftechnik*, **34(12)**, pp. 1094–1100 (2003).

Taylor Hobson Ltd. PO Box 36, 2 New Star Road, Leicester, LE4 9JQ, UK (2009).

URL: *http://www.taylor-hobson.com Last Accessed 26th April 2009*

Technical Committee ISO/TC 150, Subcommittee 1. ISO 6474: Non-metallic materials for surgical implants - part 2: Specification for ceramic materials based on high purity alumina. Technical Report ISO 6474, International Standards Organization (1994).

Technical Committee ISO/TC 150 Subcommittee 1. ISO 5832: Metallic materials for surgical implants - part 1: Specification for wrought titanium 6-aluminium 4-vanadium alloy. Technical Report ISO 5832-3, International Standards Organization (1996).

Technical Committee ISO/TC 150 Subcommittee 1. ISO 5832: Metallic materials for surgical implants - part 1: Specification for wrought stainless steel. Technical Report ISO 5832-1, International Standards Organization (1997a).

Technical Committee ISO/TC 150 Subcommittee 1. ISO 5832: Metallic materials for surgical implants - part 4: Specification for cobalt-chromium-molybdenum casting alloy. Technical Report ISO 5832-4, International Standards Organization (1997b).

Technical Committee ISO/TC 150, Subcommittee 1. ISO 6474: Non-metallic materials for surgical implants - part 6: Specification for ceramic materials based on yttria-stabilized tetragonal zirconia (y-tzp). Technical Report ISO 13356, International Standards Organization (1997).

Technical Committee ISO/TC 150, Subcommittee 4. ISO 7206: Orthopaedic joint prostheses - part 4: Specification for articulating surfaces made of metallic, ceramic and plastics materials of hip joint prostheses. Technical Report ISO 7206, International Standards Organization (1996).

Technical Committee ISO/TC 150, Subcommittee 4. ISO 14242: Implants for surgery - wear of total hip-joint prostheses - part 1: Loading and displacement parameters for wear-testing machines and corresponding environmental

conditions for test. Technical Report ISO 14242-1, International Standards Organization (2002).

Teer, D. G. Magnetron sputter ion plating. UK Patent No. GB 2 258 343B (1991).

Teer, D. G. New solid lubricant coatings. *Wear*, **251**, pp. 1068–1074 (2001).

Teer, D. G., Camino, D. and Jones, A. H. S. Carbon coatings, method and apparatus for applying them, and articles bearing such coatings. US Patent No. 6,726,993 (2004).

Teer Coatings Ltd. West Stone House, Berry Hill Industrial Estate, Droitwich, Worcestershire, WR9 9AS, UK (2004).
URL: *http://www.teercoatings.co.uk Last Accessed 26th April 2009*

Thompson, C. W. and Floyd, R. T. *Manual of Structural Kinesiology*. Mosby College (1997).

Tiainen, V.-M. Amorphous carbon as a bio-mechanical coating - mechanical properties and biological applications. *Diamond and Related Materials*, **10**, pp. 153–160 (2001).

Tipper, J. L., Firkins, P. J., Ingham, E., Fisher, J., Stone, M. H. and Farrar, R. Quantitative analysis of the wear and wear debris from low and high carbon content cobalt chrome alloys used in metal on metal total hip replacements. *Journal of Materials Science: Materials in Medicine*, **10**, pp. 353–362 (1999).

Torregrosa, F., Barrallier, L. and Roux, L. Phase analysis, microhardness and tribological behaviour of ti-6al-4v after ion implantation of nitrogen in connection with its application for hip joint prosthesis. *Thin Solid Films*, **266**, pp. 245–253 (1995).

University of Huddersfield. Centre for Precision Technologies, Queensgate, Huddersfield, HD1 3DH, UK (2006).
URL: *http://www.hud.ac.uk Last Accessed 26th April 2009*

University of Leeds. Institute of Medical and Biological Engineering, Leeds, LS2 9JT, UK (2006).
URL: *http://www.leeds.ac.uk Last Accessed 26th April 2009*

University of Surrey. Ion Beam Centre, Guildford, Surrey, GU2 7XH, UK (2007).
URL: *http://www.surrey.ac.uk Last Accessed 26th April 2009*

University of Wolverhampton. School of Engineering and the Built Environment, Wulfruna St, Wolverhampton, WV1 1LY, UK (2005).
URL: *http://www.wlv.ac.uk/EAT Last Accessed 26th April 2009*

Unsworth, A. The effects of lubrication in hip joint prostheses. *Physics in Medicine and Biology*, **23(2)**, pp. 253–268 (1978).

Unsworth, A. Tribology of artificial hip joints. *Proceedings of the Institute of Mechanical Engineers Part J: Journal of Engineering Tribology*, **220**, pp. 711–718 (2006).

Vassiliou, K., Elfick, A. P. D., Scholes, S. C. and Unsworth, A. The effect of

'running-in' on the tribology and surface morphology of metal-on-metal birmingham hip resurfacing device in simulator studies. *Proceedings of the Institute of Mechanical Engineers Part H: Journal of Engineering in Medicine*, **220**, pp. 269–277 (2006).

Vassiliou, K. and Unsworth, A. Is the wear factor in total joint replacements dependent on the nominal contact stress in ultra-high molecular weight polyethylene contacts? *Proceedings of the Institute of Mechanical Engineers Part H: Journal of Engineering in Medicine*, **218(2)**, pp. 101–107 (2004).

Visuri, T., Pukkala, E., Paavolainen, P., Pulkkinen, P. and Riska, E. B. Cancer risk after metal on metal and polyethylene on metal total hip arthroplasty. *Clinical Orthopaedics and Related Research*, **329S**, pp. S280–S289 (1996).

Voevodin, A. A., O'Neill, J. P. and Zabinski, J. S. Nanocomposite tribological coatings for aerospace applications. *Surface and Coatings Technology*, **116-119**, pp. 36–45 (1999).

Wang, A., Lin, R., Stark, C. and Dumbleton, J. H. Suitability and limitations of carbon fiber reinforced peek composites as bearing surfaces for total joint replacements. *Wear*, **225-229**, pp. 724–727 (1999a).

Wang, A., Polineni, K., Essner, A., Stark, C. and Dumbleton, J. H. The impact of lubricant protein concentration on the outcome of hip simulator testing. In *Proceedings of the 45th Annual Meeting of the Orthopaedic Research Society*, p. 52 (1999b).

Wang, A., Stark, C. and Dumbleton, J. H. Mechanistic and morphological origins of ultra-high molecular weight polyethylene wear debris in total joint replacement prostheses. *Proceedings of the Institute of Mechanical Engineers Part H: Journal of Engineering in Medicine*, **210(3)**, pp. 141–155 (1996).

Wang, A., Sun, D. C., Yau, S., Edwards, B., Sokol, M., Essner, A., Polineni, V. K., Stark, C. and Dumbleton, J. H. Orientation softening in the deformation and wear of ultra-high molecular weight polyethylene. *Wear*, **203-204**, pp. 230–241 (1997).

Wang, M., Jiang, X. and Stritzker, B. Adhesion of hydrogenated amorphous carbon films on silicon substrates and its enhancement. *Thin Solid Films*, **197**, pp. 57–66 (1991).

Waugh, W. *John Charnley: The man and the hip*. Springer-Verlag (1990).

Weisse, B., Zahner, M., Weber, W. and Rieger, W. Improvement of the reliability of ceramic hip joint implants. *Journal of Biomechanics*, **36**, pp. 1633–1639 (2003).

Wells, V. M., Hearn, T. C., McCaul, K. A., Anderton, S. M., Wigg, A. E. R. and Graves, S. E. Changing incidence of primary total hip arthroplasty and total knee arthroplasty for primary osteoarthritis. *Journal of Arthroplasty*, **17(3)**, pp. 267–273 (2002).

Williams, S., Topper, J. L., Ingham, E., Stone, M. H. and Fisher, J. In vitro analysis of the wear, wear debris and biological activity of surface-engineered coatings for use in metal-on-metal total hip replacements. *Proceedings of the*

Institute of Mechanical Engineers Part H: Journal of Engineering in Medicine, **217(3)**, pp. 155–163 (2003).

Wimmer, M. A., Loos, J., Nassutt, R., Heitkemper, M. and Fischer, A. The acting wear mechanisms on metal-on-metal hip joint bearings: in vitro results. *Wear*, **250**, pp. 129–139 (2001).

Windischmann, H. Intrinsic stress in sputter-deposited thin films. *Critical Reviews in Solid Sate Materials Sciences*, **17(6)**, pp. 547–596 (1992).

Window, B. and Savvides, N. Charged particle fluxes from planar magnetron sputtering sources. *Journal of Vacuum Science Technology A*, **4(2)**, pp. 196–202 (1986).

Yang, S., Camino, D., Jones, A. H. S. and Teer, D. G. Deposition and tribological behaviour of sputtered carbon hard coatings. *Surface and Coatings Technology*, **124**, pp. 110–116 (2000).

Yatsuzuka, M., Oka, Y., Nishijima, M. and Hiraga, K. Microstructure of interface for high-adhesion dlc film on metal substrates by plasma-based ion implantation. *Vacuum*, **83**, pp. 190–197 (2009).

Yeh, T.-S., Wu, J.-M. and Hu, L.-J. The properties of TiN thin films deposited by pulsed direct current magnetron sputtering. *Wear*, **516**, pp. 7294–7298 (2008).

Zeeko Ltd. 4 Vulcan Court, Vulcan Way, Coalville, Leicestershire, LE67 3FW, UK (2009).

URL: *http://www.zeeko.co.uk Last Accessed 26th April 2009*

Zhang, S., Sun, D., Fu, Y. and Du, H. Toughness measurement of thin films: a critical review. *Surface and Coatings Technology*, **198**, pp. 74–84 (2005a).

Zhang, S., Zeng, X. T., Xie, H. and Hing, P. A phenomenological approach for the i_d/i_g ratio and sp^3 fraction of magnetron sputtered a-c films. *Surface and Coatings Technology*, **123**, pp. 256–260 (2000).

Zhang, W., Tanaka, A., Xu, B. S. and Koga, Y. Study on the diamond-like carbon multilayer films for tribological application. *Diamond and Related Materials*, **14(8)**, pp. 1361–1367 (2005b).

Zhang, Z. X., Dong, H., Bell, T. and Xu, B. S. The effect of deep-case oxygen hardening on the tribological behaviour of a-c:h dlc coatings on ti6al4v alloy. *Journal of Alloys and Compounds*, **464**, pp. 519–525 (2008).

Ziegler, J. F., Biersack, J. P. and Littmark, U. *The Stopping and Range of Ions in Solids*. Pergamon Press, New York (1985).

Ziegler, J. F., Biersack, J. P. and Littmark, U. The stopping and range of ions in solids software (pc) (2008).

URL: *http://www.srim.org/*

Zu, M., Zhou, Z., Kapsa, P. H. and Vincent, L. Radial fretting damage of surface coatings. *Wear*, **250**, pp. 650–657 (2001).

Appendices

Appendix A: Process Parameters

This appendix details the penetration of nitrogen ion depth penetration through UHMWPE with increasing implantation energy; as calculated using the SRIM software written by Ziegler *et al.* (2008).

Ion Energy (KeV)	Projected Range (A)
10	457
15	663
20	867
25	1,066
30	1,262
35	1,456
40	1,648
45	1,837
50	2,024
55	2,208
60	2,390
65	2,571
70	2,750
80	3,104
90	3,453
100	3,798
150	5,462
200	7,032
250	8,510
300	9,898
350	11,200
400	12,400
450	13,600
500	14,700
1,000	23,700
2,000	36,800
2,500	42,200
5,000	66,000
10,000	111,800

Appendix B: Nano-Indentation

The Figures within this appendix are depth-load profiles resulting from the nano-indentation of the coatings deposited for this study.

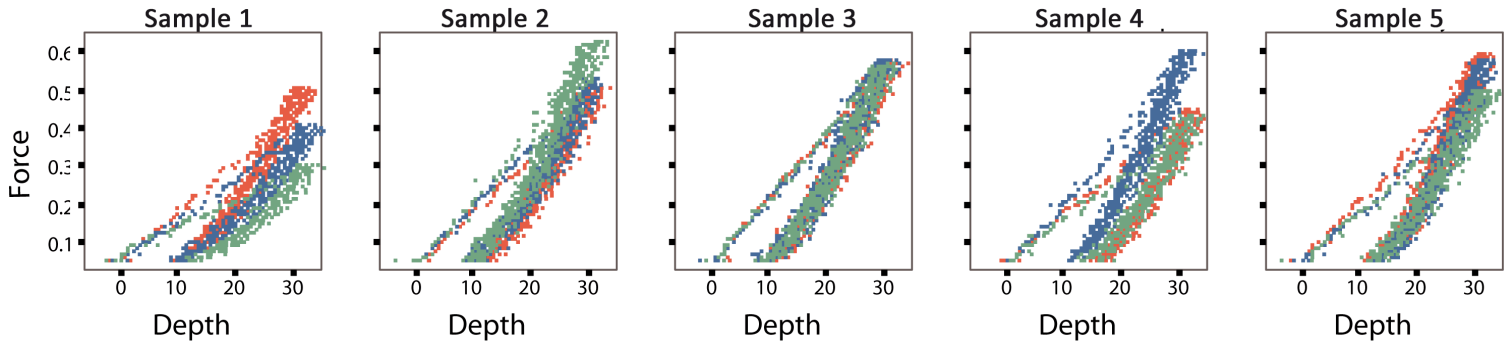

Figure B.1: Nano-indentation of coated CoCr to 30nm depth (Force scale mN)

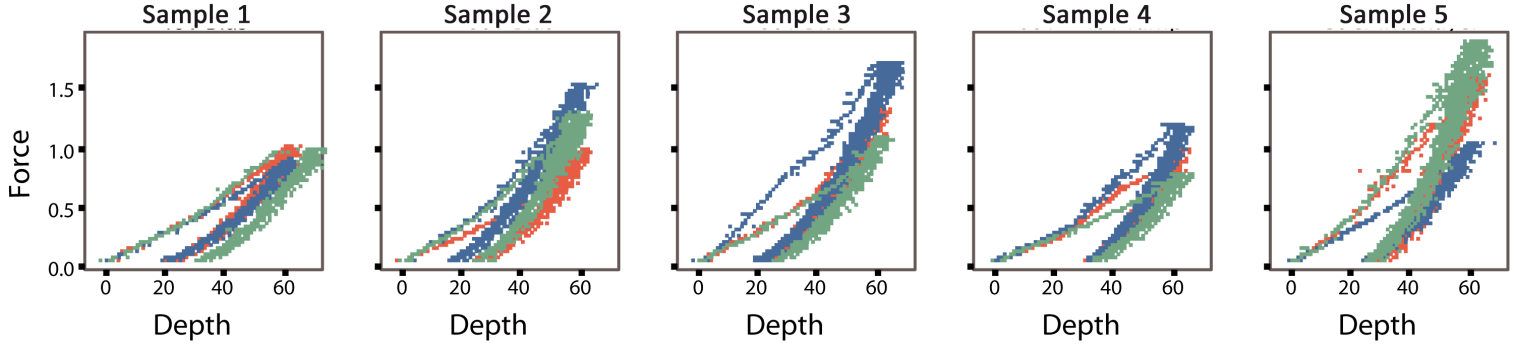

Figure B.2: Nano-indentation of coated CoCr to 60nm depth (Force scale mN)

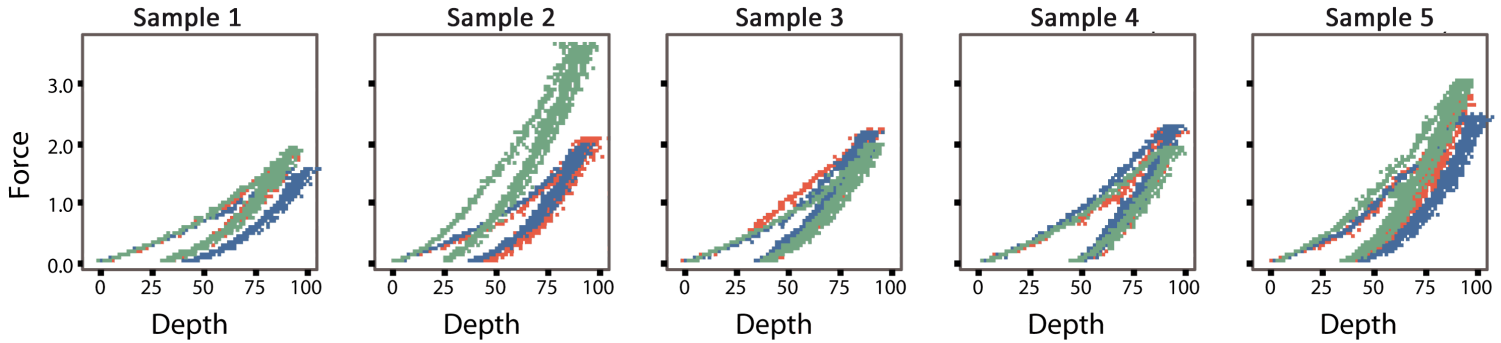

Figure B.3: Nano-indentation of coated CoCr to 90nm depth (Force scale mN)

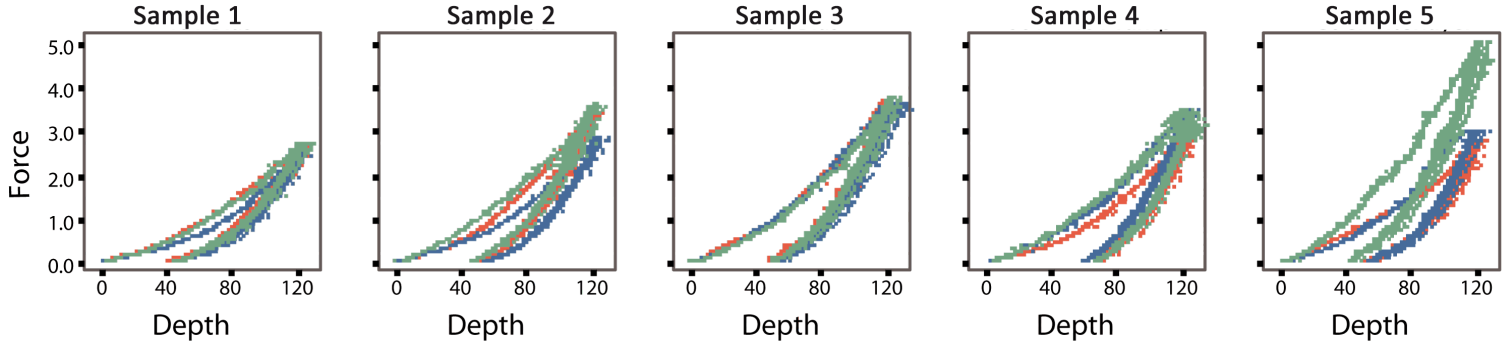

Figure B.4: Nano-indentation of coated CoCr to 120nm depth (Force scale mN)

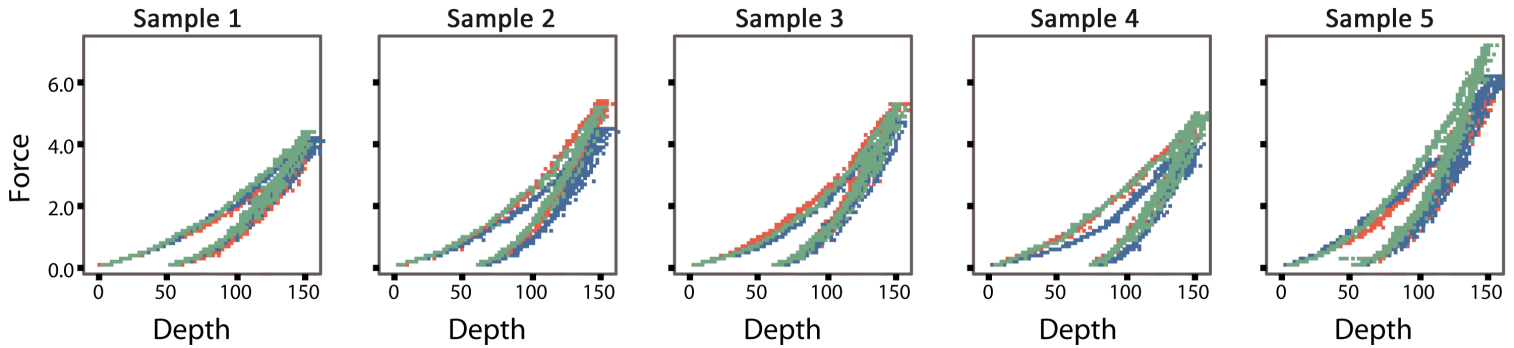

Figure B.5: Nano-indentation of coated CoCr to 150nm depth (Force scale mN)

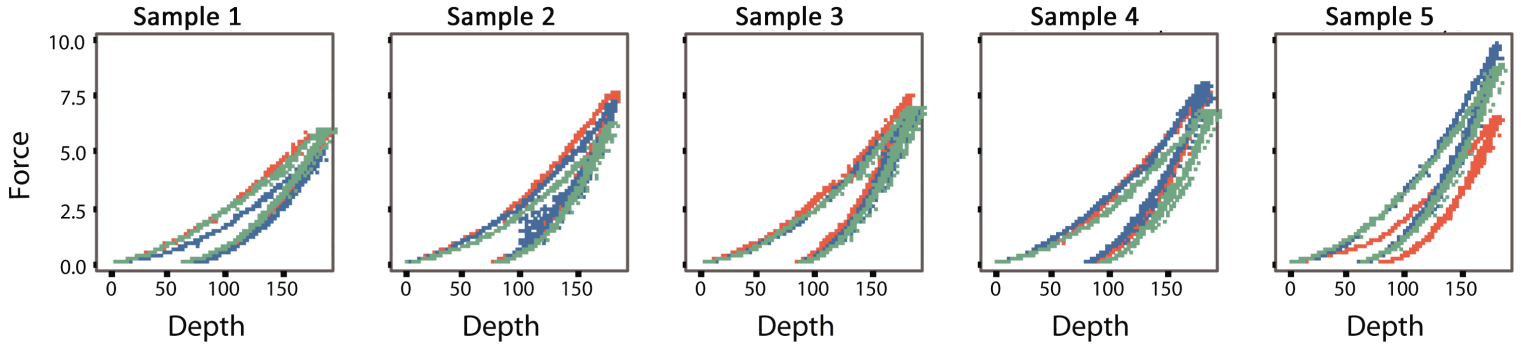

Figure B.6: Nano-indentation of coated CoCr to 180nm depth (Force scale mN)

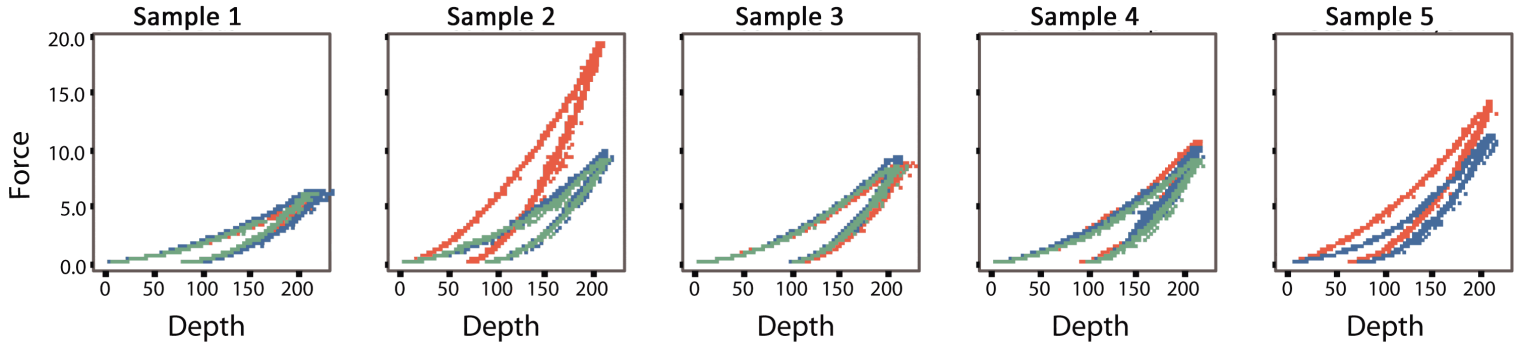

Figure B.7: Nano-indentation of coated CoCr to 210nm depth (Force scale mN)

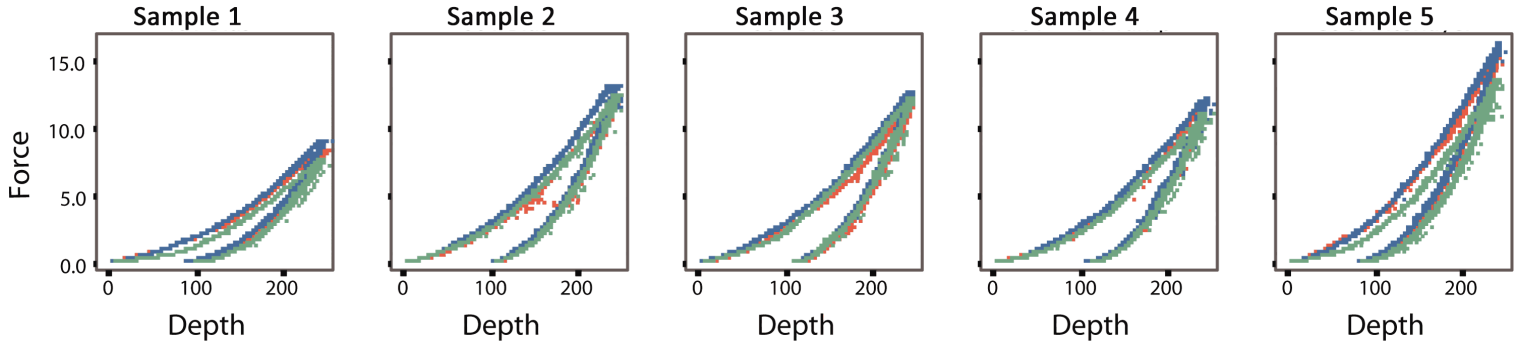

Figure B.8: Nano-indentation of coated CoCr to 240nm depth (Force scale mN)

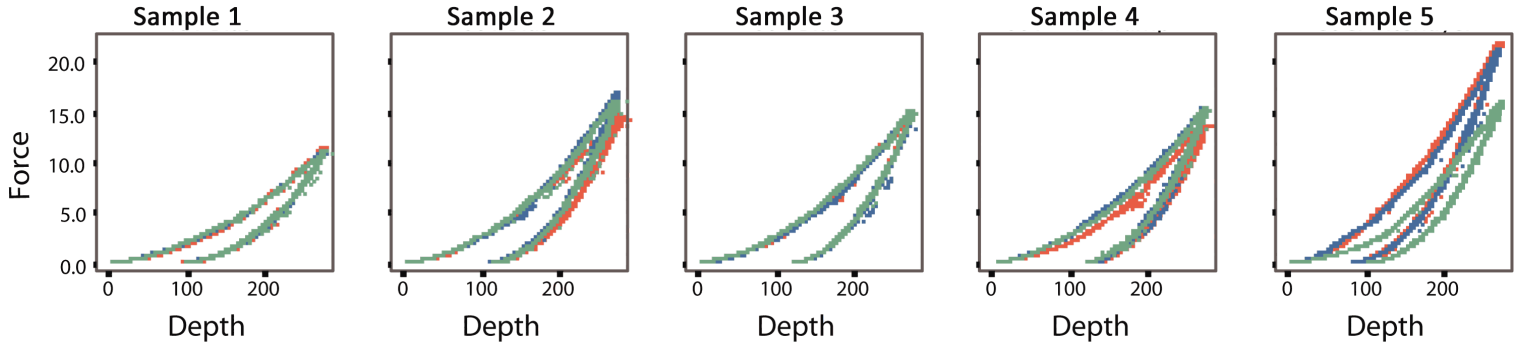

Figure B.9: Nano-indentation of coated CoCr to 270nm depth (Force scale mN)

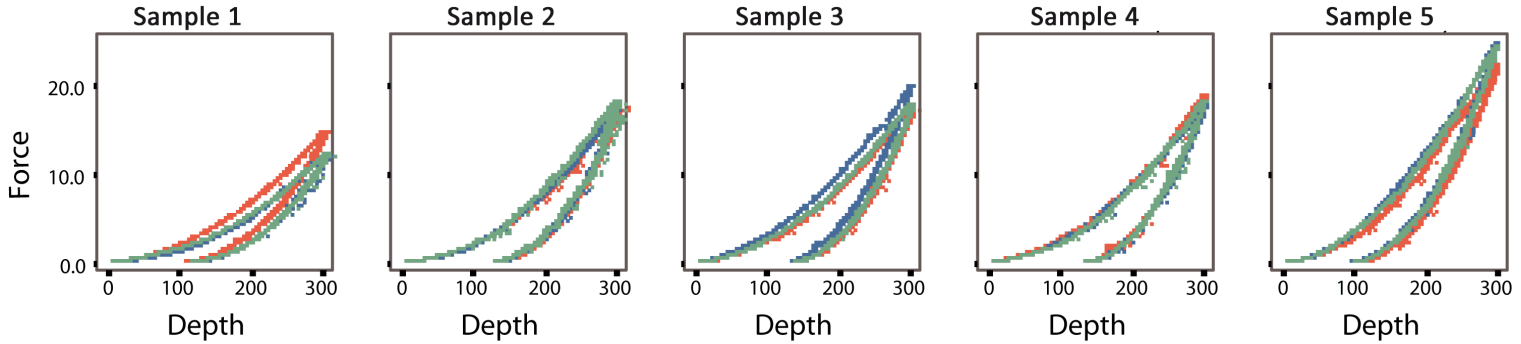

Figure B.10: Nano-indentation of coated CoCr to 300nm depth (Force scale mN)

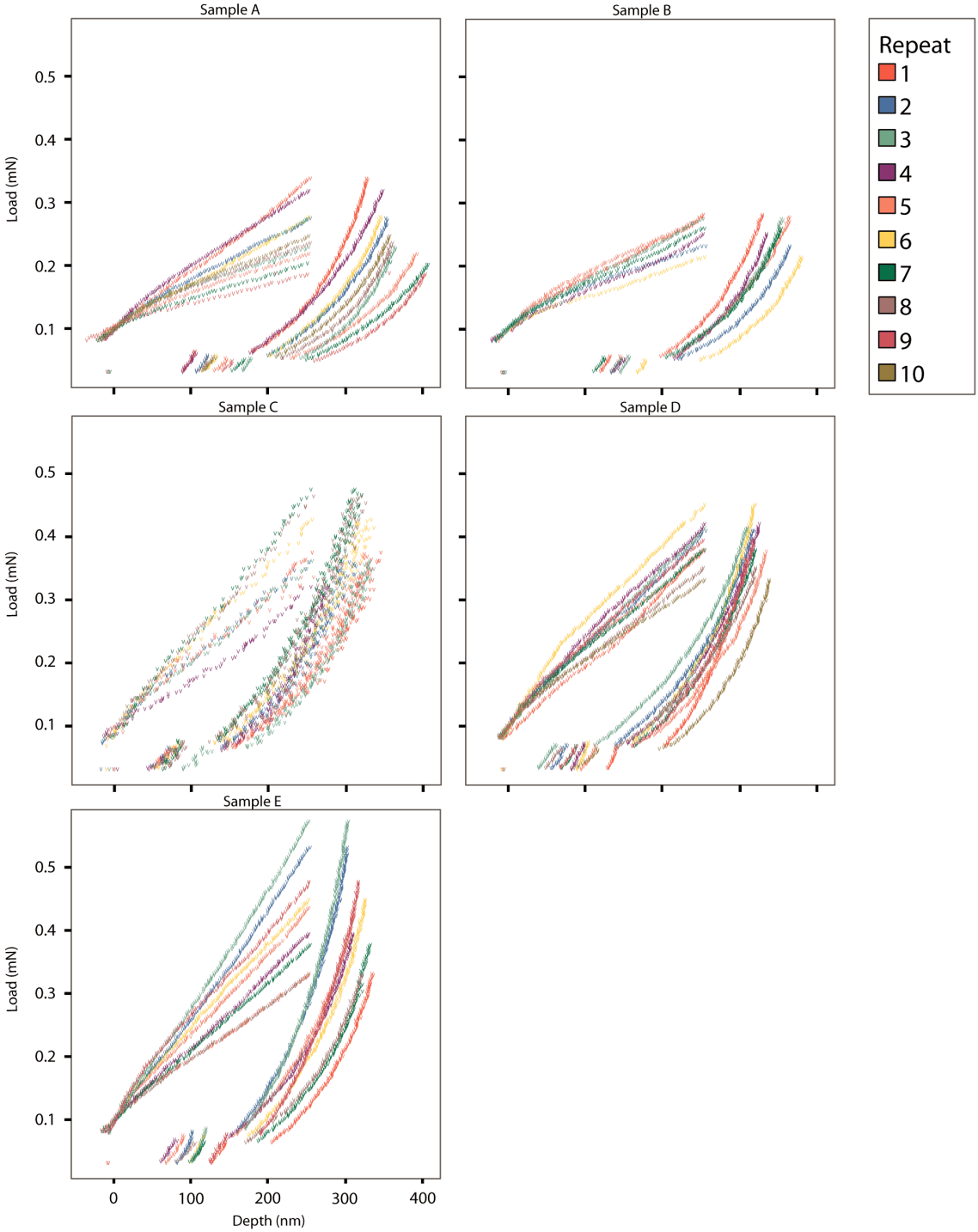

Figure B.11: Depth-load nano-indentation graphs of ion implanted UHMWPE

Appendix C: Equations

C.1 Coordinate Transfer Derivation

Figure C.1 illustrates the notation used for determining position in the z axis of the point of the pin in contact with the polishing pad on the Zeeko CNC polishing machine. When $\theta = 0$, z is equal to the disc radius; however as the disc is rotated so that the disc edge can be polished z will change; therefore to maintain the same contact with the polishing pad it must be moved closer. In order to calculate this, z must be known.

From Figure C.1 the only values known are R_d (disc radius), R_e (disc edge radius) and θ (the angle the disc is being held at). In order to illustrate the derivation a formula for z with respect to these known values, the variables γ, ϵ, τ have been arbitrarily named; they represent the various geometric features that are marked in Figure C.1

$$z = \gamma \cos \varepsilon \tag{C.1}$$

By cosine rule:

$$\gamma = \sqrt{(R_d - R_e)^2 + R_e^2 - 2(R_d - R_e)R_e \cos \phi} \tag{C.2}$$

$$\phi = \pi - \theta \tag{C.3}$$

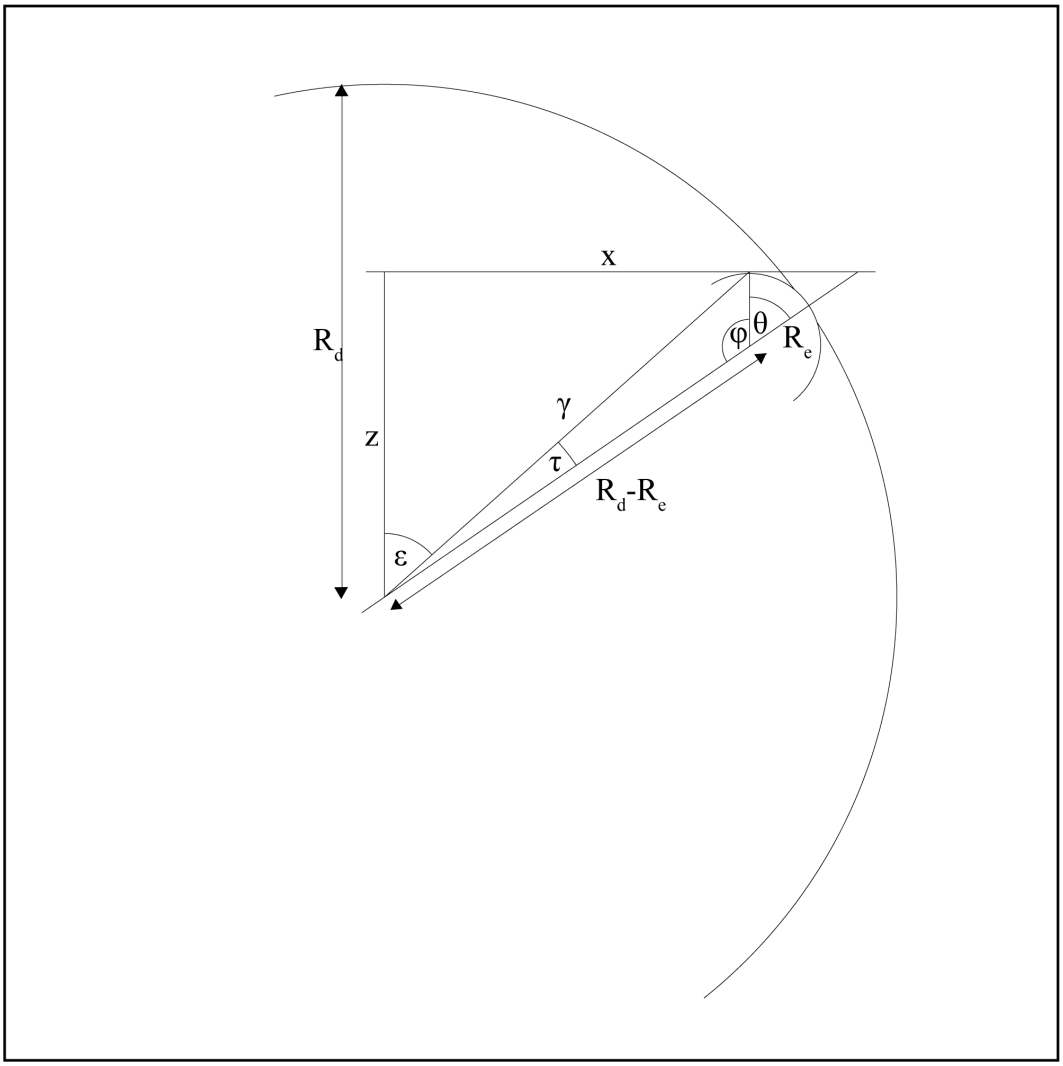

Figure C.1: Coordinate transfer geometry notation

$$\therefore \gamma = \sqrt{(R_d - R_e)^2 + R_e^2 - 2(R_d - R_e)R_e \cos(\pi - \theta)} \tag{C.4}$$

$$\varepsilon = \theta - \tau \tag{C.5}$$

By sine rule

$$\frac{\sin\phi}{\gamma} = \frac{\sin\tau}{R_e} \tag{C.6}$$

$$\therefore \varepsilon = \theta - \arcsin\left(\frac{R_e \sin\phi}{\gamma}\right) \tag{C.7}$$

$$\therefore z = \sqrt{(R_d - R_e)^2 + R_e^2 - (2(R_d - R_e)R_e \cos(\pi - \theta))}$$
$$\cos\left(\theta - \arcsin\left(\frac{\theta - (R_e \sin(\pi - \theta))}{\sqrt{(R_d - R_e)^2 + R_e^2 - (2(R_d - R_e)R_e \cos(\pi - \theta))}}\right)\right) \tag{C.8}$$

C.2 Calculation of Wear Volume from Observation of an Elliptical Wear Scar

C.2.1 Equation

If the wear scar of a pin with two radii is examined, the shape observed will be elliptical; the dimensions of the ellipse will be related to the two radii and the quantity of wear. As the two radii are known, the depth of the wear scar can be

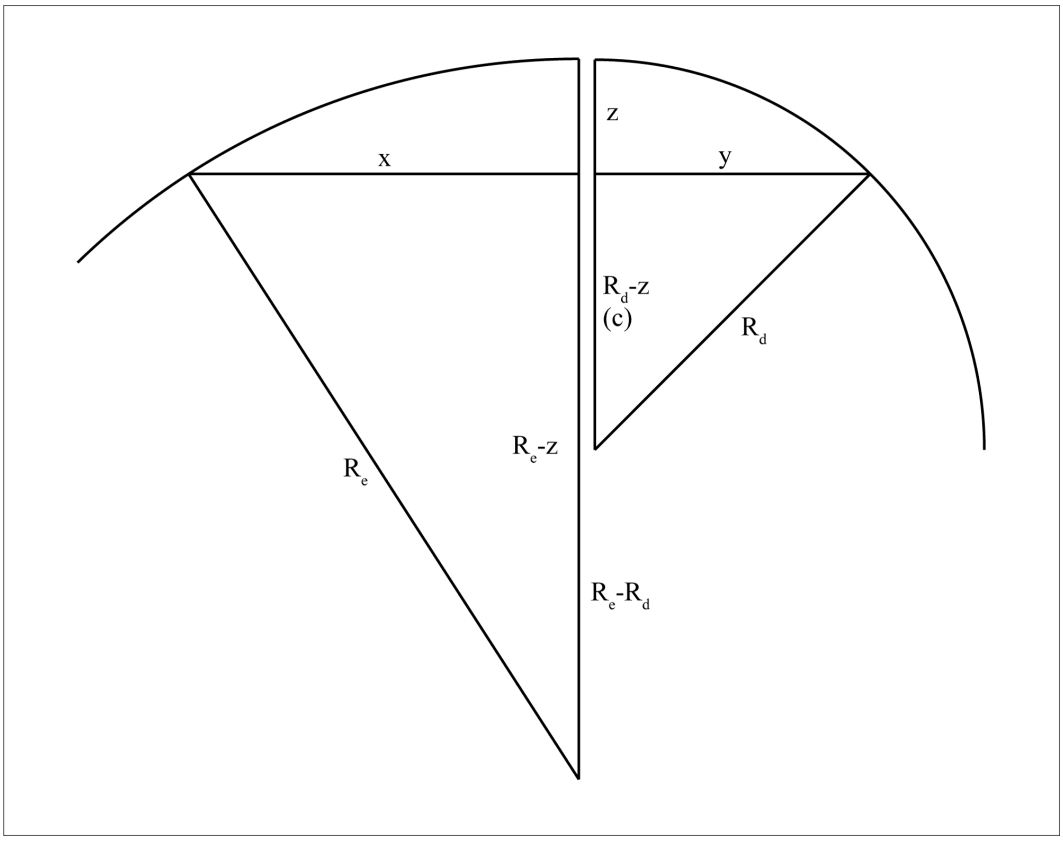

Figure C.2: Multi-edge disc schematic

calculated and vice versa.

$$z = R_d - \sqrt{R_d^2 - y^2} \tag{C.9}$$

$$z = R_e - \sqrt{R_e^2 - x^2} \tag{C.10}$$

Consequently, by knowing the depth of wear and the two radii, it will be possible to calculate the area of the ellipse. To integrate from the wear depth through one of the radii will result in a volume calculation. Therefore the following equations stand (Figure C.2 illustrates the relationship between variables)

The area of an ellipse is defined by equation C.11 where A = area; x and y are

the two ellipse radii:

$$A = \pi xy \tag{C.11}$$

by integrating through depth of scar the volume can be calculated:

$$V = \pi \int_{R_d}^{c} xydc \tag{C.12}$$

dimension x with respect to c:

$$x = \sqrt{R_e^2 - (c + (R_e - R_d))^2} \tag{C.13}$$

dimension y with respect to c:

$$y = \sqrt{R_d^2 - c^2} \tag{C.14}$$

$$\therefore V = \pi \int_{R_d}^{\sqrt{R_d^2 - X^2}} \sqrt{R_d^2 - x^2}\sqrt{R_e^2 - (x + (R_e - R_d))^2}dx \tag{C.15}$$

C.2.2 Excel Macro

Equation C.15 can only be solved using numerical methods. In order to speed calculation of the wear volume a Microsoft Excel macro was written to automatically calculate the wear when the disc radii and wear scar diameter had been input; this code was written by Burley (2006). The numerical method used to

solve the equation is Romberg Integration (Hazewinkel, 2002)

```
Function Integrate(ByVal disc As Double, ByVal edge As Double,
ByVal y As Double, ByVal order As Integer) As Double
    Dim a As Double
    a = ( disc ^ 2 - ( y / 2) ^ 2) ^ 0.5
    Integrate = ComputeT_l_k(order, 1, a, disc, disc, edge)
End Function
```

```
Function ComputeT_l_k(ByVal l As Integer, ByVal k As Integer,
ByVal a As Double, ByVal b As Double, ByVal disc As Double,
ByVal edge As Double) As Double
        Dim h As Double
        Dim working_l As Integer
        Dim result As Double
        Dim temp2 As Double
        Dim j As Double
        temp2 = 0
        h = (b - a) / (2 ^ (k - 1))
        If l = 1 Then
            working_l = (2 ^ (k - 1)) - 1

            result = f(a, disc, edge) + f(b, disc, edge)

            For j = 1 To working_l
                temp2 = temp2 + f(a + (j * h), disc, edge)
            Next j
            result = result + temp2 * 2

            result = result * (h / 2)
        Else
            result = (4 ^ (l - 1)) *
            ComputeT_l_k(l - 1, k + 1, a, b, disc, edge)
            result = result - ComputeT_l_k(l - 1, k, a, b, disc, edge)
            result = result / ((4 ^ (l - 1)) - 1)
        End If

        ComputeT_l_k = result
End Function
```

```
Public Function f(ByVal x As Double, ByVal disc As Double,
ByVal edge As Double) As Double
        f = 3.14159265358979 * (disc ^ 2 - x ^ 2) ^ 0.5 *
        (edge ^ 2 - (x + (edge - disc)) ^ 2) ^ 0.5
End Function
```

References

Hazewinkel, M., editor. *Encyclopaedia of Mathematics.* Kluwer Academic (2002).

Burley, M., University of Wolverhampton, School of Computing and Technology, Wulfruna St., Wolverhampton, WV1 1LY, UK (2009).

URL: *http://www.wlv.ac.uk Last Accessed 26th April 2009*

Appendix D: XPS spectra

Figures D.1 and D.2 are the XPS spectra produced from the analysis of the deposits left on the 40V bias coating.

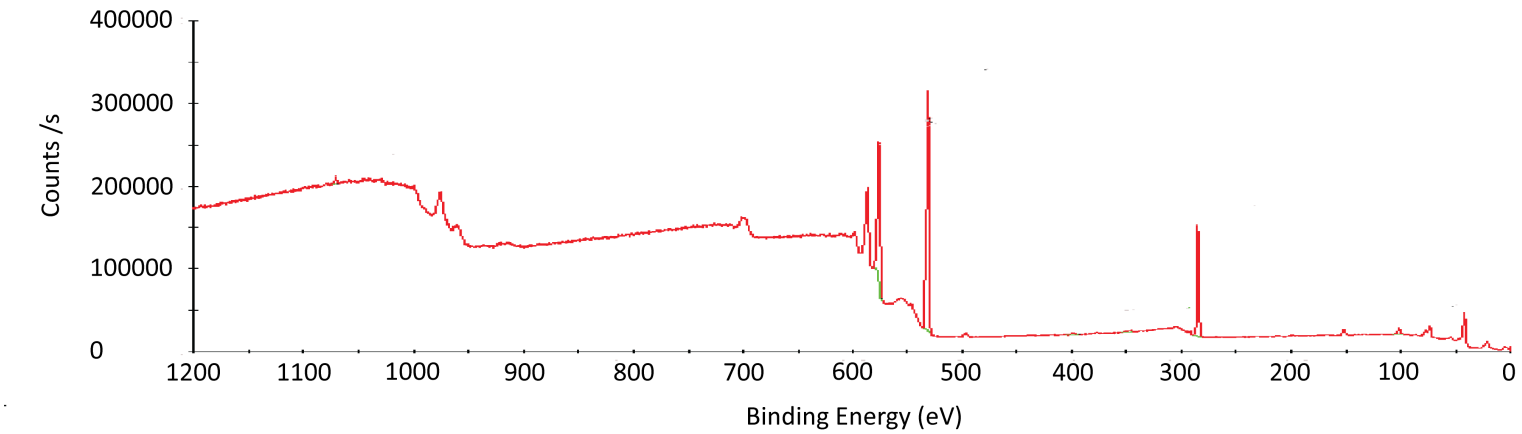

Figure D.1: XPS survey of 40V bias coating on CoCr substrate

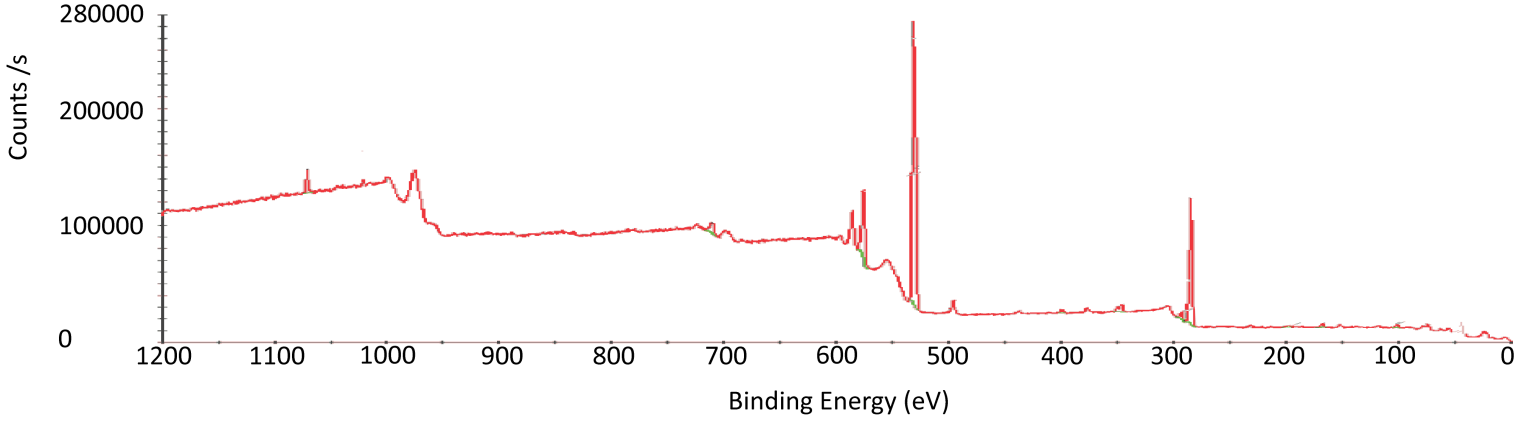

Figure D.2: XPS survey of deposit found at wear point of 40V bias coating on CoCr substrate

Appendix E: Publications

This appendix lists the presentations and posters that have been presented at various conferences related to the work in this thesis.

E.1 Conference Articles

E.1.1 Laser Metrology and Machine Performance VIII, 2007, Cardiff, UK: The significance of sample preparation when testing surface coatings for orthopaedic implants

P. Knox, P. Charlton, T. Laoui, G. Pearce, L. Blunt

In the UK there are over 50,000 hip replacement operations annually, of which approximately 10% are revision surgeries, most commonly necessitated by aseptic loosening. By improving implant design the number of risky and costly revision surgeries can be significantly reduced.

Aseptic loosening is mainly caused by osteolysis, a condition that occurs when the body attempts to break down wear particles produced from the articulation of the artificial joint; the chemicals used by the body have limited effect on the wear particles but do start to cause the bone to reabsorb. By reducing the production of wear particles and making those that are produced as biocompatible as possible, the incidence of aseptic loosening can be reduced. Surface coatings are prime

candidates for achieving this.

By modifying the surface of the implant using coatings, it is possible to modify the tribology of the joint while retaining the bulk properties. This not only enables the increase of wear resistance of the joint but introduces a barrier between the blood and the metal components which are causing increased concern among medical professionals who are worried about the toxic effect of metal ions being released into the body.

For orthopaedic implants to reach the market, stringent testing is required. Joint simulators are used for testing, machines that attempt to mimic the movement and loading expected in the body. Unfortunately tests can take months to complete; this is unsuitable for initial development of coatings numerous iterations of which can be produced in a few days. Consequently preliminary testing is carried out using other techniques, such as pin on disc, which sacrifices elements of the simulation of the joint movement for speed.

Initial pin on disc tests used to identify potential coating candidates identified a need to accurately control the geometry and surface characteristics of the test samples used for short tests (<1 day) so as to be able to accurately measure the small amounts of wear created by the measurement techniques described within this paper. Control of surface finish was also important to ensure that there were no significant surface defects which may act as stress concentrators and result in premature failing of the coating.

By using a 7 axis CNC Zeeko polishing machine, it has been possible to accurately

control the surface roughness and form of samples and characterise their effect on the wear of surface coatings that are being developed for orthopaedic applications.

E.2 Poster Abstracts

E.2.1 Materials Congress 2006, London, UK: Evaluation of wear behaviour of amorphous carbon coatings developed for application onto hip joints

P. A. Knox, T. Laoui, S. Field

Hip joint prostheses are being implanted into the young with increasing frequency. The active lifestyle that younger people enjoy results in an increased incidence of aseptic loosening compared to that seen in elderly patients (Swedish Hip Arthroplasty Register, 2004).

By applying an amorphous carbon coating known as Graphit-iC^{TM} to the femoral-acetabular interface it is predicted that the wear of the implant can be reduced, decreasing the incidence of aseptic loosening.

The Graphit-iC^{TM} coating developed by Teer Coatings Ltd. has been successfully used in a wide range of low to heavily loaded applications where its low wear and friction characteristics have demonstrated considerable benefits. It is anticipated that it can be further optimised for orthopaedic applications. Initial studies have demonstrated wear rates as low as 1.87×10^{-18} m^3/Nm on CoCr substrates during

pin-on-disc testing in bovine serum. Coatings that perform well in pin-on-disc will be applied to hip prostheses and tested using a hip simulator.

E.2.2 UK Society of Biomaterials 2006: Development of an amorphous carbon coating for application onto hip joints and other prostheses. A preliminary study

P. A. Knox, T. Laoui, S. Field

Aseptic loosening is the most common medium to long term cause of failure in hip joints and other prostheses, it is exasperated by placing implants into younger, more active patients. By developing an improved amorphous carbon coating for the implant at the acetabular and femoral interface, it is hoped that the rate of wear can be reduced, thereby reducing the incidence of aseptic loosening and associated revision surgeries.

Coatings were deposited using a closed field unbalanced magnetron sputtering technique developed by Teer Coatings Ltd and based upon their Graphit-iC^{TM} coating. Preliminary studies were carried out using a pin on disc technique to identify potential coatings for further testing in a hip simulator.

Initial results are promising, with wear rates to the order of 1.87×10^{-18} m^3/Nm with amorphous carbon coated CoCr samples sliding against each other in 20% bovine serum diluted with deionised water under a 40N load.

Studies are continuing with further promising and improved results expected.

Coatings system parameters will be adjusted to optimise the coatings for this application and further analysis of the coatings will be carried out to characterise their structure.